Proton shuttle mechanism in the transition state of lipase catalyzed N-acylation of amino alcohols

Per-Olof Syren, Florian Le Joubioux, Yesmine Ben Henda, Thierry Maugard, Karl Hult, Marianne Graber

DOI: 10.1002/cctc.200((will be filled in by the editorial staff))

Proton shuttle mechanism in the transition state of lipase catalyzed *N*-acylation of amino alcohols

Per-Olof Syrén*[a],[c], Florian Le Joubioux[b], Yesmine Ben Henda[b], Thierry Maugard[b], Karl Hult[c], Marianne Graber*[b]

Dedication ((optional))

An increased reaction rate for lipase catalyzed *N*-acylation of amino alcohols compared to monofunctionalized amines can be explained by a hydrogen shuffling mechanism that avoids nitrogen inversion in the transition state. The mechanism does not involve acyl migration from an ester intermediate which would be formed first, an explanation that permeates the literature. Our suggested reaction mechanism is dependent on the preference of amino alcohols to form intramolecular hydrogen bonds and the capability of the enzyme to accommodate and exploit the specific hydrogen bonding pattern provided by the ligand during catalysis. Our proposed proton shuttle mechanism involves the transfer of two protons in the transition state concomitant with nucleophilic attack on the acyl enzyme and provides an explanation to the high reaction rate and chemoselectivity for lipase catalyzed *N*-acylation of amino alcohols. Moreover the proton shuttle mechanism explains the increased reaction rate for the enzyme catalyzed *N*-acylation of diamines and of methoxy-2-propylamine for which *O*- to *N*-acyl migration is impossible. A Linear Free Energy Relationship (LFER) analysis based on the experimental results showed that all of our investigated difunctionalized amine substrates afforded a substrate assisted rate acceleration of *N*-acylation by the same reaction mechanism. Furthermore the LFER analysis was consistent with partial proton transfer in the rate limiting transition state which further supports our suggested proton shuttle mechanism.

Introduction

Amino alcohols are used as chiral auxiliaries and chiral ligands in a plethora of asymmetric transformations.[1] The fully reduced equivalent of amino acids, 1,2-amino alcohols, have received most of the attention.[2] Moreover, amino alcohols constitute important compounds in the pharmaceutical, agrochemical, cosmetic and beauty industries[3] and they are readily available from a vast source of precursor molecules including amino acids, imines, epoxides and isoxazolines.[4] Besides being important molecules in synthetic chemistry, amino alcohols and derivatives thereof including sphingosine ((2*S*, 3*R*, 4*E*)-2-amino-octadec-4-ene-1,3-diol), ceramide and the sphingolipids are crucial for the cell as mediators of signalling cascades.[5] Therefore expanding our understanding on how amino alcohols function at the molecular level is of significant importance. Herein we propose a new reaction mechanism for lipase catalyzed *N*-acylation of amino alcohols and related compounds in which the enzyme is able to exploit a specific hydrogen bonding pattern, provided by the ligand, for catalysis by proton shuttling in the transition state (TS). The proton shuttling is mediated by the two functional groups present in the amino alcohol (or in the related difunctionalized amine substrate) linked together by an intramolecular hydrogen bond and by the availability of a suitable base to act as proton acceptor in the enzyme active site. Our suggested proton shuttle mechanism is thus not limited to the α,β-hydrolase fold. The fact that amino alcohols can participate in such concerted proton shuffling using a suitable base in an enzyme scaffold constitutes an interesting inherent property of amino alcohols that to our best knowledge was previously not known.

Transacylation reactions involving amino alcohols have recently gained attention.[6] In acylation reactions of amino alcohols, the alcohol and amino groups have different reactivities. It has been found that 1,2-amino alcohols react to give the *N*-acylated product in water in the absence of catalyst through a suggested mechanism that involves intramolecular general base

[a] *Dr. P.-O. Syrén*
Present address:
Institute of Technical Biochemistry
University of Stuttgart
Allmandring 31, D-70569 Stuttgart, Germany
Fax: (+49)-(0)711-685-63196
E-mail: per-olof.syren@itb.uni-stuttgart.de
[b] *Prof. M. Graber, F. Le Joubioux, Y. Ben Henda, Prof. T. Maugard*
UMR CNRS 7266 LIENSs
Université de La Rochelle,
Bâtiment Marie Curie, Avenue Michel Crépeau 17042 La Rochelle cedex 1, France
E-mail: mgraber@univ-lr.fr
[c] *Prof. K. Hult*
Department of Biochemistry
School of Biotechnology
Royal Institute of Technology (KTH)
AlbaNova University Centre
SE-106 91 Stockholm, Sweden

Supporting information for this article is available on the WWW under http://dx.doi.org/10.1002/cctc.200xxxxxx.((Please delete if not appropriate))

catalysis followed by *O*- to *N*-acyl migration.[7] It is interesting to note that the reaction rate for the uncatalyzed acylation of amino alcohols is higher than expected based on nitrogen basicity solely indicative of cooperation between the nitrogen and the oxygen atoms in the reaction mechanism.[7-8] In chemical acylation of amino alcohols, the *N,O*-diacylated product is observed[9] although the chemoselectivity can be significantly enhanced in favor of *O*-acylation by using tertiary amino alcohols[10] or a tetranuclear zinc cluster as catalyst.[11] Recently focus has been on using enzymes as catalysts for the chemoselective acylation of amino alcohols.[12] Interestingly the selectivity in enzyme catalyzed acylation of amino alcohols is the opposite to the selectivity obtained using metal catalysis.[6, 11] It has been suggested that the lipase catalyzed chemoselective *N*-acylation of 1,2-amino alcohols proceeds through initial *O*-acylation followed by spontaneous *O*- to *N*-acyl migration.[13] Herein we report experimental results on the lipase catalyzed acylation of amino alcohols and related compounds that are not in accordance with that hypothesis of acyl migration as an explanation of the observed chemoselectivity and rate enhancement for *N*-acylation. Furthermore by using density functional theory (DFT) calculations at the B3LYP/6-31G(d,p) level using an active site model containing 205 atoms and MD-simulations we identified a previously unknown reaction mechanism in which the enzyme is able to take advantage of an intramolecular hydrogen bond of the amino alcohol substrate during catalysis. Our proposed mechanism involves a concerted nucleophilic attack by the lone pair of the nitrogen on the acyl enzyme concomitant with an intramolecular proton transfer from the nitrogen and the transfer of the hydroxyl proton of the amino alcohol to the enzyme catalytic base. This proton shuttling in the TS in the enzyme active site leads to the formation of a stereoelectronically favorable intermediate for facile amide bond synthesis (Scheme 1). Moreover our proposed proton shuttle mechanism explains the rate enhancement for the enzyme catalyzed *N*-acylation of other difunctionalized amines including methoxy-2-propylamine and diamines for which *O*- to *N*-acyl migration is not applicable.

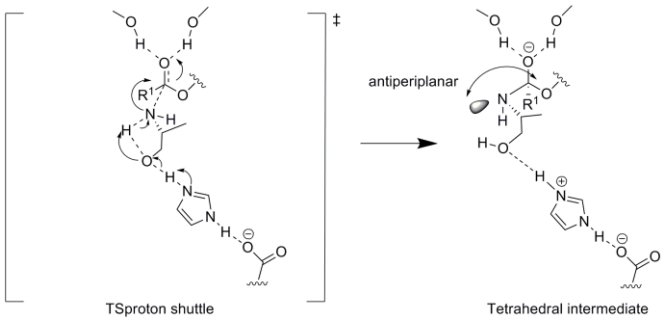

Scheme 1. Proposed proton shuttle reaction mechanism in TS (labelled $TS_{proton\ shuttle}$) for lipase catalyzed *N*-acylation of amino alcohols which leads to the formation of a tetrahedral intermediate in a stereoelectronically favourable[14] conformation for amide bond synthesis without the need for nitrogen inversion. Our suggested reaction mechanism is shown using (*R*)-alaninol as substrate. Note that the proton shuttle mechanism works in the same way for diamines where a nitrogen replaces the oxygen as the substrate assisted acceptor.

Results and Discussion

The enzyme catalyzed acylation of amino alcohols (**1a-d)** is outlined in Scheme 2. Three different types of acylated products are possible: the *O*-acylated amino alcohol (**2a-d**)**,** the *N*-acylated amino alcohol (**3a-d**) and the diacylated amino alcohol (**4a-d**). For comparison, the substrate scope was extended by analyzing the lipase catalyzed acylation of a secondary alcohol, a secondary amine, a diol and a diamine. The initial kinetics for lipase catalyzed *N*-acylation and *O*-acylation respectively were measured and the resulting apparent k_{cat} values ($k_{cat,app}$) are given in Table 1.

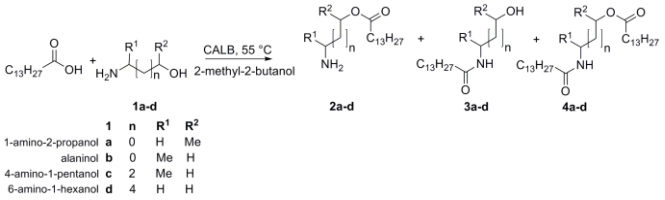

	1	n	R^1	R^2
1-amino-2-propanol	a	0	H	Me
alaninol	b	0	Me	H
4-amino-1-pentanol	c	2	Me	H
6-amino-1-hexanol	d	4	H	H

Scheme 2. Acylation of amino alcohols catalyzed by *Candida antarctica* lipase B (CALB, *EC* 3.1.1.3) using myristic acid as acyl donor.

Table 1. Experimentally determined apparent k_{cat} values for *N*-acylation and *O*-acylation using *Candida antarctica* lipase B in 2-methyl-2-butanol as solvent at 55 ºC. Myristic acid was used as acyl donor.

Substrate[a]		*N*-acylation $k_{cat,app}$ [min^{-1}]	*O*-acylation $k_{cat,app}$ [min^{-1}]
acylation of amino alcohols			
1a	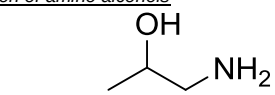	29	*n.d.*[b],[c]
1b	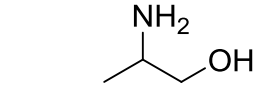	50	*n.d.*[b],[c]
1c	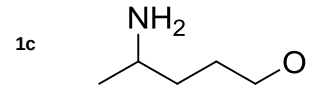	13	85
1d	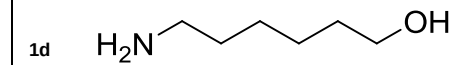	12	130
acylation of a monofunctional group			
5	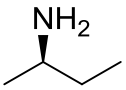	2.3	-
6	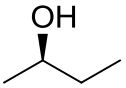	-	54
acylation of a diol and diamine			
7	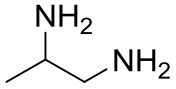	89	-
8	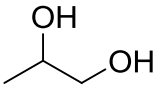	-	320[d]
Negative control for O- to N- acyl migration			
9	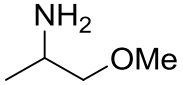	19	*n.d.*[b]

[a] The pure (*R*)-enantiomer of 2-butanol (**6**) and 2-butylamine (**5**) was used, respectively [b] The *O*-monoacylated product was not detected. [c] Trace amounts of the *N*,*O*-diacylated product were detected, formed at a $k_{cat,app}$ tenfold lower than the $k_{cat,app}$ value for *N*-acylation [d] $k_{cat,app}$ for *O*-acylation of the primary hydroxyl group was 260 min^{-1} and $k_{cat,app}$ for *O*-acylation of the secondary hydroxyl group was 60 min^{-1}

The enzyme catalyzed acylation of amino alcohols (**1a** and **1b**) was compared with the acylation of monofunctional substrates (Table 1, substrate **5** and **6**). The apparent k_{cat} for *N*-acylation using (*R*)-2-butylamine (**5**) as nucleophile was found to be 25 fold lower than the apparent k_{cat} value for *O*-acylation using (*R*)-2-butanol (**6**), in contrast with the intrinsic chemical reactivities of these two functional groups[15] but in accordance with the well known fact that lipases and esterases are very poor catalysts in the hydrolysis and synthesis of amide bonds.[16]

For the homo difunctionalized substrate 1,2-diaminopropane (**7**) the apparent k_{cat} value for *N*-acylation was found to be the highest of the investigated substrates (40 times higher compared to the value for (*R*)-2-butylamine (**5**)) and only fourfold lower than the rate constant for *O*-acylation of 1,2-propanediol (**8**). The enhanced apparent k_{cat} for *N*-acylation displayed by 1,2-diaminopropane can not be explained by enhanced nucleophilicity[17] and indicates a cooperative interaction between the two amino groups facilitating *N*-acylation in the enzyme active site. Such cooperative interaction was not observed for 1,2-propanediol (**8**) for which the primary hydroxyl did not assist in the *O*-acylation of the secondary hydroxyl. Moreover the hydroxyl group present in the investigated amino alcohols leads to an increased k_{cat} value for *N*-acylation of 5 to 25 times compared to the value for (*R*)-2-butylamine (**5**).

In the literature, the observed rate increase and chemoselectivity for lipase catalyzed *N*-acylation of amino alcohols has been attributed to initial *O*-acylation followed by *O*- to *N*-acyl migration.[13, 18] Acyl migrations are well known phenomena in chemistry and are used for converting prodrugs with beneficial properties such as increased solubility, to their corresponding parent molecules.[19] However, we did not observe any *O*-acylated intermediate of the amino alcohols or of methoxy-2-propylamine (**9**) from which the presumed *O*- to *N*-acyl migration would occur (the experimental detection limit was 2 µM, see Supporting Information). Such *O*- to *N*-acyl migration would need to proceed faster than the enzyme catalyzed reaction in order for the *O*-acylated intermediate to remain undetected. Acyl migrations between two oxygens in glucose and in a glyceride have been reported to occur at a rate of 0.005 min^{-1} and 0.002 min^{-1} respectively.[20] Acid catalyzed *N*- to *O*-acyl migrations in phosphopeptides have been studied[21] and the reported conversions correspond to an acyl migration rate of 0.002 min^{-1}. The *O*- to *N*-acyl migration in ethanol amine was found to proceed with rates much lower than 1 min^{-1}.[22] In a study of the acyl migration in *O*-arachidonoylethanolamine and *O*-palmitoylethanolamine the published data corresponded roughly to a base promoted *O*- to *N*- acyl migration rate of less than 0.02 min^{-1}.[23] The experimentally determined reaction rates for base catalyzed *O*- to *N*-acyl migrations are at least one to two orders of magnitude slower than our experimentally determined reaction rates for enzyme catalyzed acylation of amino alcohols. Since the acyl donor myristic acid was used in slight excess in our experiments, an acid catalyzed *N*- to *O*- acyl migration would be more likely than the corresponding *O*- to *N*- transfer.[23] If *O*- to *N*-acyl migration would play a major role for lipase catalyzed *N*-acylation of amino alcohols, the *O*-acylated intermediate would build up and reach a steady-state concentration. Under our experimental conditions the steady-state concentration of this intermediate would reach 1-100 mM (Supporting Information). No *O*-acylated intermediate was found despite that our detection limit was 2 µM. To further confirm the fact that acyl migrations can not explain our experimental results, we performed an enzyme catalyzed acylation of methoxy-2-propylamine (**9**, Table 1) with a poor nucleophilic oxygen which lacks the capability of *O*- to *N*-acyl migration. The apparent k_{cat} value for *N*-acylation of methoxy-2-propylamine was found to be tenfold higher than for (*R*)-2-butylamine (**5**) and only twofold lower than the corresponding value for alaninol (**1b**). This is in sharp contrast to chemical *N*-acylation as well as to metal catalysis where it has been found that methylation of the oxygen atom in the amino alcohol molecule leads to a decrease in reaction rate of two orders of magnitude.[6-8] Furthermore, 1,2-diaminopropane (**7**) afforded the highest rate acceleration that can not be explained by the acyl migration hypothesis for obvious reasons.

Since an *O*- to *N*-acyl migration could not explain our experimental results we came up with the alternative hypothesis that the additional functional group besides the nitrogen atom (-OH for amino alcohols, $-NH_2$ for the diamine (**7**) and -OMe for methoxy-2-proylamine (**9**)) participated in the reaction mechanism and afforded a substrate assisted rate acceleration for *N*-acylation. The hydroxyl group in amino alcohols promote the formation of intramolecular hydrogen bonds.[24] It has been shown experimentally that ethanol amine exists predominantly in its *gauche* conformation in solution[25] for which such interactions are facilitated. Two different types of intramolecular hydrogen bonds can exist in amino alcohols (Table 2).

Table 2. Relative distribution of amino alcohol conformers with an intramolecular hydrogen bond based on DFT single-point calculations at the B3LYP/ 6-311+G(2d,2p) level in 2-methyl-2-butanol.

Conformer	Relative energy[a] [kcal/mol]	Relative abundance
(*R*)-Alaninol		
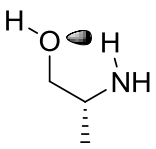	0.2	0.44
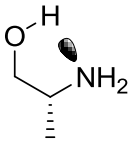	0	0.56
R)-4-Amino-1-pentanol		
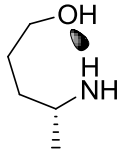	4.7	0.0007
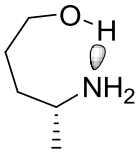	0	0.9993

[a] Using DFT at the B3LYP/6-311+G(2d,2p) level of theory including ZPVE. A Conductor-like Polarizable Continuum Model was used to account for the solvent. Geometry optimizations were performed using B3LYP/6-31G(d,p) level of theory.

The first set of conformations contains an intramolecular hydrogen bond between one of the amine hydrogens and one of the lone pairs of the oxygen. In the second conformation, the hydroxyl group binds to the lone pair of the nitrogen. We used DFT calculations at the B3LYP/6-311+G(2d,2p) level to assess the relative abundances of substrate conformers containing an intramolecular hydrogen bond for (*R*)-alaninol (**1b**) and (*R*)-4-amino-1-pentanol (**1c**) (Table 2). For (*R*)-alaninol, the conformation for which the hydrogen bond is donated by the hydroxyl and accepted by the nitrogen lone pair is slightly preferred in accordance with previously published results on ethanol amine.[26] For the longer amino alcohol, (*R*)-4-amino-1-pentanol, only one type of intramolecular hydrogen bond is possible, reflecting an almost perfect -OH---N hydrogen bond. Can such substrate conformational distributions be linked to catalysis? It is interesting to note that the major shift in the relative distribution of substrate conformations displayed by the amino alcohol containing a longer chain is accompanied with an enhanced preference for *O*-acylation (Table 1). We therefore decided to investigate the putative role of an intramolecular hydrogen bond on the reaction mechanism in the enzyme active site that could explain the increased activity for *N*-acylation for *all* of the investigated difunctionalized amine substrates.

We have recently discovered a previously unacknowledged hydrogen bond donated by the substrate reacting amide NH-group in the transition state for amide bond hydrolysis of amidases with a spatial arrangement to assist nitrogen inversion in the enzyme active site.[27] The hydrogen bond is important for reaction specificity since esterases that are poor in the hydrolysis/synthesis of an amide bond lack this interaction.[27-28] In order to analyse if such a substrate assisted hydrogen bond donated by the NH_2-group of the amino alcohol substrate in the transition state could facilitate enzymatic *N*-acylation, we performed MD-simulations on the acylation of (*R*)-alaninol (**1b**). From the MD-simulations, in which the tetrahedral intermediate represented the transition state for *N*-acylation, it was concluded that the reacting NH-group of (*R*)-alaninol did *not* function as hydrogen bond donor in the modelled transition state. Rather the lone pair of the reacting nitrogen atom accepted a hydrogen bond donated by the hydroxyl (Figure S1, Table S1, Supporting Information). Moreover by using *ab initio* calculations on *N*-methyl alaninol we concluded that nitrogen inversion is not facilitated in an amino alcohol compared to an alkyl amine (rather the calculated barrier for inversion was found to be higher for amino alcohols, Table S2, Supporting information). Proton transfer has been discussed in the context of the rate enhancement observed for the chemical catalyzed acylation of diamines.[29] Such proton transfer would be facilitated by the intramolecular hydrogen bonding pattern present in amino alcohols.[30] Interestingly spontaneous proton transfers have been observed in the gas-phase in cationic clusters of phenol and ethanol amine.[31] By using *ab initio* DFT calculations on a small model of a lipase catalytic machinery we found a new alternative mechanism for enzyme catalyzed *N*-acylation of amino alcohols (Figure S2). In this new, previously undescribed mechanism, the neutral nitrogen atom of the amino alcohol attacks the acyl enzyme coincidently with the transfer of two protons, thus forming a "proton shuttle" (a proton is transferred from the NH_2-group to the hydroxyl and at the same time the hydroxyl proton is transferred to the enzyme catalytic base H224). Interestingly, a proton shuttle in the transition state has been suggested to occur for the ribosome via a water molecule[32] and for Mycolic Acid Cyclopropane Synthase involving a bicarbonate.[33] In order to understand the impact on catalysis of our discovered proton shuttle reaction mechanism for *N*-acylation of amino alcohols, a very large *ab initio* model of the active site of *Candida antarctica* lipase B was constructed. It is advantageous to perform calculations in a large model of the active site since such model provides a more realistic reaction environment compared to a small model in the gas-phase. By performing cluster *ab initio* calculations using this very large model of the active site to simulate the protein environment it is possible to compare the proton shuttle mechanism with the "traditional" reaction mechanism The hypothetical "traditional" mechanism for *N*-acylation of an amino alcohol is the pathway that would be displayed by a monofunctionalized amine and for which proton shuttling does not occur. Note that the traditional mechanism uses the open chain of the amino alcohol substrate whereas it is known that amino alcohols adopt conformations with an intramolecular hydrogen bond[24] that thus has to be broken to obtain the non-cyclic conformation. Cluster *ab initio* calculations have previously been used to analyze reaction mechanisms in enzymes.[33-34] Our model of the enzyme active site consisted of 205 atoms and contained 14 amino acids in and around the active site. The geometry of the transition state for *N*-acylation of (*R*)-alaninol (**1b**) for our suggested proton shuttle reaction mechanism, calculated at B3LYP/6-31G(d,p) level of theory using the large active site model, is shown in Figure 1. The transition state had one imaginary frequency (1030i cm^{-1}) that corresponded to nucleophilic attack of the nitrogen atom of the amino alcohol on the acyl enzyme coincidently with the transfer of two protons that form the proton shuttle (Figure 1).

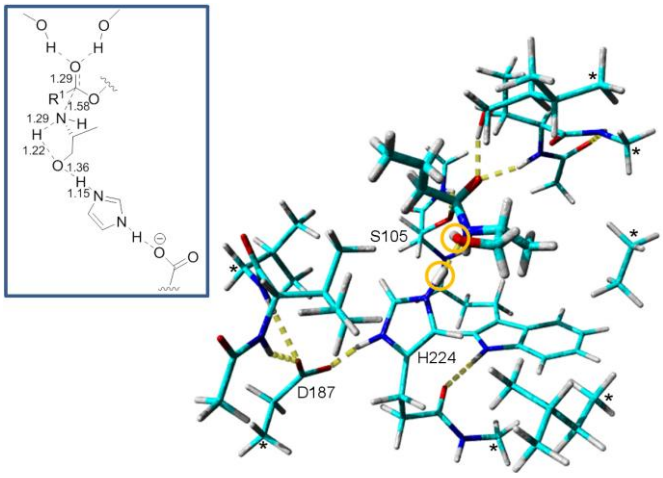

Figure 1. The figure shows the geometry of the transition state for the proposed proton shuttle reaction mechanism obtained at B3LYP/6-31G(d,p) level of theory. A large model of the active site of *Candida antarctica* lipase B consisting of 205 atoms was used for the cluser *ab initio* calculations. The scissile nitrogen atom of (*R*)-alaninol is attacking the carbonyl carbon of the acyl enzyme concomitant with the transfer of two protons (encircled). The lengths of the bonds being formed/broken in the transition state are shown in the panel in the top left corner. Atoms marked with an asterisk (*) were kept fixed during the geometry optimization since the corresponding backbone atoms in the enzyme does not have the ability to move freely. The acyl enzyme with the carbon chain originating from the acyl donor (containing four carbon atoms in our model) and the substrate, (*R*)-alaninol are shown in thick sticks. Color code: Cyan- carbon, Red - oxygen, Blue - nitrogen, White - hydrogen. Hydrogen bonds are indicated with dashed yellow lines. The residues constituting the Ser/His/Asp catalytic triad are labelled. A larger picture of the geometry of the transition state is shown in Figure S3 in Supporting Information.

The proton shuttle mechanism is facilitated by the preference of amino alcohols to form intramolecular hydrogen bonds and the (*R*)-alaninol (**1b**) substrate is already preorganized for catalysis in the ES-complex, since it contains the necessary intramolecular hydrogen bond for the "proton shuffling" to occur (Table 2, Row 1). Next, the transition states and intermediates for the hypothetical traditional reaction mechanism for *N*-acylation of (*R*)-alaninol, for which proton shuttling does not occur, was calculated (Figure S7, for a definition of the different mechanisms discussed, see Supporting Information, Figure S4-S6). For the traditional mechanism of *N*-acylation, the open chain conformation of (*R*)-alaninol was used, for which proton shuttling can not occur and which would mimic the pathway for a mono substituted amine. The calculated barriers of activation, using the large model of the active site, for *N*-acylation of (*R*)-alaninol are shown in Figure 2 (with the rate limiting transition states shown, See Also Supporting Information, Figure S7). The nitrogen inversion step for the traditional mechanism (TS_{inv} in Figure 2) was found to be concerted with (and thus part of) amide bond formation at the B3LYP/6-31G(d,p) level of theory (see also supporting information, Figure S4). Using DFT at the B3LYP/6-31G(d,p) level of theory, our proposed reaction mechanism was found to have a barrier of activation that is 1.1 kcal/mol lower than the barrier for the "traditional" mechanism in the enzyme (the traditional mechanism is outlined in Figure S4) . This energy difference corresponds roughly to an increase by a factor of 10 of the rate constant k_{cat} which is in good agreement with the rate enhancement of enzyme catalyzed *N*-acylation of amino alcohols that we observed experimentally. The calculated barrier for our proposed alternative mechanism (18.5 kcal/mol) can be translated into a calculated k_{cat} value of approximately 2 min^{-1} at 55 °C using transition state theory, which is in reasonable agreement with the experimentally determined k_{cat} values for *N*-acylation of amino alcohols (Table 1). Although the calculated energy difference of 1.1 kcal in the very large active site model between our suggested proton shuttle mechanism and the "traditional mechanism" is in accordance with the experimental results (Table 1), it is quite small (it corresponds to a 10 times rate enhancement).

Additional calculations showed that the proton shuttle mechanism works for other substrate assisted acceptors besides a hydroxyl group. We calculated the TS for *N*-acylation of 1,2-diaminoethane (representing 1,2-diaminopropane (**7**)) by the proton shuttle mechanism (Supporting Information, Figure S8). As for (*R*)-alaninol, nucleophilic attack was concerted with proton shuttling. When constructing the proton shuttle for 1,2-diaminoethane in the large active site model of 205 atoms, the barrier was found to be 17.2 kcal/mol including ZPVE which is 1.3 kcal/mol lower than the calculated barrier for *N*-acylation of (*R*)-alaninol. More importantly the barrier for the proton shuttle mechanism for 1,2-diaminoethane was found to be 5 kcal/mol lower than the barrier for the traditional mechanism (with nitrogen inversion) thus further corroborating the importance of the proton shuttle and in accordance with our experimental results that 1,2-diaminopropane (**7**) afforded the highest substrate assisted rate acceleration of *N*-acylation (Table1). MD-simulations of the tetrahedral intermediate representing the transition state for *N*-acylation of methoxy-2-propylamine (**9**) showed that the oxygen can accept a proton from the reacting NH-group (Supporting Information, Figure S9). Obviously proton transfer to the enzyme catalytic base occurs in a second step since the methoxylated group lacks a hydrogen. To further corroborate that the proton shuttle mechanism can explain the rate enhancement for enzyme catalyzed *N*-acylation of all of our investigated substrates, we note that the proton shuttle mechanism involves partial proton transfer in the rate limiting transition state. Therefore, for the proton shuttle mechanism the apparent k_{cat} value for *N*-acylation should depend on the pK_a of the substrate as opposed to the "traditional mechanism" for which no partial proton transfer from the reacting NH-group occurs in the rate limiting transition state (nitrogen inversion). A Linear Free Energy Relationship (LFER) analysis showed that the amino alcohols, the diamine and methoxy-2-propylamine (**9**) afforded a rate acceleration by the same reaction mechanism of *N*-acylation and the slope of -0.24 was in accordance with partial proton transfer in the transition state (Supporting Information, Figure S10). It should be noted that (*R*)-2-butylamine (**5**) that lacks the possibility of proton shuffling does not follow the trend observed for the difunctionalized amines and thus operates by a different reaction mechanism of *N*-acylation (nitrogen inversion).

For the smaller amino alcohols, the rate for enzyme catalyzed *O*-acylation was very low (the *O*-monoacylated intermediate was not detected). We decided to analyze this experimental finding by computing the transition state and intermediates for enzyme catalyzed *O*-acylation starting from the other possible conformation of (*R*)-alaninol that is preorganized for a proton shuttle mechanism with an intramolecular hydrogen bond donated by the hydroxyl (Table 2, second row). As mentioned previously smaller amino alcohols form intramolecular hydrogen bonds[30] and such a ring structure is preorganized to react through a proton shuttle mechanism as described for *N*-acylation. It was found that the mechanism for *O*-acylation of (*R*)-alaninol by such proton shuttle (Figure S11) has a much higher barrier compared to *N*-acylation, clearly demonstrating that the proton shuttle mechanism disfavors *O*-acylation. In our very large model of the active site, the proton shuttle for *O*-acylation was found to have a barrier that was approximately 20 kcal/mol higher in energy than for *N*-acylation based on using a TS-model that was optimized at the B3LYP/6-31G(d,p) level (see Figure S12-S13). This is because of the fact that the remaining free lone pair on the oxygen atom will be close in space to the developing negative charge on the carbonyl oxygen of the acyl enzyme in TS (see Figure S6, S11 and S12 in Supporting Information). The long distance between the nucleophilic oxygen and the carbonyl carbon in the TS for *O*-acylation that minimizes this electrostatic repulsion results in the catalytic base H224 no longer being in an optimal position for catalysis, thus disfavoring proton shuffling (Figure S12). Obviously this unfavorable interaction in the TS does not occur for "normal" *O*-acylation operating on the open chain conformer of the substrate for which the catalytic base (H224) adopts its normal position where a hydrogen bond is formed directly with the substrate nucleophilic hydroxyl group. As noted previously no substrate assisted rate acceleration was observed for 1,2-propanediol (**8**) (Table 1) in consistence with the fact that the proton shuttle mechanism is highly disfavoured for *O*-acylation. Vicinal diols display a significant relative abundance of substrate conformations that do not contain an intramolecular hydrogen bond[35] and experimental data from the gas phase further shows that the strain energy related to intramolecular hydrogen bond formation is much higher for molecular ions of vicinal diols as compared to corresponding diamines and amino alcohols.[30]

The lower barrier of activation for the new proton shuttle mechanism of *N*-acylation compared to "traditional" *N*-acylation

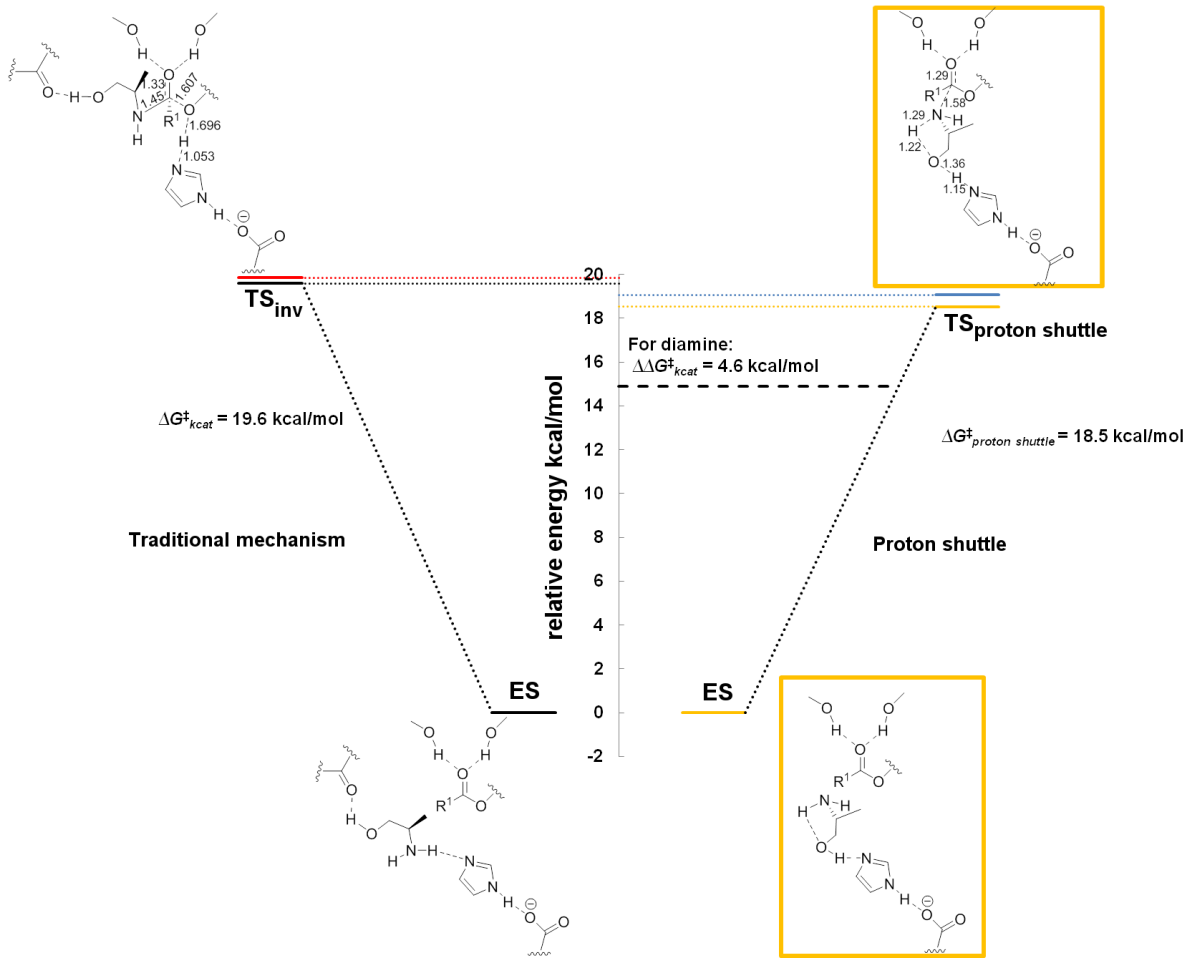

Figure 2. Energy profile diagram for comparison of enzyme catalyzed *N*-acylation of (*R*)-alaninol for the novel proton shuttle mechanism (right) and the hypothetical traditional mechanism that would be the pathway for an amine and for which proton shuttling does not occur (left). The calculated energy difference (4.6 kcal/mol in the gas-phase) in favour of the proton shuttle mechanism over the traditional mechanism for 1,2-diaminoethane (representing 1,2-diaminopropane (**7**)) is indicated by the bold dashed line. The tetrahedral intermediate produced from the proton shuttle mechanism has the nitrogen lone pair in the stereoelectronically required conformation for amide bond synthesis which makes nitrogen inversion obsolete (see Scheme 1). Note that the hydrogen bond donated by the (*R*)-alaninol substrate hydroxyl and accepted by the backbone of T40 that we used in our model for the hypothetical traditional mechanism (left) replaces the hydrogen bond to the $N_{\varepsilon 2}$ of the H224 and does not contribute to catalysis since it is fully developed in the ES-complex (the corresponding interaction is formed for the corresponding hypothetical *O*-acylation as well, see also Figure S4, Supporting Information). The $\Delta G^{\ddagger}_{kcat}$ values given are the calculated activation energies for *N*-acylation of (*R*)-alaninol for the two mechanisms in the gas-phase including ZPVE (orange and black dotted lines respectively, geometry optimizations and vibrational analysis were performed at the B3LYP/6-31G(d,p) level of theory using the large quantum model presented in Figure 1). For the proton shuttle mechanism (right), the ES-complex and the transition state are schematically shown within orange frames with the lengths of the bonds being formed/broken in the transition state ($TS_{proton\ shuttle}$) given in Å. The rate limiting transition state for *N*-acylation for the traditional mechanism (left) is the nitrogen inversion step (TS_{inv}, top left) in which the nitrogen atom has sp^2 like character and the Ser O_γ-former carbonyl carbon bond is being broken (the lengths of the bonds being formed/broken in TS_{inv} are given in Å). The inversion step is necessary in order for the lone pair of the nitrogen atom to be pointing antiperiplanar to the Ser Oγ-former carbonyl carbon bond, which is the well known[14a] stereoelectronically required conformation for amide bond synthesis (see also Figure S4). It should be noted that nitrogen inversion and amide bond formation is a concerted process at the B3LYP/6-31G(d,p) level of theory. To simulate the protein and water shell surrounding the large active site model, single-point calculations using a conductor-like polarizable continuum model[36] were performed for ε=2 (the level of the rate limiting transition states shown in red and blue for the two mechanisms for (*R*)-alaninol) and ε=80 (levels not shown in the figure). The relative energies were essentially unaffected by a continuum surrounding the active site model and for water the activation barriers were 20.1 kcal/mol for the traditional mechanism and 19.7 kcal/mol for the proton shuttle. The reduced barrier for the proton shuttle mechanism of *N*-acylation for (*R*)-alaninol compared to the traditional mechanism, that would be the pathway for a (monosubstituted) amine, is in accordance with the experimental results that amino alcohols display increased k_{cat}-values for *N*-acylation (Table 1). The proton shuttle does not work for *O*-acylation since a lone pair of the oxygen will point towards the (developing) negative charge of the carbonyl oxygen of the acyl enzyme or towards a lone pair on Ser105 O_γ in TS (see Figure S6, S11-S13). This causes the hydroxyl oxygen-carbonyl carbon distance to increase in transition state for the proton shuttle of *O*-acylation and the position of the catalytic base (H224) is no longer optimal as compared to *N*-acylation. We estimate that the barrier for the proton shuttle of *O*-acylation is 39 kcal/mol at the B3LYP/6-31G(d,p) level of theory in the large active site model (Figure S12) thus making *O*-acylation highly disfavoured.

(Figure 2) can be understood in terms of orbitals and stereoelectronic effects. To clarify this it is adequate to compare lipase catalyzed *N*-acylation of amino alcohols with the reaction mechanism of amidases. It is well known that esterases are poor catalysts in the hydrolysis/synthesis of amide bonds.[16] Nitrogen inversion or rotation is required in the enzymatic mechanism for amide bond hydrolysis/synthesis[37] (see Figure S14 in Supporting Information). This is because the nitrogen lone pair needs to be situated antiperiplanar to the bond formed/cleaved between the nucleophilic group and the carbonyl carbon of the amide in

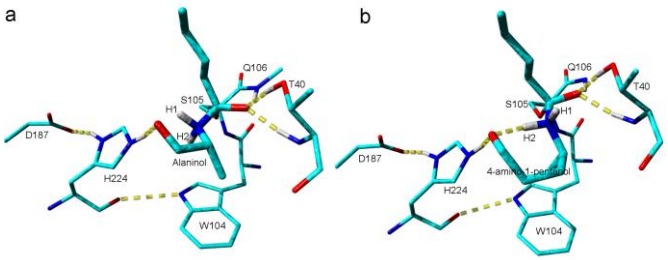

Figure 3. Snapshots from the MD-simulations of the tetrahedral intermediate representing the transition state for the proton shuttle mechanism of *N*-acylation ($TS_{proton\ shuttle}$ in Figure 2) of amino alcohols catalyzed by *Candida antarctica* lipase B. **(A)** *N*-acylation of (*R*)-alaninol (**1b**) **(B)** *N*-acylation of (*R*)-4-amino-1-pentanol (**1c**). The catalytic amino acids (S105, H224, D187) as well as oxyanion hole (T40 and Q106) are shown. W104 forms the bottom of the so called stereoselectivity pocket in *Candida antarctica* lipase B. Substrates are shown in thick sticks. Color code: Cyan - carbon, Red - oxygen, Blue - nitrogen, White - hydrogen. Not all atoms are shown for clarity reasons. Hydrogen bonds are indicated with dashed yellow lines. The two protons sitting on the scissile nitrogen are labelled (H1 and H2).

Table 3. Distances and angles between atoms involved in proton transfer for the proton shuttle mechanism of *N*-acylation of amino alcohols using *Candida antarctica* lipase B.[a]

Hydrogen bond	Distance [Å]	Angle D-H---A[b] [degrees]	Angle –H---AX[b] [degrees]
(*R*)-Alaninol			
NH1---O[c]	1.6 (2.5)	141 (96)	85 (74)
NH2---O[c]	1.8 (2.8)	134 (77)	81 (75)
HisNH to O in alaninol	1.5 (1.8)	171 (156)	104 (112)
(*R*)-4-amino-1-pentanol			
NH1---O[c]	1.6 (2.7)	168 (107)	90 (88)
NH2---O[c]	1.6 (2.6)	171 (111)	105 (78)
HisNH to O in 4-amino-1-pentanol	1.5 (1.9)	163 (147)	142 (96)

[a] Based on the 8 ns "production phase" of the MD-simulations of the tetrahedral intermediate representing transition state ($TS_{proton\ shuttle}$ in Figure 2). The values for the best hydrogen bond are given, with average values for all 8000 snapshots given within brackets. [b] The two angles involved in hydrogen bond formation (donor-H---acceptor and –H---acceptor-X). [c] The two individual protons sitting on the scissile nitrogen in the transition state model. See Figure 3.

accordance with stereoelectronic theory in chemistry introduced by Deslongchamps.[14] The stereoelectronic effect is caused by a stabilizing n-σ^* orbital interaction in the TS worth several kcal/mol. Our proposed reaction mechanism for lipase catalyzed *N*-acylation of amino alcohols and 1,2-diaminopropane (**7**) (involving the transfer of two protons in the transition state) and methoxy-2-propylamine (involving the transfer of one proton in the transition state) leads to the direct formation of a tetrahedral intermediate in a stereoelectronically favourable conformation for facile amide bond synthesis without the need for nitrogen inversion (Scheme 1, Figure S4-S6 Supporting Information).

In order to make the picture of enzyme catalyzed *N*-acylation of amino alcohols more complete it is important to include the amino alcohols of longer chain length (**1c-d**) in the analysis as well. For shorter amino alcohols only the *N*-acylated product was observed experimentally whereas *O*-acylation was predominant for the longer amino alcohols 4-amino-1-pentanol (**1c**) and 6-amino-1-hexanol (**1d**) (Table 1). We performed 10 ns MD-simulations of an intermediate mimicking the transition state for the proton shuttle mechanism ($TS_{proton\ shuttle}$ in Figure 2) to analyze this difference in more detail. A snapshot from the MD-simulations of (*R*)-alaninol and (*R*)-4-amino-1-pentanol is shown in Figure 3. The average lengths and angles for the hydrogen bonds relevant for the proton shuttle mechanism are given in Table 3. A hydrogen bond donated by the amino group and accepted by the hydroxyl oxygen of the amino alcohol can be formed at the same time as the hydroxyl proton forms a hydrogen bond with the enzyme catalytic base (H224), which will lead to our proposed "proton shuttle" mechanism in accordance with the *ab initio* calculations. However, the two protons sitting on the amino group of the amino alcohol (labelled H1 and H2 in Figure 3A and Figure 3B respectively) are not identical since upon proton transfer they lead to different conformations of the nitrogen lone pair in the formed tetrahedral intermediate. Only abstraction of the proton for which the NH-bond is pointing antiperiplanar to the Ser O_γ-C bond (the proton labelled H1 in Figure 3) will lead to a tetrahedral intermediate with a stereoelectronically favourable conformation for amide bond synthesis (the abstraction of this proton was accounted for in our *ab initio* calculations of the proton shuttle mechanism of *N*-acylation using the large active site model, Figure 1 and Figure 2). Interestingly, from the MD-simulations we found that for the shorter amino alcohol (*R*)-alaninol (**1b**) there was a preference for the hydrogen bond donated by the NH-group pointing antiperiplanar to the Ser O_γ-C bond to form (i.e. involving H1 in Figure 3). We found the situation to be the opposite for the longer amino alcohol (*R*)-4-amino-1-pentanol where a hydrogen bond involving the other proton was preferred (the proton labelled H2 in Figure 3). For the longer amino alcohol the formation of a tetrahedral intermediate in an unfavourable stereoelectronic conformation will result from such proton abstraction (as shown in the snapshot in Figure 3B). Nitrogen inversion (or rotation) in such an unfavourable tetrahedral intermediate is necessary to prepare for the breakdown of the intermediate and no advantage over "traditional" *N*-acylation of an alkylamine is expected. This is in accordance with the fact that *O*-acylation was predominant for the larger amino alcohols (Table 1). Furthermore, from Table 2 it can be concluded that formation of the required intramolecular hydrogen bond for the proton shuttle mechanism of *N*-acylation is difficult for longer amino alcohols. Moreover entropic effects disfavours the formation of larger rings for amino alcohols[38] and consequently the importance of the proton shuttle mechanism, dependant on such ring formation, will decrease. This is in accordance with the experimental finding that *O*-acylation becomes predominant for the longer amino alcohols caused by nucleophilic attack of the open chain. In fact the entropic cost of ring formation can be estimated to be 5 kcal/mol higher for the longer amino alcohol 4-amino-1-pentanol (**1c**) as compared to alaninol (**1b**) based on gas-phase experimental data.[38] 1,2-Diaminopropane (**7**) showed the highest reaction rate for *N*-acylation (Table 1) which is in accordance with the fact that the intramolecular hydrogen bond in the molecular ion of diamines is considerably stronger than for corresponding amino alcohols.[30] It is interesting to see that the reaction rate for lipase catalyzed *N*-acylation of methoxy-2-propylamine (**9**) is only two fold lower than the reaction rate for (*R*)-alaninol (**1b**). A reduction in rate is expected since the methylated oxygen in methoxy-2-propylamine

lacks a hydrogen to donate to the enzyme catalytic base during proton shuttling. Therefore the ether oxygen works as a bridging atom between the amino group and the enzyme catalytic base with proton transfer in two steps in this case. The molecular ions of polyethers are known to form very strong intramolecular hydrogen bonds.[38]

Finally there is an additional driving force for *N*-acylation to occur according to our proposed mechanism. Upon formation of the tetrahedral intermediate, an NH---O hydrogen bond in the near attack complex is replaced with a stronger OH---N hydrogen bond (Table 2). Ring formation in the enzyme active site is further promoted by the formation of a hydrogen bond between H224 and the additional functional group present in the substrate.

Conclusion

We propose a proton shuttle reaction mechanism for lipase catalyzed *N*-acylation of amino alcohols in which two protons are transferred in transition state coincidently with nucleophilic attack. Our proton shuttle mechanism is not dependent on acyl migration from an ester intermediate and can explain the enhanced reaction rate for enzyme catalyzed *N*-acylation of diamines and methoxy-2-propylamine for which *O*- to *N*-acyl migration can not occur. A Linear Free Energy Relationship (LFER) analysis indicated that the difunctionalized amines afforded a substrate assisted rate acceleration by the same reaction mechanism. Furthermore the LFER analysis was consistent with partial proton transfer in the rate limiting transition state which is in accordance with our suggested proton shuttle reaction mechanism. By using DFT *ab initio* calculations on a very large active site model we found that our proposed mechanism had a lower barrier of activation compared to traditional *N*-acylation for which proton shuffling does not occur. Moreover we demonstrated the feasibility of using quantum mechanics on very large active site models to study complex biochemical problems. The proton shuttle reaction mechanism leads to the formation of a tetrahedral intermediate in a stereoelectronically favourable conformation for facile amide bond synthesis which provides a physical explanation of the rate increase for enzyme catalyzed *N*-acylation of amino alcohols and other difunctionalized amines. The mechanism is facilitated by the preference of amino alcohols to form intramolecular hydrogen bonds which makes the substrate amino alcohol adopting a conformation that is preorganized for proton shuttling, a property that to our best knowledge was previously not known. Our proposed proton shuttle mechanism for lipase catalyzed *N*-acylation of amino alcohols provides an interesting link to amidases, for which the production of a stereoelectronically favourable conformation of the nitrogen lone pair is facilitated by a hydrogen bond in transition state.[27] Likewise, in the ribosome, proton shuttling is lowering the barrier of activation for peptide bond synthesis.[32b]

Experimental Section

Enzyme and chemicals

Novozym® 435 (immobilized *Candida antarctica* lipase B), was kindly provided by Novozymes A/S, Bagsvaerd, Denmark. (*R*)-2-butanol (99%), (*R*)-2-butylamine (99%), 1,2-propanediol (≥99.5%), 1,2-diaminopropane (≥98%), 1-amino-2-propanol (93%), alaninol (98%), 1-methoxy-2-propylamine (95%) and 6-amino-1-hexanol (≥97%), as well as 2-methyl-2-butanol (99%) and acetonitrile for luminescence were purchased from Sigma-Aldrich (St Louis, USA). 4-amino-1-pentanol was from Santa Cruz Biotechnology (USA). Myristic acid and acetic acid were from Fluka (St Quentin-Fallavier, Switzerland). All chemicals were dried over molecular sieves. Pure water was obtained via a Milli-Q system (Millipore, France). Acetonitrile and methanol were purchased from Carlo ERBA (Val-de-Reuil, France).

Active site titration

Active site titration was performed by using the suicide inhibitor 4-methylumbelliferyl hexylphosphonate. The inhibitor was added to beads (10 mg), which contained immobilized lipase, to a final concentration of 50 µM. Acetonitrile was added to a final volume of 1 mL. The fluorescence intensity was analyzed by adding 100 µL sample solution to 900 µL buffer containing 100 mM Tris-HCl, 1 mM $CaCl_2$, pH 8.0 and by measuring the signal by using a luminescence spectrometer (Luminescence Spectrometer Model LS-50B, PerkinElmer, MA, USA). The excitation wavelength was λ=360 nm and the emission wavelength was λ =445 nm. The amount of active sites were calculated from a standard curve of the linear relationship between fluorescence intensity and the concentration of the leaving group 4-methylumbelliferone. The relationship between fluorescence intensity and the amount of beads containing immobilized enzyme was linear. The resulting active protein load on the support (%weight/weight) was found to be 4.7% which corresponds to an active site concentration of 14 µM when 10 mg beads per ml are used.

Enzymatic reactions

Initial rate measurements were performed at 55 °C in 2-methyl-2-butanol as solvent. Various amounts of acyl acceptor (25-350 mM) and 175 mM of myristic acid as acyl donor were incubated for 10 minutes prior to addition of 10 or 50 gl^{-1} of beads with immobilized *Candida antarctica* lipase B for the acylation of 2-butanol and 2-butylamine respectively. For the other acyl acceptors 5 gl^{-1} of beads with immobilized enzyme was used. 100 µl samples were taken at intervals and centrifuged at 10000 x g. The supernatant was analyzed by LC-MS. Initial rates were calculated from the linear relationship of the total concentration of products against reaction time. These results were used to determine apparent k_{cat} values from Lineweaver-Burk reciprocal plots.

HPLC analysis

Structural and quantitative analysis of reaction products were conducted using a LC/MS-ES system from Agilent (1100 LC/MSD Trap mass spectrometer VL) with a C18 Uptisphere 300 A OD column (250×4 mm, 5 µm, Interchim) for the analysis of reaction media for acylation of (*R*)-2-butanol and a C18 Prontosil 120-5-C18-AQ column (250×4 mm, 5 µm; Bischoff Chromatography) for the analysis of other reaction media. Products were detected and quantified by differential refractometry and UV detection at 210 nm. Low-resolution mass spectral analyses were obtained by electrospray in the positive detection mode. Nitrogen was used as the drying gas at 15 l min-1 and 350 °C at a nebulizer pressure of 4 bars. The scan range was 50–1000 m/z using five averages and 13,000 m/z per second resolution. The capillary voltage was 4000 V. Processing was done offline using HP Chemstation software.

Various eluent systems were used depending on the acyl acceptor used. Reaction samples resulting from the acylation of (*R*)-2-butanol and (*R*)-2-butylamine were eluted with acetonitrile/water/acetic acid (90:10:0.1, v/v/v) at room temperature and at a flow rate of 1 ml min-1. Reaction samples resulting from the acylation of 1-methoxy-2-propylamine and 1,2-diaminopropane were eluted with methanol/water/acetic acid (95:5:0.1 and 93:7:0.1, v/v/v, respectively) at room temperature and at a flow rate of 1 ml min-1. Concerning the separation of products resulting from the acylation of other acyl acceptors, two solvent gradients were used. These gradients were

derived from two eluent mixtures, solvent A: acetonitrile / water / acetic acid (77:23:0.1, v / v / v) and solvent B: methanol / acetic acid (100:0.1, v / v). Analysis of products resulting from the acylation of 1,2-propanediol and the disappearance of myristic acid were performed by using the gradient described in Table S3 (Supporting Information) at room temperature and for analysis of products resulting from acylation of amino-alcohols and the disappearance of myristic acid, by using the gradient described in Table S4 at room temperature.

Product Characterization

The products formed were characterized and confirmed by 1H NMR, mass spectroscopy and infrared spectroscopy after purification via preparative HPLC. ^{1}H-NMR were recorded on a JEOL-JNM LA400 spectrometer (400 MHz) with tetramethylsilane as an internal reference. Samples were prepared in $CDCl_3$. Infra-Red (IR) spectra were recorded using a Perkin-Elmer Spectrum 100 ATR spectrometer.

***N*-myristyl 1-amino-2-propanol (3a)**: ^{1}H NMR (400 MHz, $CDCl_3$, δ ppm): δ 0.88 (t, 3H, *J* = 6.55 Hz, -CH_2-C*H*$_3$), 1.19 (d, 3H, *J* = 5.61 Hz, –CH-C*H*$_3$), 1.25 (m, 20H, -CH_2- of myristyl chain), 1.64 (m, 2H, -C*H*$_2$-CH_2-CO-NH- of myristyl chain), 2.21 (t, 2H, *J* = 7.49 Hz, -CH_2-C*H*$_2$-CO-NH- of myristyl chain), 2.72 (d, 1H, *J* = 3.74 Hz, -OH), 3.13 (m, 1H, –CH-C*H*$_2$-NH-), 3.44 (m, 1H, –CH-C*H*$_2$-NH-), 3.92 (m, 1H, -CH-), 5.95 (s, 1H, -NH-). IR ν_{max} (cm^{-1}): 3100-3500 (O-H, alcohol and N-H, amide), 2800-3000 (CH of myristyl chain), 1619 (C=O, amide), 1571 (N-H, amide). *m/Z* (LR-ESI$^+$) $C_{17}H_{36}NO_2$ (M + H^+), found: 286.4 (theoretical: 286.48).

***N,O*-dimyristyl 1-amino-2-propanol (4a)**: ^{1}H NMR (400 MHz, $CDCl_3$, δ ppm): δ 0.88 (t, 6H, *J* = 6.55 Hz, 2x -CH_2-C*H*$_3$), 1.22 (d, 3H, *J* = 6.39 Hz, –CH-C*H*$_3$), 1.25 (m, 40H, -CH_2- of myristyl chain), 1.61 (m, 4H, 2x -C*H*$_2$-CH_2-CO- of myristyl chain), 2.16 (t, 2H, *J* = 6.62 Hz, -CH_2-C*H*$_2$-CO-O- of myristyl chain), 2.30 (t, 2H, *J* = 6.62 Hz, -CH_2-C*H*$_2$-CO-NH- of myristyl chain), 3.37 (m, 1H, –CH-C*H*$_2$-NH-), 3.45 (m, 1H, –CH-C*H*$_2$-NH-), 4.99 (m, 1H, -CH-), 5.69 (s, 1H, C-N*H*-CH_2-). IR ν_{max} (cm^{-1}): 3291 (N-H, amide), 2800-3000 (CH of myristyl chain), 1725 (C=O, ester), 1641 (C=O, amide), 1557 (N-H, amide). *m/Z* (LR-ESI$^+$) $C_{31}H_{62}NO_3Na$ (M + Na^+), found: 518.6 (theoretical: 518.85).

***N*-myristyl 2-amino-1-propanol (3b)**: ^{1}H NMR (400 MHz, $CDCl_3$, δ ppm): δ 0.88 (t, 3H, *J* = 6.06 Hz, -CH_2-C*H*$_3$), 1.17 (d, 3H, *J* = 6.06 Hz, –CH-C*H*$_3$), 1.25 (m, 20H, -CH_2- of myristyl chain), 1.63 (m, 2H, -C*H*$_2$-CH_2-CO-NH- of myristyl chain), 2.19 (t, 2H, *J* = 6.06 Hz, -CH_2-C*H*$_2$-CO-NH- of myristyl chain), 3.04 (s, 1H, -OH), 3.27 (dd, 1H, *J* = 5, 10 Hz, –CH-C*H*$_2$-OH), 3.46 (dd, 1H, *J* = 3.7, 11 Hz, –CH-C*H*$_2$-OH), 4.07 (m, 1H, -CH-), 5.7 (s, 1H, -NH-). IR ν_{max} (cm^{-1}): 3100-3500 (O-H, alcohol and N-H, amide), 2800-3000 (CH of myristyl chain), 1638 (C=O, amide), 1543 (N-H, amide). *m/Z* (LR-ESI$^+$) $C_{17}H_{36}NO_2$ (M + H^+), found: 286.4 (theoretical: 286.48).

***N,O*-dimyristyl 2-amino-1-propanol (4b)**: ^{1}H NMR (400 MHz, $CDCl_3$, δ ppm): δ 0.88 (t, 6H, *J* = 7.6 Hz, 2x -CH_2-C*H*$_3$), 1.16 (d, 3H, *J* = 7.6 Hz, –CH-C*H*$_3$), 1.25 (m, 40H, -CH_2- of myristyl chain), 1.6 (m, 4H, 2x -C*H*$_2$-CH_2-CO- of myristyl chain), 2.14 (t, 2H, *J* = 7.2 Hz, -CH_2-C*H*$_2$-CO-O- of myristyl chain), 2.32 (t, 2H, *J* = 7.2 Hz, -CH_2-C*H*$_2$-CO-NH- of myristyl chain), 4 (dd, 1H, *J* = 4.4, 10.7 Hz, –CH-C*H*$_2$-O-), 4.13 (dd, 1H, *J* = 4.9, 10 Hz, –CH-C*H*$_2$-O-), 4.29 (m, 1H, -CH-), 5.54 (d, 1H, *J* = 7.3 Hz, C-NH-CH_2-). IR ν_{max} (cm^{-1}): 3301 (N-H, amide), 2800-3000 (CH of myristyl chain), 1737 (C=O, ester), 1643 (C=O, amide), 1542 (N-H, amide). *m/Z* (LR-ESI$^+$) $C_{31}H_{62}NO_3Na$ (M + Na^+), found: 518.6 (theoretical: 518.85).

***O*-myristyl 4-amino-1-pentanol (2c):** ^{1}H NMR (400 MHz, $CDCl_3$, δ ppm): δ 0.88 (t, 3H, *J* = 6.99 Hz, -CH_2-C*H*$_3$), 1.14 (d, 3H, *J* = 8 Hz, –CH-C*H*$_3$), 1.25 (m, 20H, -CH_2- of myristyl chain), 1.52 (m, 4H, –CH-C*H*$_2$-C*H*$_2$-CH_2-O-), 1.62 (m, 2H, -C*H*$_2$-CH_2-CO-O- of myristyl chain), 2.22 (t, 1H, *J* = 7.16 Hz, -CH_2-C*H*$_2$-CO-O- of myristyl chain), 2.29 (t, 1H, *J* = 7.5 Hz, -CH_2-C*H*$_2$-CO-O- of myristyl chain), 3.43 (m, 1H, –CH_2-C*H*$_2$-O-), 3.69 (m, 1H, –CH_2-C*H*$_2$-O-), 4.1 (m, 1H, -CH-). IR ν_{max} (cm^{-1}): 3291 (N-H, amine), 2800-3000 (CH of myristyl chain), 1736 (C=O, ester), 1557 (N-H, amine). *m/Z* (LR-ESI$^+$) $C_{19}H_{40}NO_2$ (M + H^+), found: 314.2 (theoretical: 314.53).

***N*-myristyl 4-amino-1-pentanol (3c):** ^{1}H NMR (400 MHz, $CDCl_3$, δ ppm): δ 0.88 (t, 3H, *J* = 6.58 Hz, -CH_2-C*H*$_3$), 1.14 (d, 3H, *J* = 6.23 Hz, –CH-C*H*$_3$), 1.25 (m, 20H, -CH_2- of myristyl chain), 1.53 (m, 4H, –CH-C*H*$_2$-C*H*$_2$-CH_2-OH), 1.63 (m, 2H, -C*H*$_2$-CH_2-CO-NH- of myristyl chain), 2.14 (t, 2H, *J* = 7.27 Hz, -CH_2-C*H*$_2$-CO-NH- of myristyl chain), 2.94 (s, 1H, -OH), 3.67 (m, 2H, –CH_2-C*H*$_2$-OH), 4.06 (m, 1H, -CH-), 5.28 (s, 1H, -NH-). IR ν_{max} (cm^{-1}): 3200-3500 (O-H, alcohol and N-H, amide), 2800-3000 (CH of myristyl chain), 1639 (C=O, amide), 1545 (N-H, amide). *m/Z* (LR-ESI$^+$) $C_{19}H_{40}NO_2$ (M + H^+), found: 314.2 (theoretical: 314.53).

***N,O*-dimyristyl 4-amino-1-pentanol (4c):** ^{1}H NMR (400 MHz, $CDCl_3$, δ ppm): δ 0.88 (t, 6H, *J* = 7.43 Hz, 2x -CH_2-C*H*$_3$), 1.14 (d, 3H, *J* = 6.83 Hz, –CH-C*H*$_3$), 1.25 (m, 40H, -CH_2- of myristyl chain), 1.53 (m, 4H, –CH-C*H*$_2$-C*H*$_2$-CH_2-O-C), 1.6 (m, 4H, 2x -C*H*$_2$-CH_2-CO- of myristyl chain), 2.14 (t, 4H, *J* = 7.08 Hz, -CH_2-C*H*$_2$-CO- of myristyl chain), 3.68 (m, 2H, –CH_2-C*H*$_2$-O-C), 4.07 (m, 1H, -CH-), 5.27 (d, 1H, *J* = 6.86Hz, -NH-). IR ν_{max} (cm^{-1}): 3304 (N-H, amide), 2800-3000 (CH of myristyl chain), 1732 (C=O, ester), 1640 (C=O, amide), 1546 (N-H, amide). *m/Z* (LR-ESI$^+$) $C_{33}H_{66}NO_3Na$ (M + Na^+), found: 546.2 (theoretical: 546.9).

***O*-myristyl 6-amino-1-hexanol (2d):** ^{1}H NMR (400 MHz, $CDCl_3$, δ ppm): δ 0.88 (t, 3H, *J* = 7.28 Hz, -CH_2-C*H*$_3$), 1.25 (m, 20H, -CH_2- of myristyl chain), 1.55 (m, 2H, -C*H*$_2$-CH_2-CO-O- of myristyl chain), 1.62 (m, 4H, –CH_2-C*H*$_2$-C*H*$_2$-CH_2-NH_2), 2.28 (t, 2H, *J* = 7.65 Hz, -CH_2-C*H*$_2$-CO-O- of myristyl chain), 2.81 (s, 2H, -NH_2), 3.64 (t, 2H, *J* = 6.47 Hz, –CH_2-C*H*$_2$-NH_2), 4.04 (t, 2H, *J* = 6.47 Hz, –CH_2-C*H*$_2$-O-CO-CH_2). IR ν_{max} (cm^{-1}): 3400 (N-H, amine), 2800-3000 (CH of myristyl chain), 1736 (C=O, ester), 1544 (N-H, amine). *m/Z* (LR-ESI$^+$) $C_{20}H_{42}NO_2$ (M + H^+), found: 329.5 (theoretical: 328.56).

***N*-myristyl 6-amino-1-hexanol (3d):** ^{1}H NMR (400 MHz, $CDCl_3$, δ ppm): δ 0.88 (t, 3H, *J* = 7.5 Hz, -CH_2-C*H*$_3$), 1.25 (m, 20H, -CH_2- of myristyl chain), 1.51 (m, 2H, -C*H*$_2$-CH_2-CO-O- of myristyl chain), 1.59 (m, 4H, –CH_2-C*H*$_2$-C*H*$_2$-CH_2-OH), 2.26 (t, 2H, *J* = 7.65 Hz, -CH_2-C*H*$_2$-CO-OH of myristyl chain), 2.72 (s, 1H, -OH), 3.25 (t, 2H, *J* = 7.07 Hz, –CH_2-C*H*$_2$-OH), 3.63 (t, 2H, *J* = 7.29 Hz, –CH_2-C*H*$_2$-NH-CO-CH_2), 5.41 (s, 1H, -NH-). IR ν_{max} (cm^{-1}): 3385 (O-H, alcohol), 3314 (N-H, amide), 2800-3000 (CH of myristyl chain), 1634 (C=O, amide), 1534 (N-H, amide). *m/Z* (LR-ESI$^+$) $C_{20}H_{42}NO_2$ (M + H^+), found: 329.5 (theoretical: 328.56).

***N,O*-dimyristyl 6-amino-1-hexanol (4d):** ^{1}H NMR (400 MHz, $CDCl_3$, δ ppm): δ 0.88 (t, 6H, *J* = 6.48 Hz, 2x -CH_2-C*H*$_3$), 1.25 (m, 40H, -CH_2- of myristyl chain), 1.5 (m, 4H, -C*H*$_2$-CH_2-CO- of myristyl chain), 1.6 (m, 4H, –CH_2-C*H*$_2$-C*H*$_2$-CH_2-O-C), 2.15 (t, 2H, *J* = 7.8 Hz, -CH_2-C*H*$_2$-CO-NH-), 2.29 (t, 2H, *J* = 7.8 Hz, -CH_2-C*H*$_2$-CO-NH-), 3.24 (q, 2H, *J* = 6.5 Hz, –CH_2-C*H*$_2$-NH-), 4.06 (t, 2H, *J* = 5.9 Hz, –CH_2-C*H*$_2$-O-CO-CH_2), 5.4 (s, 1H, -NH-). IR ν_{max} (cm^{-1}): 3298 (N-H, amide), 2800-3000 (CH of myristyl chain), 1726 (C=O, ester), 1635 (C=O, amide), 1547 (N-H, amide). *m/Z* (LR-ESI$^+$) $C_{34}H_{67}NO_3Na$ (M + Na^+), found: 560.7 (theoretical: 560.93).

***N*-myristyl 1-methoxy-2-propylamine:** ^{1}H NMR (400 MHz, $CDCl_3$, δ ppm): δ 0.88 (t, 3H, *J* = 6.79 Hz, -CH_2-C*H*$_3$), 1.17 (d, 3H, *J* = 6.17 Hz, –CH-C*H*$_3$), 1.26 (m, 20H, -CH_2- of myristyl chain), 1.62 (m, 2H, -C*H*$_2$-CH_2-CO-NH- of myristyl chain), 2.15 (t, 2H, *J* = 6.8 Hz, -CH_2-C*H*$_2$-CO-NH- of myristyl chain), 2.19 (t, 1H, *J* = 6.8 Hz, –CH-C*H*$_2$-OCH_3), 3.36 (m, 3H, -O*CH*$_3$), 4.06 (t, 1H, *J* = 6.45 Hz, –CH-C*H*$_2$-OCH_3), 4.16 (m, 1H, -CH-), 5.62 (d, 1H, *J* = 5.84 Hz, -NH-). IR ν_{max} (cm^{-1}): 3304 (N-H, amide), 2800-3000 (CH of myristyl chain), 1634 (C=O, amide), 1544 (N-H, amide). *m/Z* (LR-ESI$^+$) $C_{18}H_{38}NO_2$ (M + H^+), found: 300.3 (theoretical: 300.51).

1-*N*-myristyl 1,2-diaminopropane: ^{1}H NMR (400 MHz, $CDCl_3$, δ ppm): δ 0.88 (t, 3H, *J* = 6.67 Hz, -CH_2-C*H*$_3$), 1.22 (d, 3H, *J* = 6.67 Hz, –CH-C*H*$_3$), 1.25 (m, 20H, -CH_2- of myristyl chain), 1.61 (q, 2H, *J* = 6.67 Hz, -C*H*$_2$-CH_2-CO-NH- of myristyl chain), 1.96 (s, 2H, -NH_2), 2.19 (t, 2H, *J* = 7.3 Hz, -CH_2-C*H*$_2$-CO-NH- of myristyl chain), 3.21(st, 1H, *J* = 5.9 Hz, -CH-), 3.27 (qd, 1H, *J* = 2.6, 11.8 Hz, –CH-C*H*$_2$-NH-), 3.46 (qd, 1H, *J* = 3.24, 13.6 Hz, –CH-C*H*$_2$-NH-), 7.22 (t, 1H, *J* = 4.42 Hz, -NH-). *m/Z* (LR-ESI$^+$) $C_{17}H_{37}N_2O$ (M + H^+), found: 285.4 (theoretical: 285.49).

1-*O*-myristyl 1,2-propanediol: ^{1}H NMR (400 MHz, $CDCl_3$, δ ppm): δ 0.88 (t, 3H, *J* = 6.65 Hz, -CH_2-C*H*$_3$), 1.22 (d, 3H, *J* = 3.3 Hz, –CH-C*H*$_3$), 1.24 (m, 20H, -CH_2- of myristyl chain), 1.63 (m, 2H, -C*H*$_2$-CH_2-CO-O- of myristyl chain), 2.2 (s, 1H, -OH-), 2.35 (t, 2H, *J* = 7.3 Hz, -CH_2-C*H*$_2$-CO-O- of myristyl chain), 3.93 (dd, 1H, *J* = 6.3, 11 Hz, –CH-C*H*$_2$-O-), 4 (m, 1H, -CH-), 4.11 (dd, 1H, *J* = 3.1, 11 Hz, –CH-C*H*$_2$-O-). *m/Z* (LR-ESI$^+$) $C_{17}H_{35}O_3$ (M + H^+), found: 287.2 (theoretical: 287.47).

2-*O*-myristyl 1,2-propanediol: ^{1}H NMR (400 MHz, $CDCl_3$, δ ppm):δ 0.88 (t, 3H, *J* = 6.65 Hz, -CH_2-C*H*$_3$), 1.22 (d, 3H, *J* = 3.3 Hz, –CH-C*H*$_3$), 1.24 (m, 20H, -CH_2- of myristyl chain), 1.63 (m, 2H, -C*H*$_2$-CH_2-CO-O- of myristyl chain), 1.93 (s, 1H, -OH), 2.32 (t, 2H, *J* = 7.3 Hz, -CH_2-C*H*$_2$-CO-O- of myristyl chain), 3.65 (dd, 1H, *J* = 6.3, 11 Hz, –CH-C*H*$_2$-O-), 3.68 (dd, 1H, *J* = 3.1, 11 Hz, –CH-C*H*$_2$-O-), 4.99 (m, 1H, -CH-). *m/Z* (LR-ESI$^+$) $C_{17}H_{35}O_3$ (M + H^+), found: 287.2 (theoretical: 287.47).

Computational details

Calculations to obtain the distribution of ground state amino alcohol conformers were performed by employing density functional theory (DFT) using the B3LYP hybrid density functional[39] as implemented in US-GAMESS 12 JAN 2009 (R3).[40] Geometry optimizations were carried out using the 6-31G(d,p) basis set and by using the convergence criterion that the largest component of the gradient should be less than $5*10^{-4}$ Hartree/Bohr. Final energies were calculated using a larger basis set, 6-311+G(2d,2p). All structures were verified to be minima by means of vibrational analysis at the same level of theory as for the optimization. Final energies were corrected for zero-point vibrational energies (ZPVE). The effect of solvation was taken into account by performing single-point calculations on the optimized structures using the CPCM polarizable continuum model[36] using the large basis set and by adding the resulting solvation energy to the final energy. For our proposed proton shuttle mechanism of lipase catalyzed *N*-acylation of amino alcohols, calculations were initiated in a small active site model of a serine hydrolase containing 47 atoms. The classical Ser/His/Asp catalytic triad was represented by a methanol molecule, an imidazole molecule and a formate ion in order to simulate a minimal serine hydrolase active site. The oxyanion hole was represented by two methanol molecules. In our study the coordinates of the catalytic triad from PDB file 1LBT (*Candida antarctica* lipase B with Tween80) were used as a starting point. Ethanol amine was used as model of an amino alcohol molecule. Geometry optimizations were performed by DFT at the B3LYP/6-31G(d,p) level with the same convergence criterion as given above. Eigenvector-following as implemented in US-GAMESS was used to locate transition states. Vibrational analysis was performed at the same level of theory as for the optimizations and the transition state for the proton shuttle mechanism had one imaginary frequency that corresponded to nucleophilic attack and the transfer of two protons. The intrinsic reaction coordinate (IRC) was calculated to verify the reaction path. The small active site model was also used to calculate the hypothetical reaction mechanism for the proton shuttle corresponding to *O*-acylation in the same way as for *N*-acylation. The transition state for the proton shuttle mechanism of *O*-acylation of ethanol amine could be located using HF/6-31G(d,p) but could not be fully relaxed using DFT at the B3LYP/6-31G(d,p) level, presumably because of a very unfavourable interaction between the remaining free lone pair on the oxygen nucleophile and the developing negative charge on the acyl enzyme carbonyl oxygen in TS.

For the cluster *ab initio* calculations a large model of the active site of *Candida antarctica* lipase B that contained 205 atoms (which represented 14 amino acids) was used. The coordinates of the atoms were taken from the crystal structure 1LBT (to which hydrogens were added manually). A picture of the large active site model is given in Supporting Information, Figure S3. Residues were truncated such that only important side chains and/or peptide backbones were included in the model (see Figure S3). Atoms marked with an asterisk corresponds to backbone α-carbons that were kept fixed during the simulations since the enzyme backbone does not have the ability to move freely. The fixation of such atoms, a standard technique in cluster *ab initio* calculations[34b, 41], gives rise to a few small imaginary frequencies, typically less than 40i cm^{-1}. These imaginary frequencies have a very small effect on the ZPVE. As substrate, (*R*)-alaninol was used and the acyl enzyme contained four carbon atoms in the acyl chain in our large model (Figure S3). The ES-complex corresponded to the amino alcohol substrate complexed to the acyl enzyme. Intermediates and transition states in the large model were first obtained and verified (by vibrational analysis and by calculation of the intrinsic reaction coordinate (IRC)) using HF/6-31G(d,p). The resulting geometries obtained at the HF/6-31G(d,p) level were then used as the starting point for geometry optimizations using DFT at the B3LYP/6-31G(d,p) level, with the same convergence criterion as above. This strategy was especially efficient for the localization of transition states (the strategy is illustrated in Figure S7 in Supporting Information, the transition states were located by eigenvector following). The rate limiting transition state for the traditional mechanism of *N*-acylation, with ZPVEs calculated at the same level of theory as for the optimizations taken into account, was found to be the nitrogen inversion step both at HF/6-31G(d,p) and B3LYP/6-31G(d,p) (for a definition of the different mechanisms, see Figure S4-S6 in Supporting Information). Nitrogen inversion (labelled TS_{inv} in Figure S7) was found to be concerted with amide bond formation at the B3LYP/6-31G(d,p) level of theory, but a separate transition state from amide bond synthesis/breakdown at the HF/6-31G(d,p) level (TS_2 in Figure S7). Likewise by using MP2/6-31G(d,p) on the small active site model the inversion step was found to be a separate transition state that was not part of the breakdown of the tetrahedral intermediate (i.e. amide bond synthesis, see also Figure S4). It should be noted that amidases have a hydrogen bond that is in a perfect spatial arrangement for the stabilization of the transition state for nitrogen inversion, regardless of reaction mechanism.[27] Since esterases lack this interaction[27] we are not surprised to see that the transition state for nitrogen inversion was found to be rate limiting in the very large active site model of *Candida antarctica* lipase B. The proton shuttle mechanism for *N*-acylation of (*R*)-alaninol was then calculated in the large active site model using DFT, with the coordinates from HF as starting point. Frequency calculations were again performed at the same level of theory as for the optimization (B3LYP/6-31G(d,p)) and the energies were corrected for ZPVE. The DFT optimized TS for the proton shuttle mechanism of *N*-acylation obtained at the B3LYP/6-31G(d,p) level had an imaginary frequency of 1030i cm^{-1} that corresponded to nucleophilic attack and the transfer of two protons. Again the intrinsic reaction coordinate (IRC) was calculated to verify the reaction path. For the calculation of the TS-model for the proton shuttle mechanism of *O*-acylation, the His $N_{\varepsilon 2}$-H bond length was kept fixed at 1.08 Å and the distance between the hydroxyl proton and oxygen of the amino alcohol was set to 1.18 Å. These bond lengths were found from the calculations in the small active site model containing 47 atoms. A frequency calculation on the structure for the TS-model of the proton shuttle involving *O*-acylation in the large active site model was performed using HF/6-31G(d,p), which resulted in one imaginary frequency of 1429i cm^{-1} (corresponding to nucleophilic attack of the oxygen and the transfer of two protons).

The effect of solvation of our large active site model was taken into account by using single-point calculations on the optimized structures using the CPCM polarizable continuum model with ε=2 and ε=80 respectively, which resulted in small effects on the relative energies.

The software YASARA version 8.9.23[42] was used for all force field MD-simulations. All missing hydrogens were added to the starting structure 1LBT taken from the protein data bank and the hydrogen network was optimized by repeated minimizations and short molecular dynamics (MD) runs (1200 fs at 298 K) using the Amber99 force field. The tetrahedral intermediate was constructed by attaching the nitrogen or oxygen of the substrate to the acyl enzyme (containing the $C_{13}C(=O)$-group originating from myristic acid) and by using the AUTOSMILES approach implemented in YASARA.[43]10 ns MD-simulations were performed at 298 K under the canonical ensemble using a Berendsen thermostat. PME accounted for long-range electrostatics[44] during the MD-simulations of the tetrahedral intermediates and periodic boundary conditions were employed. The first 2 ns of each MD-simulation consisted of an equilibration phase.

Acknowledgements

The Royal Academy of Swedish Sciences is acknowledged for financial support as well as the Alexander von Humboldt foundation. The Swedish Center for High Performance Computing (PDC) is greatly acknowledged for computer time and technical support. This study was supported by the French ANR (National Research Agency) through the EXPENANTIO project (program CP2D). The author would like to thank R. Syrén for inspiration.

Keywords: Enzyme catalysis • Reaction mechanisms • Molecular modeling • Amino alcohols • Linear Free Energy Relationship

[1] a) F. Fache, E. Schulz, M. L. Tommasino, M. Lemaire, *Chem. Rev.* **2000**, *100*, 2159-2231; b) S. M. Lait, D. A. Rankic, B. A. Keay, *Chem. Rev.* **2007**, *107*, 767-796.

[2] D. J. Ager, I. Prakash, D. R. Schaad, *Chem. Rev.* **1996**, *96*, 835-875.

[3] a) Y. Yang, D. Wahler, J.-L. Reymond, *Helv. Chim. Acta* **2003**, *86*, 2928-2936; b) X. Chen, S.-H. Seow, T. Futterer, Rhodia Asia Pacific Pte, Limited, Singapore . **2009**, US 20090048139; c) M. Breuer, K. Ditrich, T. Habicher, B. Hauer, M. Kesseler, R. Stuermer, T. Zelinski, *Angew. Chem., Int. Ed.* **2004**, *43*, 788-824; d) M. J. Climent, A. Corma, S. Iborra, *Chem. Rev.* **2011**, *111*, 1072-1133.

[4] a) A. Abiko, S. Masamune, *Tetrahedron Lett.* **1992**, *33*, 5517-5518; b) R. Polt, M. A. Peterson, *Tetrahedron Lett.* **1990**, *31*, 4985-4986; c) D. J. Ager, M. B. East, *Tetrahedron* **1993**, *49*, 5683-5765; d) A. P. Kozikowski, *Acc. Chem. Res.* **1984**, *17*, 410-416.

[5] a) Y. A. Hannun, L. M. Obeid, *Nat. Rev. Mol. Cell Biol.* **2008**, *9*, 139-150; b) O. Cuvillier, G. Pirianov, B. Kleuser, P. G. Vanek, O. A. Coso, J. S. Gutkind, S. Spiegel, *Nature* **1996**, *381*, 800-803; c) J. M. Berg, J. L. Tymoczko, L. Stryer, *Biochemistry*, 5 ed., W H Freeman, New York, **2002**; d) S. G. Rasmussen, B. T. DeVree, Y. Zou, A. C. Kruse, K. Y. Chung, T. S. Kobilka, F. S. Thian, P. S. Chae, E. Pardon, D. Calinski, J. M. Mathiesen, S. T. Shah, J. A. Lyons, M. Caffrey, S. H. Gellman, J. Steyaert, G. Skiniotis, W. I. Weis, R. K. Sunahara, B. K. Kobilka, *Nature* **2011**, *477*, 549-555.

[6] Y. Kita, Y. Nishii, T. Higuchi, K. Mashima, *Angewandte Chemie* **2012**, *124*, 5821-5824.

[7] K. I. Skorey, V. Somayaji, R. S. Brown, *J. Am. Chem. Soc.* **1989**, *111*, 1445-1452.

[8] J. Hine, M. N. Khan, *J. Am. Chem. Soc.* **1977**, *99*, 3847-3848.

[9] T. Storz, P. Dittmar, D. Grimler, M. Testa, H. Potgeter, D. Chappel, O. Hartmann, D. Niederer, M. Trueby, *Org. Process Res. Dev.* **2006**, *10*, 1184-1191.

[10] M. M. Werber, Y. Shalitin, *Bioorg. Chem.* **1973**, *2*, 202-220.

[11] T. Ohshima, T. Iwasaki, Y. Maegawa, A. Yoshiyama, K. Mashima, *J. Am. Chem. Soc.* **2008**, *130*, 2944-2945.

[12] a) E. Husson, C. Humeau, F. Blanchard, X. Framboisier, I. Marc, I. Chevalot, *J. Mol. Catal. B: Enzym.* **2008**, *55*, 110-117; b) D. Adlercreutz, P. Tufvesson, A. Karlsson, R. Hatti-Kaul, *Ind. Biotechnol.* **2010**, *6*, 204-211; c) F. Le Joubioux, Y. Ben Henda, N. Bridiau , O. Achour, M. Graber, T. Maugard, *J. Mol. Catal. B: Enzym*. **2012**, *dx.doi.org/10.1016/j.molcatb.2012.09.006*

[13] T. Furutani, M. Furui, H. Ooshima, J. Kato, *Enzyme Microb. Technol.* **1996**, *19*, 578-584.

[14] a) P. Deslongchamps, *Tetrahedron* **1975**, *31*, 2463-2490; b) G. Deslongchamps, P. Deslongchamps, *Org. Biomol. Chem.* **2011**, *9*, 5321-5333; c) D. G. Gorenstein, *Chem. Rev.* **1987**, *87*, 1047-1077.

[15] M. M. Mojtahedi, A. M. Saeed, M. M. Heravi, F. K. Behbahani, *Monatsh. Chem.* **2007**, *138*, 95-99.

[16] a) Y. Nakagawa, A. Hasegawa, J. Hiratake, K. Sakata, *Protein Eng., Des. Sel.* **2007**, *20*, 339-346; b) A. Zaks, A. M. Klibanov, *Proc. Natl. Acad. Sci. U. S. A.* **1985**, *82*, 3192-3196.

[17] F. Brotzel, Y. C. Chu, H. Mayr, *J. Org. Chem.* **2007**, *72*, 3679-3688.

[18] L. T. Kanerva, M. Kosonen, E. Vanttinen, T. T. Huuhtanen, M. Dahlqvist, *Acta Chem. Scand.* **1992**, *46*, 1101-1105.

[19] M. Skwarczynski, Y. Kiso, *Curr. Med. Chem.* **2007**, *14*, 2813-2823.

[20] a) W. Li, W. Du, Q. Li, T. Sun, D.-H. Liu, *J. Mol. Catal. B: Enzym.* **2010**, *63*, 17-22; b) L. Iddon, S. E. Richards, C. H. Johnson, J. R. Harding, I. D. Wilson, J. K. Nicholson, J. C. Lindon, A. V. Stachulski, *Org. Biomol. Chem.* **2011**, *9*, 926-934.

[21] H. Eberhard, O. Seitz, *Org. Biomol. Chem.* **2008**, *6*, 1349-1355.

[22] R. Greenhalgh, R. M. Heggie, M. A. Weinberger, *Can. J. Chem.* **1963**, *41*, 1662-1670.

[23] S. P. Markey, T. Dudding, T.-C. L. Wang, *J. Lipid Res.* **2000**, *41*, 657-662.

[24] P. Butz, R. T. Kroemer, N. A. Macleod, E. G. Robertson, J. P. Simons, *J. Phys. Chem. A* **2001**, *105*, 1050-1056.

[25] T. D. Smith, J. B. Gerken, P. V. Jog, J. D. Roberts, *Org. Lett.* **2007**, *9*, 4555-4557.

[26] N. A. Macleod, J. P. Simons, *Phys. Chem. Chem. Phys.* **2003**, *5*, 1123-1129.

[27] P.-O. Syren, K. Hult, *ChemCatChem* **2011**, *3*, 853-860.

[28] P.-O. Syren, P. Hendil-Forssell, L. Aumailley, W. Besenmatter, F. Gounine, A. Svendsen, M. Martinelle, K. Hult, *ChemBioChem* **2012**, *13*, 645-648.

[29] M. I. Page, W. P. Jencks, *J. Amer. Chem. Soc.* **1972**, *94*, 8818-8827.

[30] M. Meot-Ner, *Chem. Rev.* **2005**, *105*, 213-284.

[31] N. A. Macleod, J. P. Simons, *Phys. Chem. Chem. Phys.* **2004**, *6*, 2821-2826.

[32] a) Q. Wang, J. Gao, Y. Liu, C. Liu, *Chem. Phys. Lett.* **2010**, *501*, 113-117; b) D. A. Hiller, V. Singh, M.-H. Zhong, S. A. Strobel, *Nature* **2011**, *476*, 236-239; c) M. Pech, K. H. Nierhaus, *ChemBioChem* **2012**, *13*, 189-192; d) G. Wallin, J. Aaqvist, *Proc. Natl. Acad. Sci. U. S. A.* **2010**, *107*, 1888-1893.

[33] R.-Z. Liao, P. Georgieva, J.-G. Yu, F. Himo, *Biochemistry* **2011**, *50*, 1505-1513.

[34] a) L. Noodleman, T. Lovell, W.-G. Han, J. Li, F. Himo, *Chem. Rev.* **2004**, *104*, 459-508; b) P. E. M. Siegbahn, F. Himo, *Wiley Interdiscip. Rev.: Comput. Mol. Sci.* **2011**, *1*, 323-356; c) O. Amata, T. Marino, N. Russo, M. Toscano, *J. Am. Chem. Soc.* **2011**, *133*, 17824-17831.

[35] C. J. Cramer, D. G. Truhlar, *J. Am. Chem. Soc.* **1994**, *116*, 3892-3900.

[36] a) V. Barone, M. Cossi, *J. Phys. Chem. A* **1998**, *102*, 1995-2001; b) M. Cossi, N. Rega, G. Scalmani, V. Barone, *J. Comput. Chem.* **2003**, *24*, 669-681.

[37] a) S. A. Bizzozero, H. Dutler, *Bioorg. Chem.* **1981**, *10*, 46-62; b) B. Liu, C. J. Schofield, R. C. Wilmouth, *J. Biol. Chem.* **2006**, *281*, 24024-24035.

[38] M. Meot-Ner, *J. Am. Chem. Soc.* **1983**, *105*, 4906-4911.

[39] a) C. Lee, W. Yang, R. G. Parr, *Phys. Rev. B: Condens. Matter* **1988**, *37*, 785-789; b) A. D. Becke, *Phys. Rev. A: Gen. Phys.* **1988**, *38*, 3098-3100; c) A. D. Becke, *J. Chem. Phys.* **1992**, *96*, 2155-2160; d) A. D. Becke, *J. Chem. Phys.* **1992**, *97*, 9173-9177; e) A. D. Becke, *J. Chem. Phys.* **1993**, *98*, 5648-5652.

[40] M. W. Schmidt, K. K. Baldridge, J. A. Boatz, S. T. Elbert, M. S. Gordon, J. H. Jensen, S. Koseki, N. Matsunaga, K. A. Nguyen, *et al*., *J. Comput. Chem.* **1993**, *14*, 1347-1363.

[41] R. Z. Liao, J. G. Yu, F. Himo, *J Phys Chem B* **2010**, *114*, 2533-2540.

[42] E. Krieger, T. Darden, S. B. Nabuurs, A. Finkelstein, G. Vriend, *Proteins: Struct., Funct., Bioinf.* **2004**, *57*, 678-683.

[43] A. Jakalian, D. B. Jack, C. I. Bayly, *J. Comput. Chem.* **2002**, *23*, 1623-1641.

[44] U. Essmann, L. Perera, M. L. Berkowitz, T. Darden, H. Lee, L. G. Pedersen, *J. Chem. Phys.* **1995**, *103*, 8577-8593.

Received: ((will be filled in by the editorial staff))
Published online: ((will be filled in by the editorial staff))

FULL PAPER

An increased reaction rate for lipase catalyzed *N*-acylation of amino alcohols and related compounds compared to amines can be explained by a hydrogen shuttle mechanism that avoids nitrogen inversion in the transition state. Our suggested mechanism leads to the formation of a tetrahedral intermediate in a stereoelectronically favorable conformation for facile amide bond synthesis.

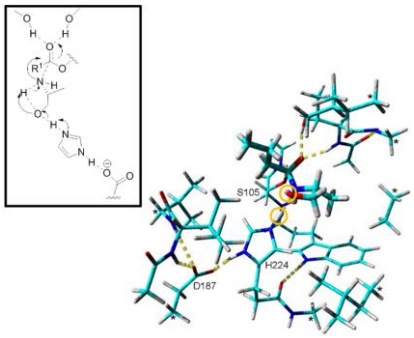

Per-Olof Syrén[*a],[c], *Florian Le Joubioux*[b], *Yesmine Ben Henda*[b], *Thierry Maugard*[b], *Karl Hult*[c], *Marianne Graber*[*b]

Page No. – Page No.

Proton shuttle mechanism in the transition state of lipase catalyzed *N*-acylation of amino alcohols

Supporting Information

Proton shuttle mechanism in the transition state of lipase catalyzed *N*-acylation of amino alcohols

Per-Olof Syrén*[a],[c],Florian Le Joubioux[b], Yesmine Ben Henda[b], Thierry Maugard[b], Karl Hult[c], Marianne Graber*[b]

[a] Dr. P.-O. Syrén, Institute of Technical Biochemistry, University of Stuttgart, Allmandring 31, D-70569 Stuttgart, Germany, Fax: (+49)-(0)711-685-63196, E-mail: per-olof.syren@itb.uni-stuttgart.de

[b] Prof. M. Graber, F. Le Joubioux, Y. Ben Henda, Prof. T. Maugard, UMR CNRS 6250 LIENSs, Université de La Rochelle, Bâtiment Marie Curie, Avenue Michel Crépeau, 17042 La Rochelle cedex 1, France, E-mail: mgraber@univ-lr.fr

[c] Prof K. Hult, Department of biochemistry, School of biotechnology, Royal Institute of Technology, AlbaNova University Centre, SE-106 91 Stockholm, Sweden

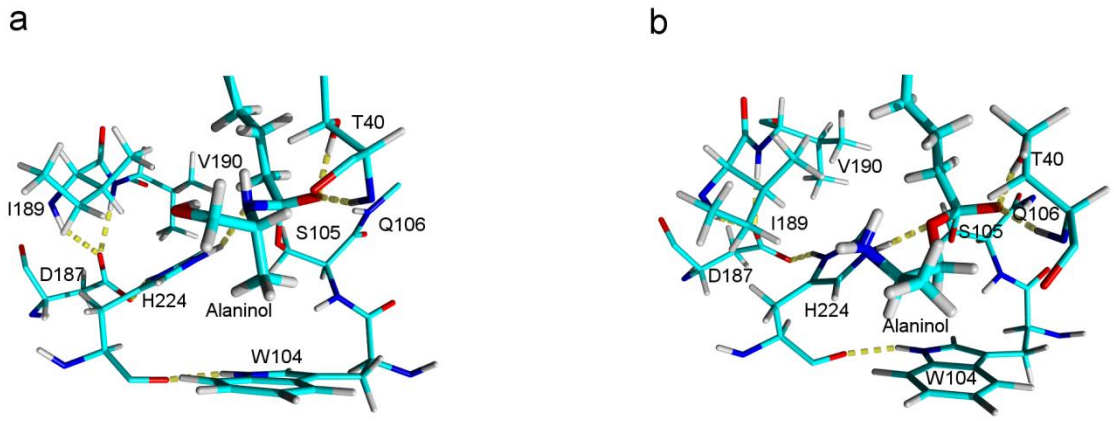

Figure S1. Snapshots from the molecular dynamics simulations of the tetrahedral intermediate representing transition state for acylation of (*R*)-alaninol using *Candida antarctica* lipase B. **a)** *N*-acylation of (*R*)-alaninol. **b)** A snapshot of *O*-acylation of (*R*)-alaninol is shown for comparison. The catalytic amino acids (S105, H224, D187) as well as oxyanion hole (T40 and Q106) are shown. W104 forms the bottom of the so called stereoselectivity pocket in *Candida antarctica* lipase B. Two amino acids, I189 and V190, were in close proximity to the substrate. (*R*)-Alaninol is shown as enlarged sticks. Color code: Cyan- carbon, Red - oxygen, Blue - nitrogen, White - hydrogen. Hydrogen bonds are indicated with dashed yellow lines.

Table S1. Average lengths and angles for the possible intramolecular hydrogen bonds formed in (*R*)-alaninol as given from MD-simulations of the tetrahedral intermediate representing the transition state for *N*-acylation in *Candida antarctica* lipase B.[a]

Average distance [Å]	Average angle NH---O (OH---N)[b] [degrees]	Average angle H---OC (H---NC)[b] [degrees]
NH---O interaction in (R)-alaninol		
2.66	77	72
OH---N interaction in (R)-alaninol		
1.86	132	159

[a] Based on 1.2 ns MD-simulation of the second tetrahedral intermediate. Values given are the average values for all 1160 snapshots generated in the simulation. [b] The atoms forming the two angles associated with the two possible hydrogen bonds, the NH---O hydrogen bond and the OH---N hydrogen bond respectively. For the OH---N interaction the relevant atoms forming the two angles are given in brackets.

Table S2. Cost for nitrogen inversion starting from the various conformations of *N*-methyl alaninol based on B3LYP/6-311+G(2d,2p) single point calculations. Solvation was taken into account by using a polarizable continuum model (CPCM). The corresponding relative energies for *N*-methyl propylamine are given for reference.

Conformer	Cost for nitrogen inversion[a] [kcal/mol]		
	In gas phase	In chloroform	In 2-methyl-2-butanol
(*R*)-*N*-Methyl alaninol			
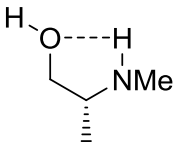	4.2	4.4	4.4
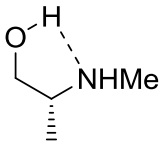	4.0	4.2	4.2
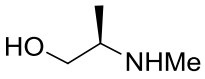	2.9	3.7	3.7
N-methyl propylamine			
	2.1	3.2	3.2

[a]The cost for nitrogen inversion is given as the energy difference between the TS for nitrogen inversion and the corresponding ground state conformer. Relative energies are based on B3LYP/6-311+G(2d,2p) single point calculations and includes ZPVE. The corresponding relative energies were calculated in the gas phase, in chloroform and in 2-methyl-2-butanol for comparison.

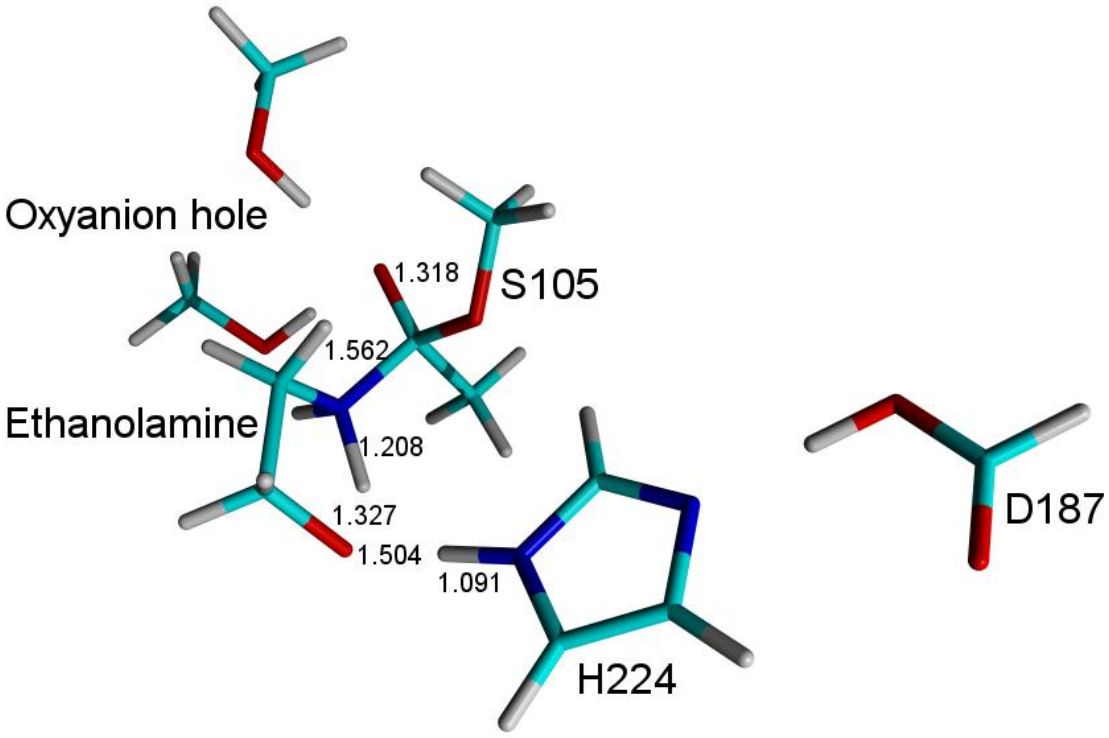

Figure S2. The transition state for *N*-acylation of ethanol amine in a small *ab initio* model of a serine hydrolase catalytic machinery calculated using DFT at the B3LYP/6-31G(d,p) level of theory. Nucleophilic attack was concomitant with the transfer of two protons. The bond lengths (l) of the bonds being formed/broken in the transition state are given in Å. The proton donated by the NH_2-group of the amino alcohol is shared between the nitrogen and oxygen of the amino alcohol (l=1.208 Å and l=1.327 Å respectively) whereas the hydroxyl proton is almost completely transferred to the enzyme catalytic base (l=1.504 Å). Methyl acetate was chosen to represent the acyl enzyme and ethanol amine was chosen to represent an amino alcohol. The catalytic triad was represented by a methanol molecule, an imidazole molecule and a formate ion. The oxyanion hole was represented by two methanol molecules. The corresponding residue numbers of amino acids in the active site of *Candida antarctica* lipase B are given. In total the small quantum model consisted of 47 atoms and the activation energy in the gas phase for the proton shuttle of *N*-acylation was 14.8 kcal/mol including ZPVE. The transition state had one imaginary frequency of 742.4i cm^{-1} that corresponded to nucleophilic attack coincidently with the transfer of two protons.

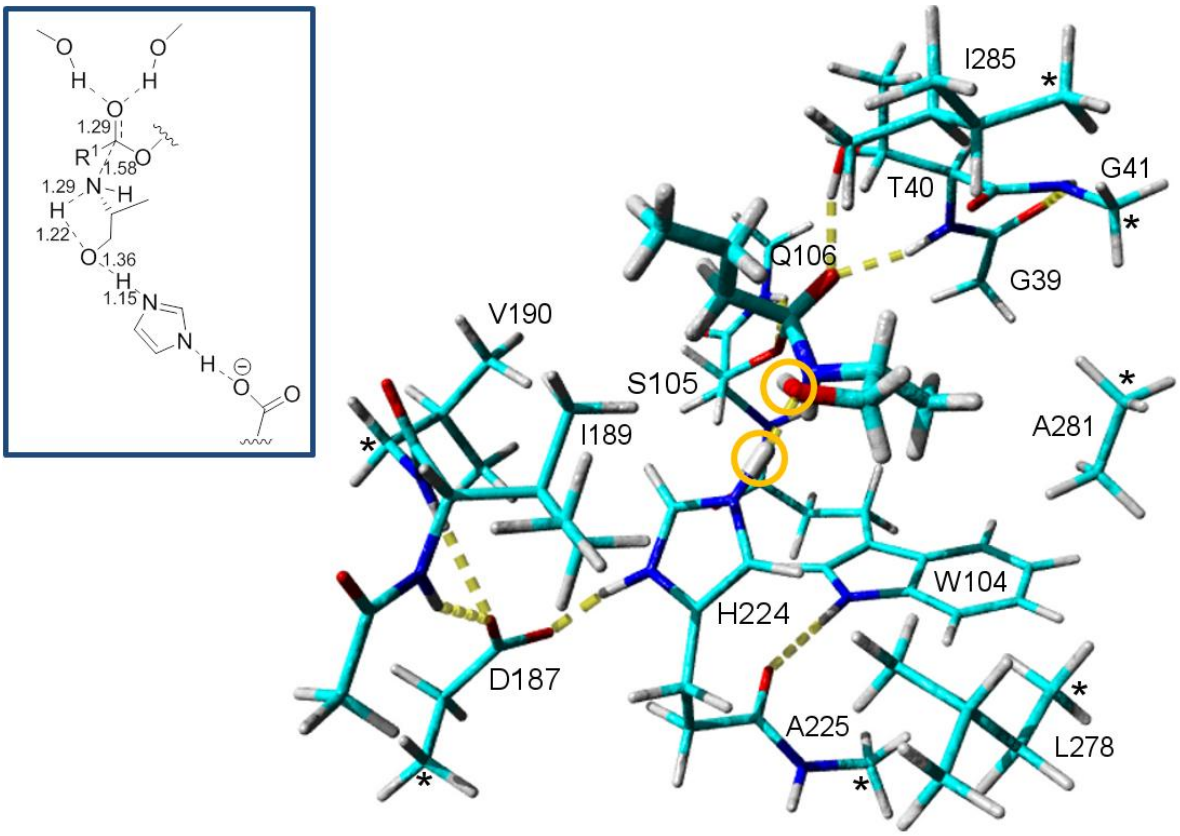

Figure S3. The large active site model of *Candida antarctica* lipase B with the calculated transition state structure for the proton shuttle mechanism of *N*-acylation of (*R*)-alaninol. The two protons encircled are being transferred in TS coincidently with nucleophilic attack. Relevant distances of bonds being formed/broken in TS are shown within the blue frame. Our large model of the active site, used for the B3LYP/6-31G(d,p) *ab initio* calculations, consisted of 205 atoms and included the side chains of G39, T40, G41, W104, S105, Q106, D187, I189, V190, H224, A225, L278, A281 and I285. The acyl enzyme with the carbon chain originating from the acyl donor (containing four carbon atoms in our model) and the substrate, (*R*)-alaninol are shown in enlarged sticks. Atoms shown with an asterisk were kept fixed during the simulations since they correspond to backbone atoms in the protein that does not have the ability to move freely. This is a standard technique in cluster *ab initio* calculations with the effect that a number of small imaginary frequencies are introduced (typically in the order of 30i cm^{-1}). These small imaginary frequencies have a neglectable effect on the energy of the system. The reaction path for the proton shuttle mechanism, obtained by computation of the intrinsic reaction coordinate (IRC), is attached as a Shockwave Flash movie (see the Shockwave Flash movies section).

Color code: Cyan- carbon, Red - oxygen, Blue - nitrogen, White - hydrogen. Hydrogen bonds are indicated with dashed yellow lines.

***N*-acylation of (*R*)-alaninol, traditional mechanism**

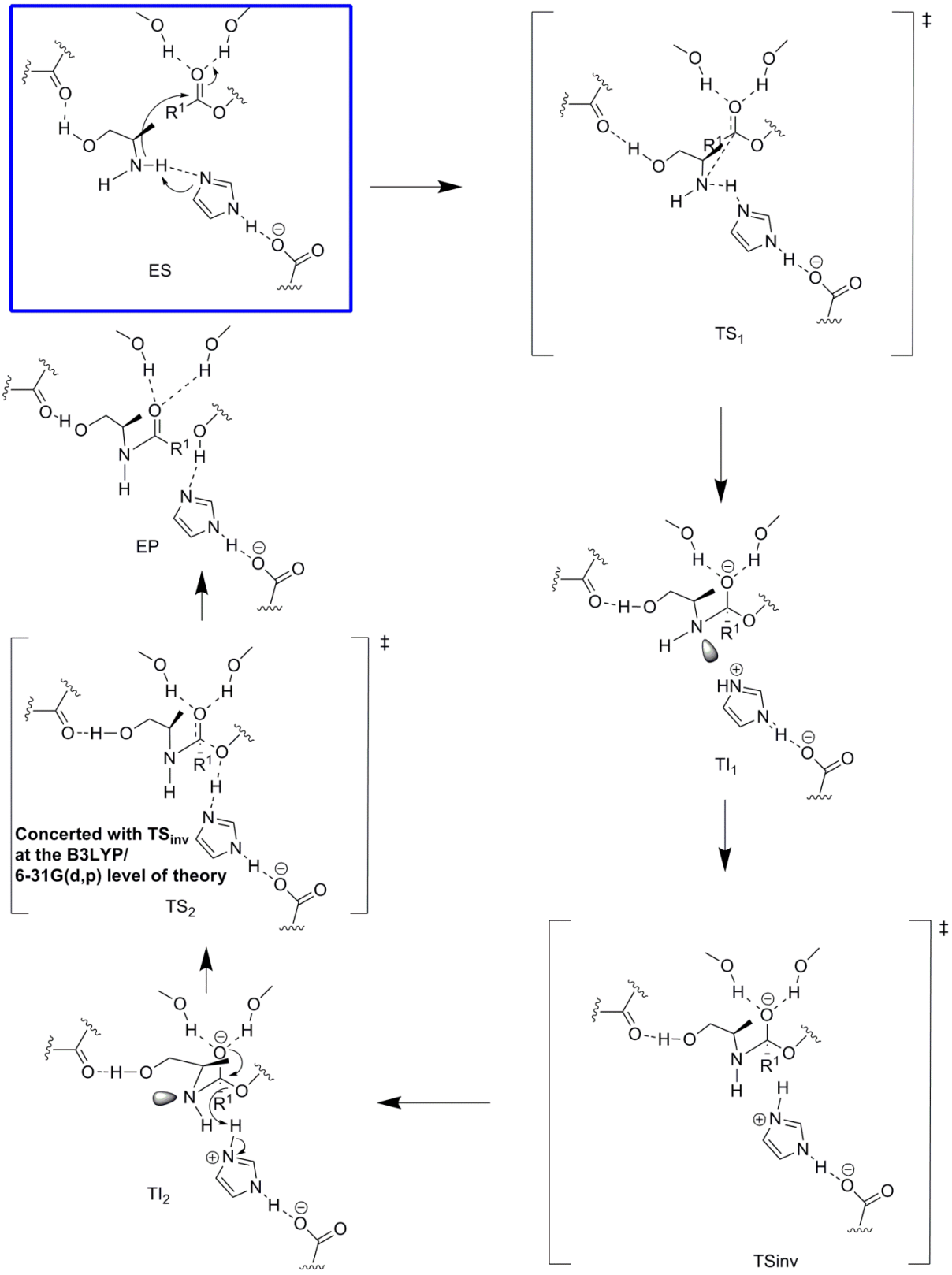

Figure S4. Schematic illustration of the "traditional" mechanism for lipase catalysed *N*-acylation of (*R*)-alaninol for which proton shuttling does not occur. Note that this hypothetical mechanism uses the open chain of the amino alcohol substrate. This traditional mechanism requires the intramolecular hydrogen bonding pattern to be broken, whereas it is known that amino alcohols adopt conformations with an intramolecular hydrogen bond[1]

By performing *ab initio* calculations for the hypothetical traditional mechanism of *N*-acylation of an amino alcohol, the catalytic effect of our suggested proton shuttle (Figure S5) can be assessed by comparison of the activation barriers for the respective mechanism. In the traditional mechanism, the open chain conformation of (*R*)-alaninol, for which proton shuttling can not occur, becomes *N*-acylated. As shown in the figure, the hydroxyl of the amino alcohol can form a hydrogen bond to the backbone of T40 in the enzyme active site and this interaction was formed upon minimization of the open chain conformation in the enzyme active site. Therefore we used this particular conformation for the *ab initio* calculations for the hypothetical traditional mechanism using the large active site model. The calculated energy difference between the ES-complex containing the open chain (shown in the blue frame in the figure) and the corresponding ES-complex for the proton shuttle mechanism, that contains an intramolecular hydrogen bond, was 3 kcal/mol at the B3LYP/6-31G(d,p) level and in favour of the ES-complex for the traditional mechanism. The corresponding hydrogen bond to the backbone of T40 was also found to be formed for the corresponding traditional mechanism of *O*-acylation with the amino group functioning as hydrogen bond donor. In this case a larger energy difference of 6 kcal/mol was found between the corresponding ES-complexes (between the ES-complex for "traditional" *O*-acylation, which was lower in energy, and the ES-complex for a proton shuttle mechanism involving *O*-acylation). The hydrogen bond that we modelled to the backbone of T40 for the hypothetical traditional mechanism of *N*-acylation does not contribute to catalysis ($k_{cat,app}$) since the hydrogen bond is already fully developed in the ES-complex. Thus this interaction is not involved in increasing the $k_{cat,app}$-values for *N*-acylation of amino alcohols or in favouring *N*-acylation over *O*-acylation. It replaces the interaction formed between the hydroxyl and the $N_{\varepsilon 2}$ of His224 in the ES-complex for the proton shuttle mechanism of *N*-acylation (Figure S5). Further the calculated barrier of activation for the traditional mechanism for *N*-acylation of (*R*)-alaninol was not lower than the corresponding calculated barrier using isopropylamine as nucleophile for which the hydrogen bond to the backbone of T40 can not form. Finally methoxy-2-propylamine displays an enhanced $k_{cat,app}$ for *N*-acylation but lacks the possibility of hydrogen bond formation to the backbone of T40.

Clarification of transition states and intermediates:

In the ES-complex (within the blue frame), the amino alcohol is complexed to the acyl enzyme. In the first transition state (TS_1) the nitrogen of the amino alcohol attacks the acyl enzyme and a proton sitting on the nitrogen is being abstracted by the enzyme catalytic base. In the first tetrahedral intermediate formed (TI_1), the lone pair of the scissile nitrogen atom is pointing towards the enzyme catalytic base. Nitrogen inversion (TS_{inv}) breaks the hydrogen bond between the scissile nitrogen atom and the catalytic histidine which causes the histidine to move towards the catalytic serine (this is clarified in the attached Shockwave Flash movies of the computed intrinsic reaction coordinate in the large active site model, see the Shockwave Flash movies section). After the inversion, the nitrogen lone pair now points antiperiplanar to the Ser O_γ-former carbonyl carbon bond in the second tetrahedral intermediate (TI_2). This orientation of the nitrogen lone pair corresponds to the stereoelectronically favourable conformation for amide bond formation/breakdown in accordance with Deslongchamps stereoelectronic theory.[2] TS_2 denotes the transition state for amide bond formation. It should be emphasized that depending on the level of theory used, nitrogen inversion is either a separate TS (which was the case when using HF/6-31G(d,p) and the large active site model containing 205 atoms) or concerted with amide bond formation, which was found to be the case at the B3LYP/6-31G(d,p) level of theory in the large active site model. Interestingly, the same result is obtained for the small serine hydrolase active site model presented in Figure S2 for which nitrogen inversion was found to be a separate transition state from amide bond synthesis at the HF/6-31G(d,p) level of theory as well as at the MP2/6-31G(d,p) level of theory (the size of the large active site model of 205 atoms prohibited an MP2 analysis in the large model). Again nitrogen inversion was found to be concerted with amide bond synthesis at the B3LYP/6-31G(d,p) level of theory. These findings are clarified in the attached Shockwave Flash movies of the reactions paths obtained by computation of the intrinsic reaction coordinate in the small active site model, see the Shockwave Flash movies section. We conclude that nitrogen inversion constituted the rate limiting transition state for the traditional mechanism in the large active site model (Figure S7). Nitrogen inversion has previously been found to be rate limiting by using MP2/6-311+G(2d,2p) calculations in a small active site model.[3] At the B3LYP/6-31G(d,p) level, the inversion step that occurs in order to avoid having the nitrogen lone pair in a stereoelectronically "forbidden" conformation, is concerted with amide bond synthesis.

EP represents the product amide complexed to the enzyme active site. $R^1 = C_3H_7$ in the large active site model used for the *ab initio* calculations.

***N*-acylation of (*R*)-alaninol, proton shuttle mechanism**

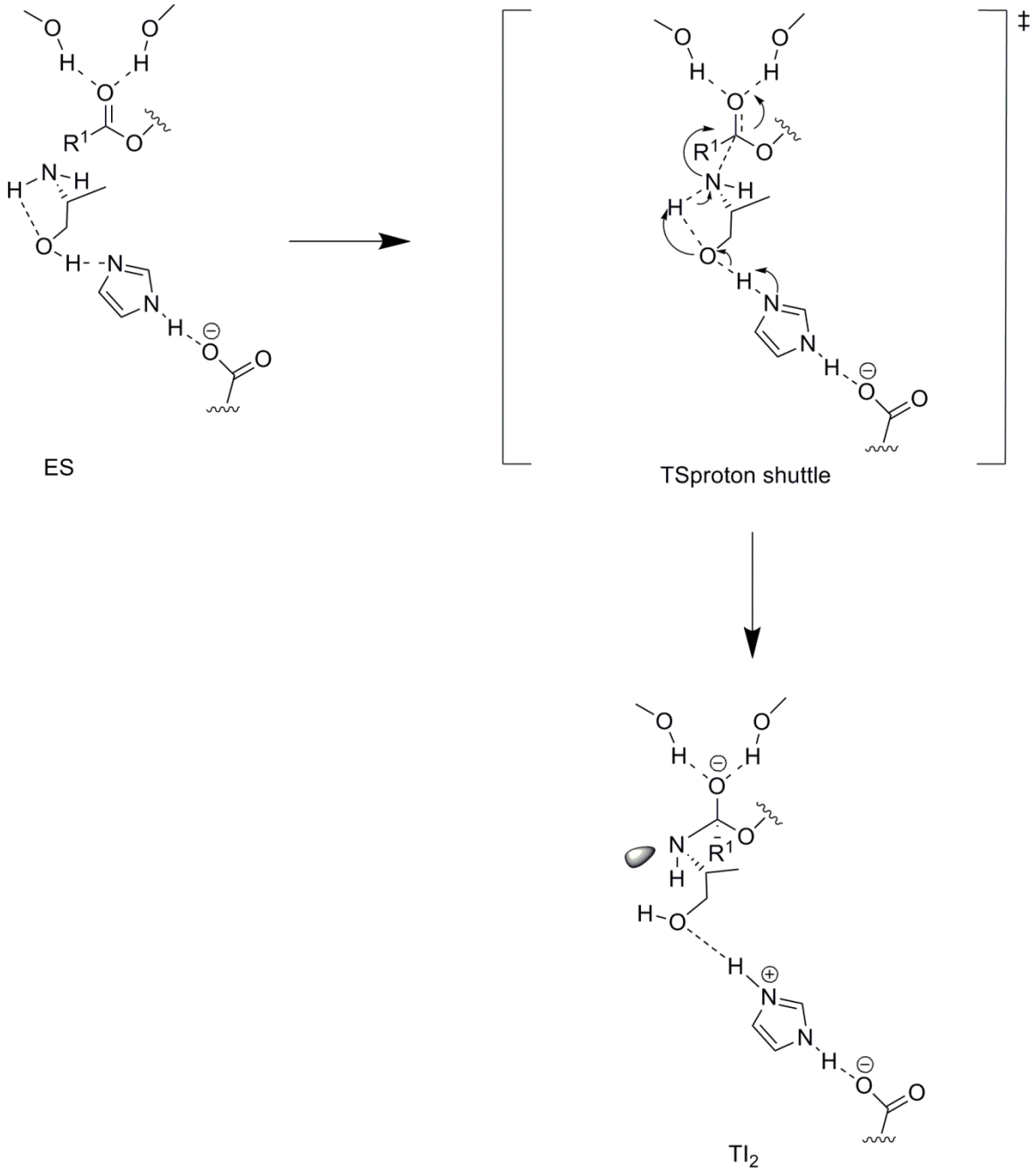

Figure S5. Schematic illustration of our suggested proton shuttle mechanism for lipase catalysed *N*-acylation of (*R*)-alaninol. Nucleophilic attack coincidently with the transfer of two protons in transition state ($TS_{proton\ shuttle}$) leads directly to the formation of a tetrahedral intermediate (TI_2) for which the lone pair of the nitrogen atom is in a stereoelectronically favourable conformation for amide bond formation. For the proton shuttle mechanism, nitrogen inversion is thus obsolete as opposed to the traditional reaction mechanism (Figure S4). $R^1 = C_3H_7$ in the large active site model used for the *ab initio* calculations.

***O*-acylation of (*R*)-alaninol, proton shuttle mechanism**

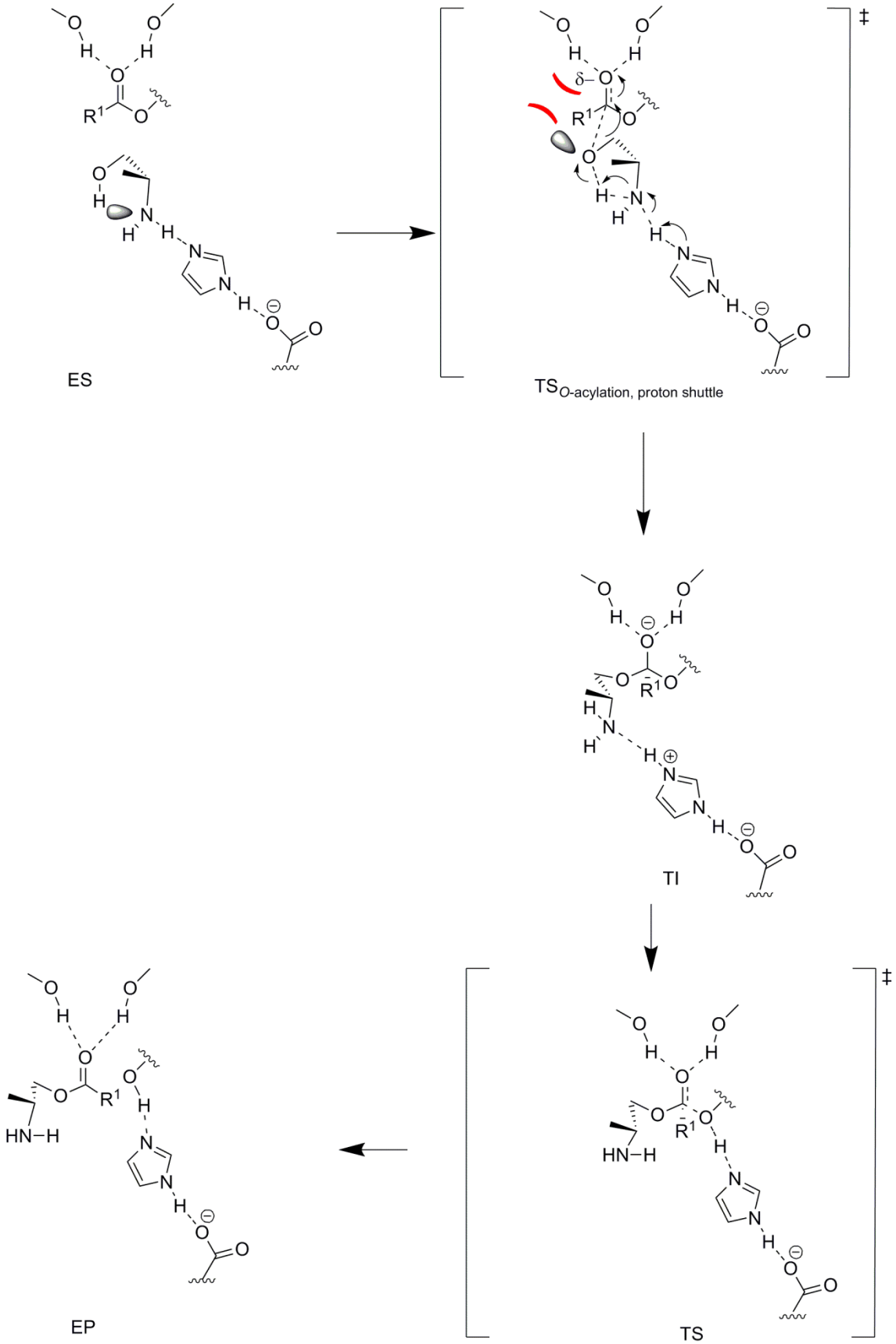

Figure S6. Proton shuttle mechanism for enzyme catalyzed *O*-acylation of (*R*)-alaninol. The preference of amino alcohols to form intramolecular hydrogen bonds makes (*R*)-alaninol adopting a conformation that is

preorganized for a proton shuttle mechanism. By inspection of Figure S6 it is seen that for the proton shuttle involving *O*-acylation, a very unfavourable interaction between the oxygen (free) lone pair and the (developing) negative charge on the carbonyl oxygen of the acyl enzyme is present in transition state (illustrated by red arcs). The other possibility is an unfavourable interaction with a lone pair of the Ser105 Oγ. This fact makes the proton shuttle for *O*-acylation unfavourable compared to the proton shuttle mechanism for *N*-acylation where a proton sitting on the nitrogen occupies the corresponding position in TS (Figure S5). The single lone pair on the scissile nitrogen atom is involved in the proton shuttle mechanism for *N*-acylation and a stereoelectronically favourable intermediate for amide bond synthesis is formed (Figure S5). For the proton shuttle involving *O*-acylation one lone pair does not participate in the proton shuttling and adopts a very unfavourable position for the mechanism to occur. This conformation is imposed by the positioning of the enzyme catalytic base (H224) which is the acceptor in the proton shuttle. Furthermore, for the proton shuttle for *O*-acylation a stable –OH---N hydrogen bond in the ES-complex is replaced by a less stable –NH---O interaction in the tetrahedral intermediate (TI) upon crossing the transition state for the proton shuttle mechanism ($TS_{O\text{-acylation, proton shuttle}}$). This fact also increases the barrier of activation for the proton shuttle mechanism involving *O*-acylation as compared to the corresponding proton shuttling for *N*-acylation (Figure S5). It should be noted that the very unfavourable interaction in TS does not occur for *O*-acylation of an alcohol that reacts through an open chain conformation since the catalytic histidine now adopts its normal position where a hydrogen bond is formed directly with the hydroxyl proton.

The tetrahedral intermediate (TI) decomposes to the product ester complexed to the active site (EP) after crossing the transition state labelled TS in the figure.

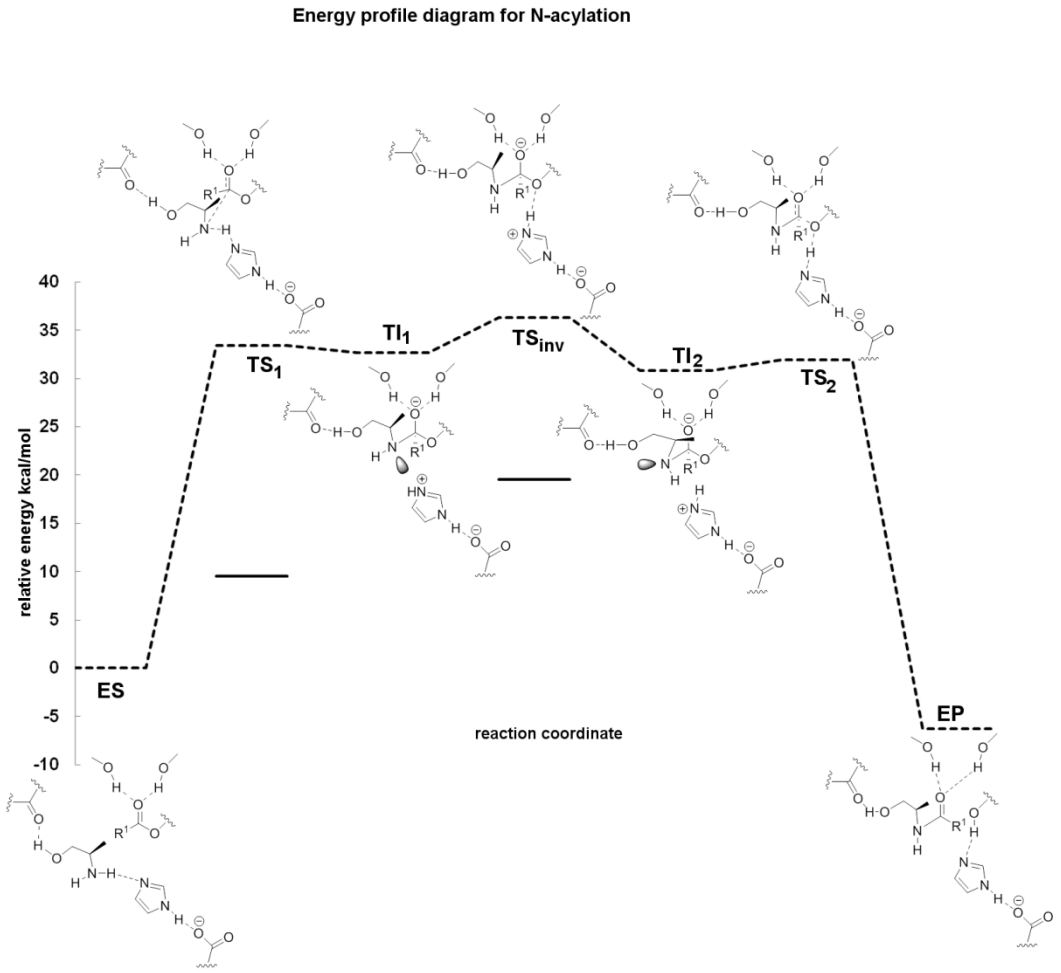

Figure S7. Strategy for the cluster *ab initio* calculations with results using HF/6-31G(d,p) and DFT at the B3LYP/6-31G(d,p) level shown for the traditional mechanism with structures of transition states and intermediates schematically drawn. By having a large model of the active site (205 atoms), calculations are tedious and time consuming. Therefore it is advantageous to optimize geometries and transition states using a lower level of theory initially (i.e. HF) and then use the obtained structures as starting point for optimization at the higher level of theory (in this case DFT at the B3LYP/6-31G(d,p) level). The whole reaction mechanism was calculated first by using HF/6-31G(d,p) (energies of transition states and intermediates according to the dotted line). Starting from the HF/6-31G(d,p) optimized structures, the mechanism was then refined using B3LYP/6-31G(d,p) (energy levels of transition states shown by solid lines). We conclude that the rate limiting transition state for *N*-acylation is nitrogen inversion (TS_{inv}) for both HF and B3LYP. In the transition state for nitrogen inversion, the nitrogen atom is sp^2-like (see figure S4 for more details on the reaction mechanism). Note that at the B3LYP/6-31G(d,p) level of theory, the TS for nitrogen inversion is concerted with amide bond formation (TS_2) and thus at this level the product amide is formed directly. The large quantum model consisting of 13 residues (205 atoms) of the active site of *Candida antarctica* lipase B was used for the calculations (the model is shown in Figure S3). In Figure 2 the proton shuttle mechanism of *N*-acylation is compared with the traditional mechanism.

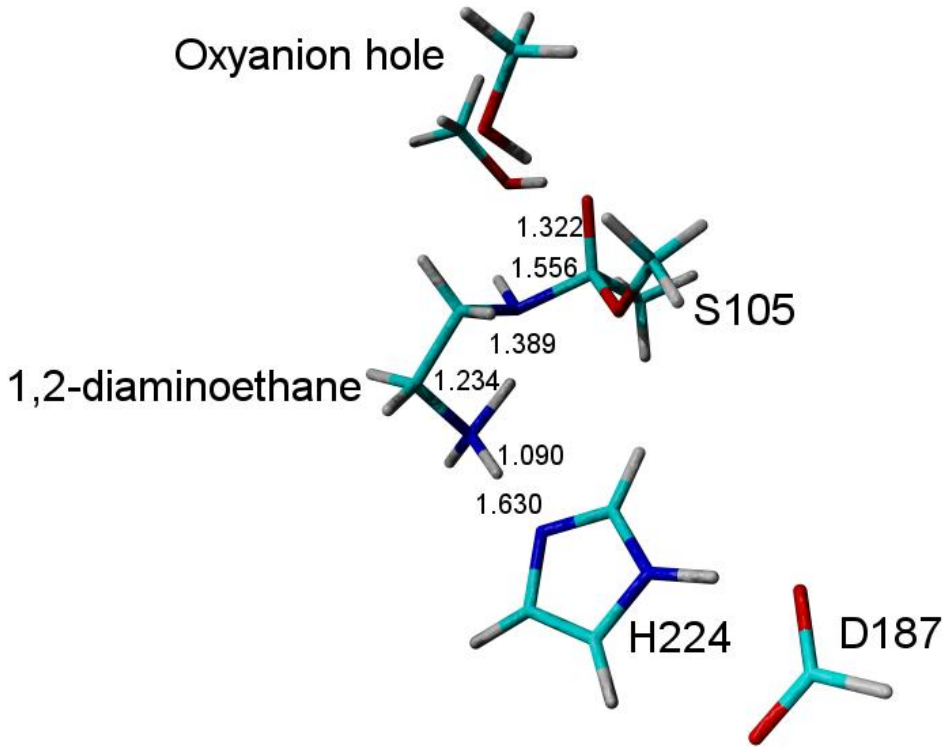

Figure S8. The transition state for the proton shuttle mechanism of *N*-acylation of 1,2-diaminoethane in a small *ab initio* model of a serine hydrolase catalytic machinery calculated using DFT at the B3LYP/6-31G(d,p) level of theory. Nucleophilic attack was concomitant with the transfer of two protons. The bond lengths (l) of the bonds being formed/broken in the transition state are given in Å. Methyl acetate was chosen to represent the acyl enzyme and 1,2-diaminoethane was chosen to represent a diamine. The catalytic triad was represented by a methanol molecule, an imidazole molecule and a formate ion. The oxyanion hole was represented by two methanol molecules. The corresponding residue numbers of amino acids in the active site of *Candida antarctica* lipase B are given. In total the small quantum model consisted of 48 atoms and the activation energy in the gas phase for the proton shuttle of *N*-acylation was 15.7 kcal/mol including ZPVE. The transition state had one imaginary frequency of 946.3i cm^{-1} that corresponded to nucleophilic attack coincidently with the transfer of two protons.

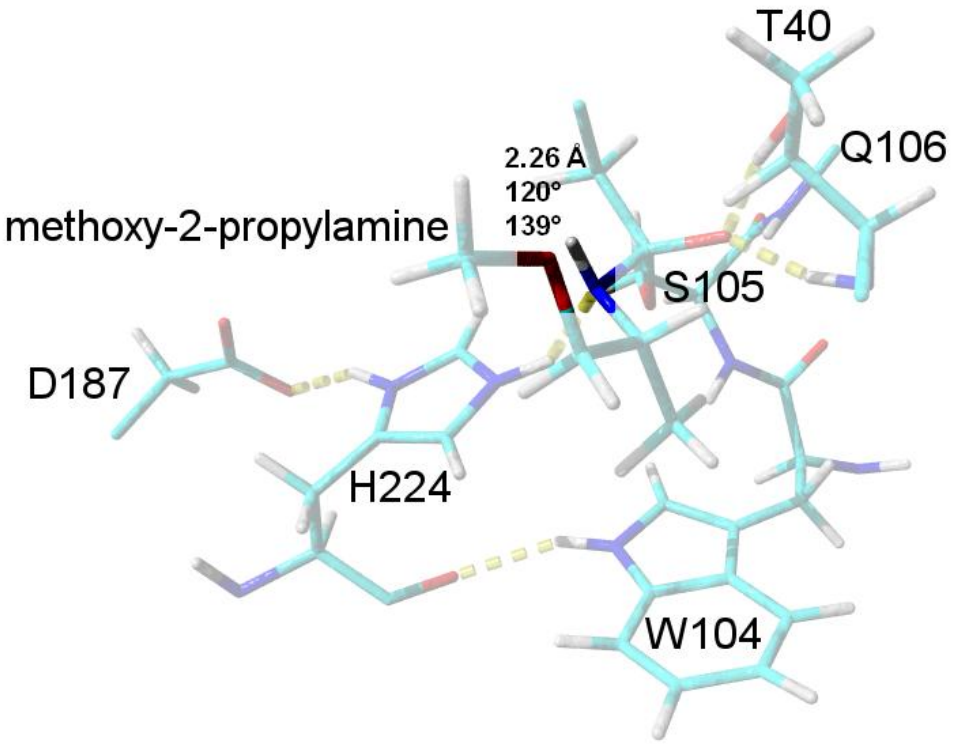

Figure S9. This figure shows a snapshot from the MD-simulation of the second tetrahedral intermediate representing the transition state for enzyme catalyzed *N*-acylation of methoxy-2-propylamine. The substrate ether oxygen (highlighted) was found to be close to the scissile NH-group (shown in highlighted sticks) throughout the 1 ns MD-simulation which shows that the proton is in a good position for transfer by a proton shuttle mechanism. The distance (2.26 Å) and the relevant angles (120° and 139°) for the hydrogen bond donated by the scissile NH-group and accepted by the ether oxygen are given in the figure. The catalytic amino acids (S105, H224, D187) as well as the oxyanion hole (T40 and Q106) are shown. W104 forms the bottom of the so called stereoselectivity pocket in *Candida antarctica* lipase B. Color code: Cyan- carbon, Red - oxygen, Blue - nitrogen, White - hydrogen. Hydrogen bonds are indicated with dashed yellow lines.

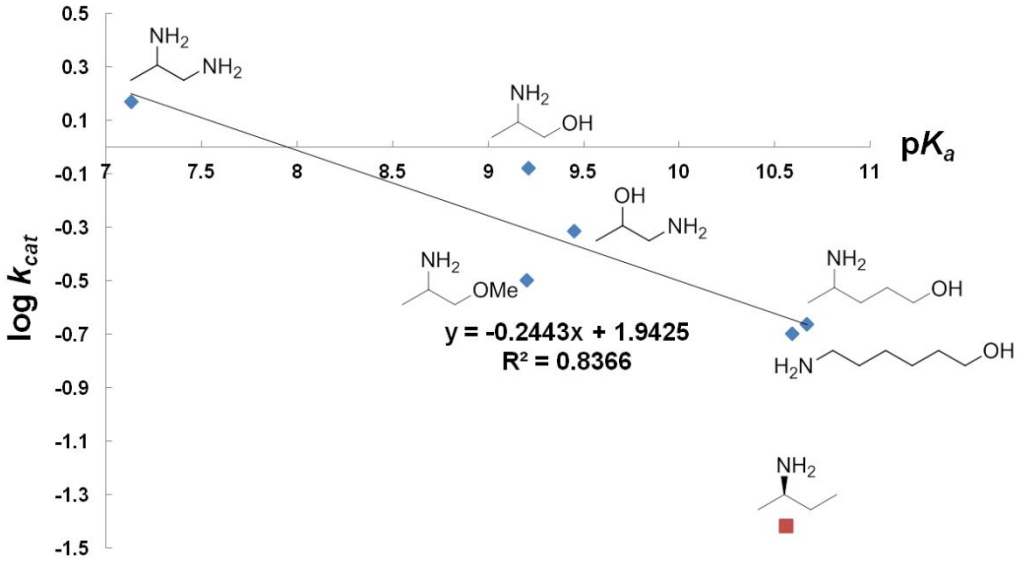

Figure S10. Linear Free Energy Relationship (LFER) analysis based on experimental k_{cat} values for enzyme catalyzed *N*-acylation (Table 1). The difunctionalized amines (blue diamonds) follow the same trend of log k_{cat} as a function of pK_a indicating that they share the same reaction mechanism. (*R*)-2-butylamine (red square) do not follow the same trend and reacts differently (through nitrogen inversion). The moderate slope of -0.24 is consistent with partial proton transfer in the rate limiting transition state which is in accordance with our suggested proton shuttle mechanism. Such partial proton transfer from the scissile NH-group in the rate limiting transition state does not occur for the "traditional" reaction mechanism involving nitrogen inversion. The pK_a values were taken from the literature.[4]

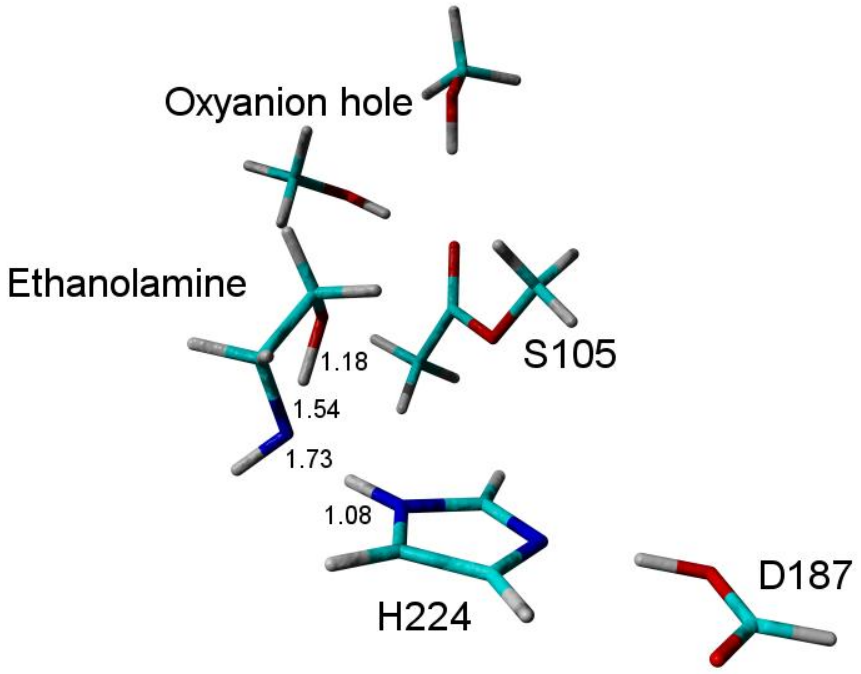

Figure S11. The proton shuttle for *O*-acylation of ethanol amine in a small *ab initio* model of a serine hydrolase catalytic machinery calculated at the B3LYP/6-31G(d,p) level of theory. Two protons are transferred in the transition state model. The distance between the hydroxyl oxygen of ethanol amine and the carbonyl carbon of the acyl enzyme in this transition state model is 2.64 Å, which is significantly longer than for *N*-acylation for which the corresponding distance was 1.56 Å (Figure S2). The bond lengths (l) of the bonds being formed/broken in the transition state model are given in Å. Methyl acetate was chosen to represent the acyl enzyme and ethanol amine was chosen to represent an amino alcohol. The catalytic triad was represented by a methanol molecule, an imidazole molecule and a formate ion. The oxyanion hole was represented by two methanol molecules. The corresponding residue numbers of amino acids in the active site of *Candida antarctica* lipase B are given. In total the small quantum model consisted of 47 atoms and the activation energy in the gas phase for the proton shuttle involving *O*-acylation was 26 kcal/mol including ZPVE. The transition state model had one imaginary frequency of 946i cm^{-1} that corresponded to the transfer of two protons and the nucleophilic oxygen approaching the carbonyl carbon. Despite many attempts, we were not able to fully relax the TS-model. By following one direction of the (imaginary) normal mode in an IRC run, the ES-complex was reached. However, in the other direction the energy increased. We were not able to relax the TS model using MP2/6-31G(d,p). However, by using HF/6-31G(d,p) the proton shuttle mechanism for *O*-acylation was found to be stepwise with an alkoxy intermediate generated by the proton shuttle (this intermediate was not viable using MP2 or DFT). B3LYP/6-31G(d,p) single point calculations on the HF generated structures resulted in an activation barrier for the proton shuttle of *O*-acylation of 21 kcal/mol. We conclude that the proton shuttle for *O*-acylation is more difficult than the corresponding shuttle for *N*-acylation (Figure S2, Figure S13) and thus provides no advantage for *O*-acylation.

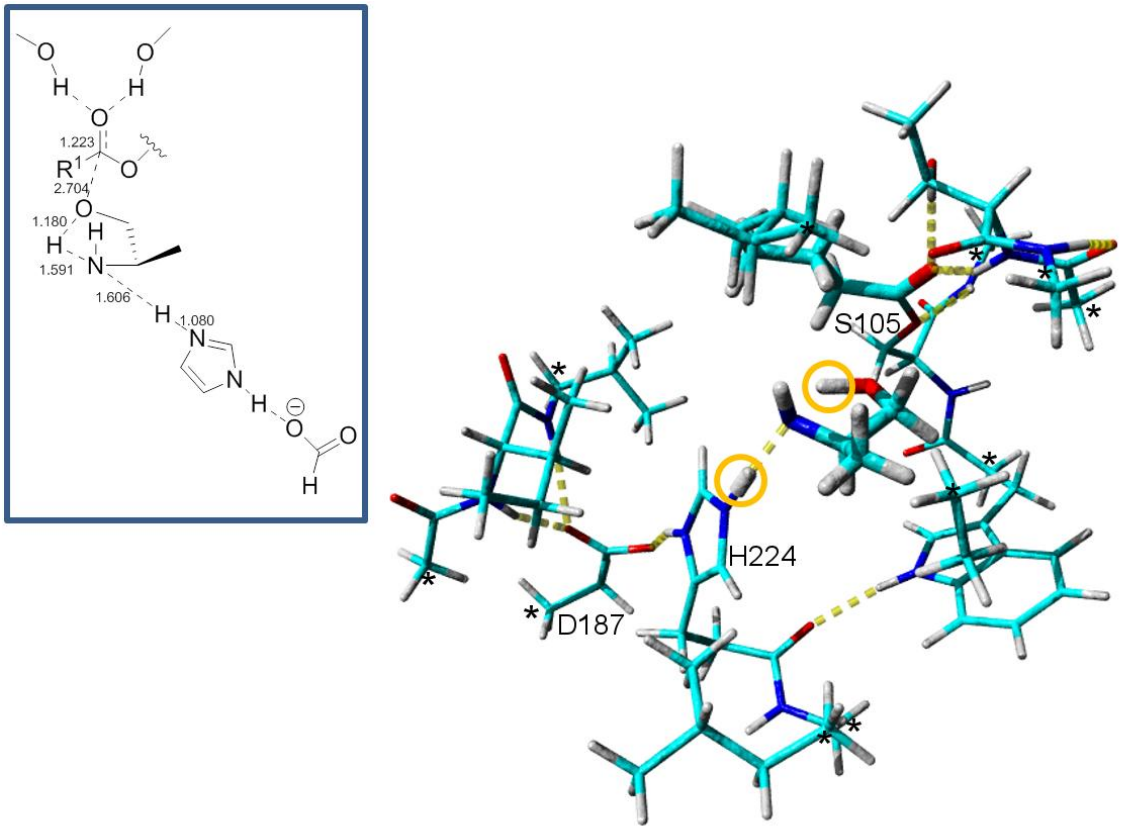

Figure S12. The structure of the calculated transition state model for the proton shuttle mechanism of *O*-acylation of (*R*)-alaninol obtained at the B3LYP/6-31G(d,p) level. The two protons encircled are being transferred in the TS. Relevant distances of bonds being formed/broken in the TS are shown within the blue frame. Note the longer distance between the nucleophile and the carbonyl carbon (2.7 Å) as compared to the proton shuttle mechanism of *N*-acylation (1.6 Å, Figure S3). This long distance is caused by an unfavourable interaction between the remaining lone pair of the amino alcohol oxygen and the lone pair on the Ser105O_γ oxygen and/or the developing negative charge on the carbonyl oxygen in TS. The model of the TS structure could not be fully relaxed and a constrained optimization was performed in which the hydroxyl O-H bond length was set to 1.18 Å and the His $N_{\varepsilon 2}$-H distance was set to 1.08 Å. These values were chosen based on using the small active site model that consisted of 47 atoms. The TS model for the proton shuttle involving *O*-acylation had an energy that was 39 kcal/mol higher than the corresponding ES-complex (B3LYP/6-31G(d,p)). We also optimized the corresponding structures using HF/6-31G(d,p) with the difference that the His $N_{\varepsilon 2}$-H distance was not constrained. This resulted in a barrier that was 10 kcal/mol higher than for *N*-acylation at the HF/6-31G(d,p) level. We conclude that a proton shuttle involving *O*-acylation is more difficult than for *N*-acylation, which is unfavourable for *O*-acylation since the amino alcohol substrate is preorganized for such proton shuttling to occur.

The acyl enzyme with the carbon chain originating from the acyl donor (containing four carbon atoms in our model) and the substrate, (*R*)-alaninol are shown in enlarged sticks. Atoms shown with an asterisk were kept fixed during the simulations since they correspond to backbone atoms in the protein that does not have the ability to move freely. This is a standard technique in cluster *ab initio* calculations with the effect that a number of small imaginary frequencies are introduced (typically in the order of 30i cm^{-1}). These small imaginary frequencies have neglectable effects on the energy of the system.

Color code: Cyan- carbon, Red - oxygen, Blue - nitrogen, White - hydrogen. Hydrogen bonds are indicated with dashed yellow lines.

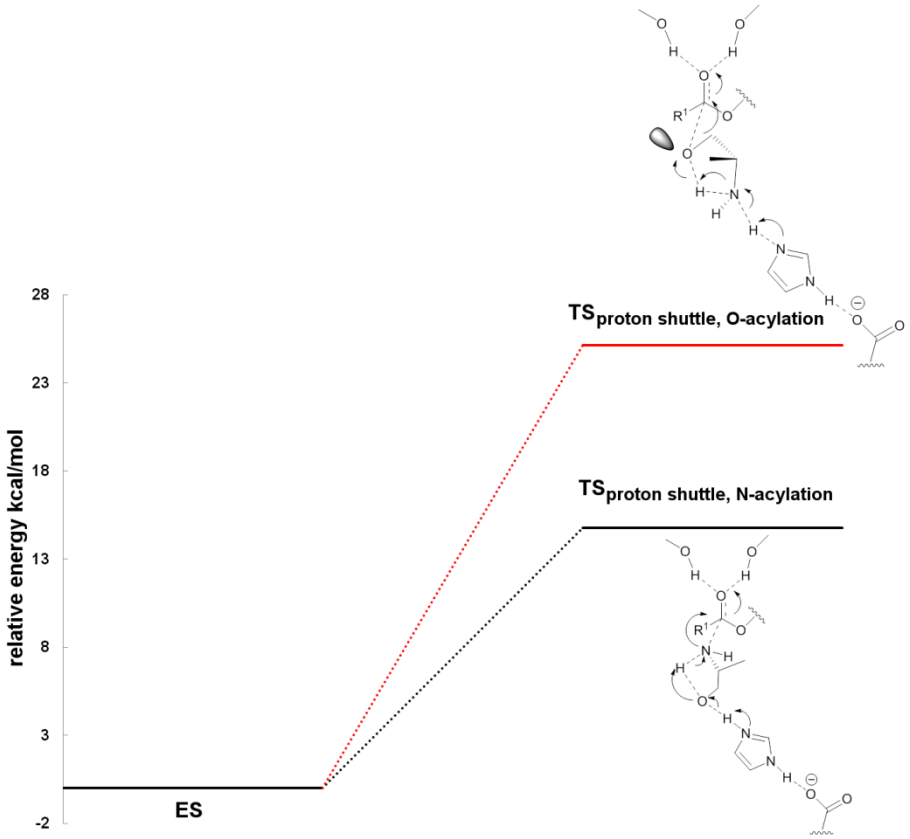

Figure S13. Energy profile diagram for proton shuttles calculated in the small active site model of a serine hydrolase consisting of 47 atoms (the model was introduced in Figure S2). In principle, a proton shuttle coincidently with nucleophilic attack, could be possible both for *N*-acylation and *O*-acylation of amino alcohols. The barrier for the proton shuttle involving *N*-acylation of (*R*)-alaninol was found to be 14.8 kcal/mol in the gas phase including ZPVE using B3LYP/6-31G(d,p). The relative energy of the TS for the proton shuttle involving *O*-acylation (red line) was found to be much higher and we estimate the barrier to be 25 kcal/mol in the gas phase including ZPVE using B3LYP/6-31G(d,p). As discussed in Figure S11 we did not manage to relax the TS structure completely but we conclude that the barrier for the proton shuttle involving *O*-acylation is much higher than for *N*-acylation. The reason for this is that the lone pair of the oxygen points towards the carbonyl oxygen of the acyl enzyme that becomes negatively charged in the TS, which causes the distance of the nucleophilic oxygen-carbonyl carbon to increase significantly in TS (Figure S11-S12).

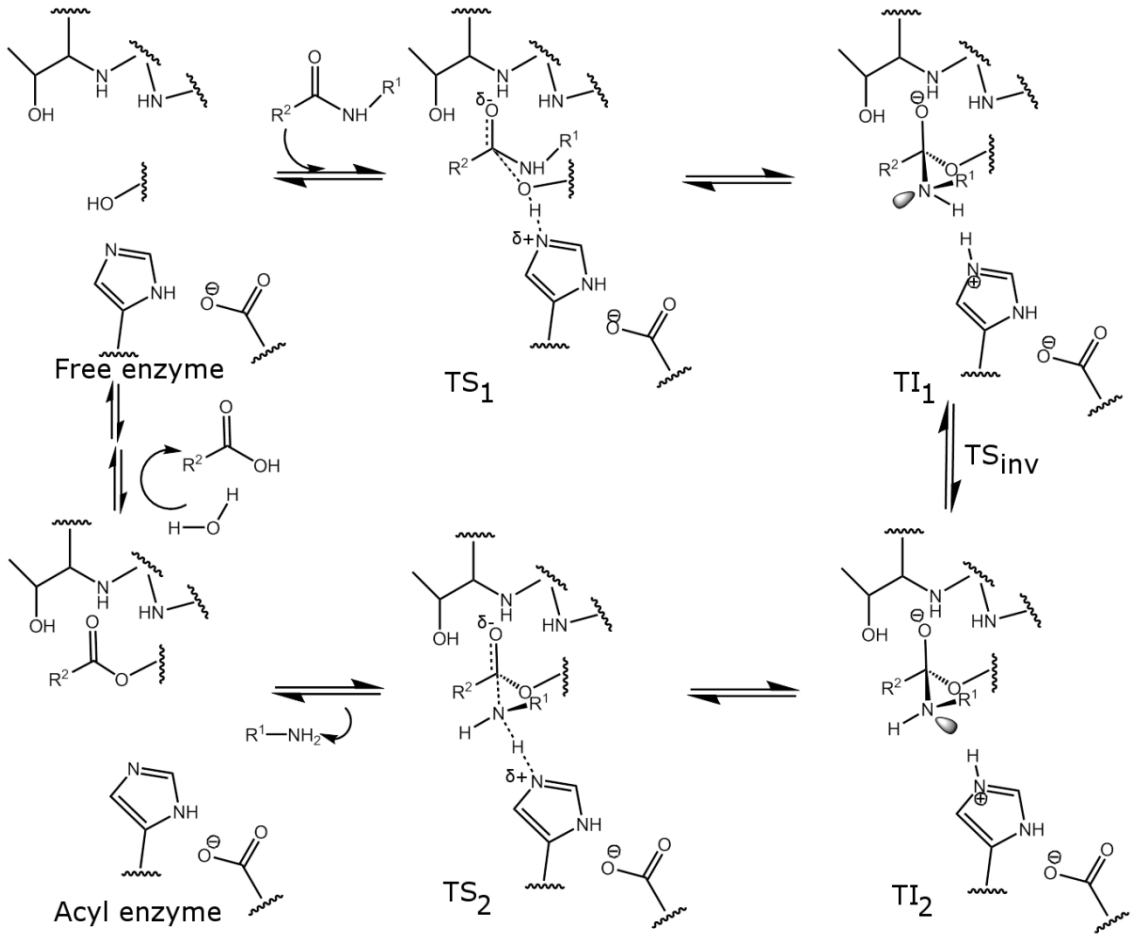

Figure S14. Reaction mechanism for amide bond hydrolysis catalyzed by *Candida antarctica* lipase B with transition states and intermediates schematically shown. The oxyanion hole is composed of T40 and Q106 in *Candida antarctica* lipase B and the residues S105, H224 and D187 form the catalytic triad. The amide substrate binds in to the free enzyme (top left) and after productive binding, the first transition state (TS_1) is reached which involves proton transfer from S105 to the catalytic base and nucleophilic attack on the carbonyl carbon. The produced tetrahedral intermediate (TI_1) has the lone pair pointing away from the catalytic base. In this conformation the scissile nitrogen is unable to accept a proton from the catalytic base (H224). Nitrogen inversion (or rotation) occurs and the second tetrahedral intermediate (TI_2) is produced which can proceed to the second transition state. In the second transition state (TS_2) the catalytic base donates a proton to the scissile nitrogen and the C-N bond breaks, forming the acyl enzyme. A water molecule functions as nucleophile during the deacylation step which proceeds through two transition states and one tetrahedral intermediate. Hydrogen bonds are indicated with dashed lines. Note that as discussed previously, at the B3LYP/6-31G(d,p) level of theory, nitrogen inversion is concerted with nucleophilic attack (TS_1, or amide bond synthesis in the reverse direction).

Supplementary Note on acyl migration

Scheme S1. The hypothetical lipase catalyzed *O*-acylation of an amino alcohol followed by chemical catalyzed *O*- to *N*-acyl migration. HO-R^2-NH_2 corresponds to an arbitrary amino alcohol. The *O*-acylated intermediate is labeled and E indicates the enzyme.

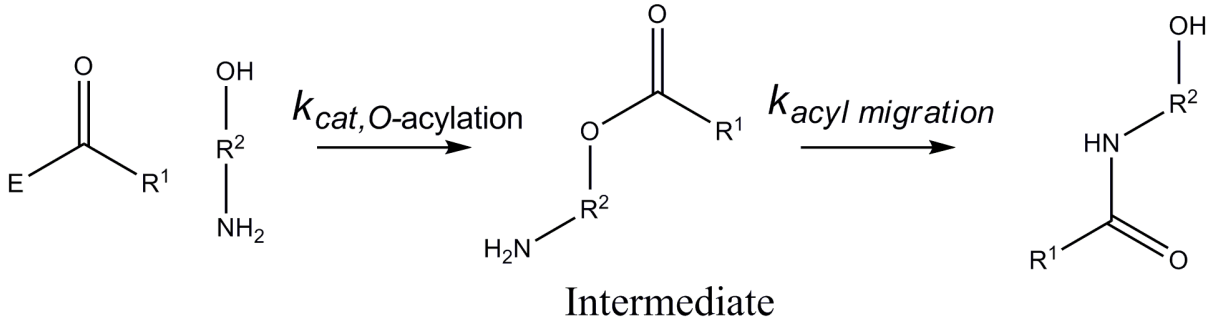

Intermediate

The steady-state concentration of the mono *O*-acylated intermediate can be calculated from:

$V_{O\text{-}acylation} - k_{acyl\ \text{migration}} * [\text{Intermediate}] = 0$ **(1)**

where the intermediate refers to the *O*-acylated intermediate from which *O*- to *N*-acyl migration would occur. $V_{O\text{-}acylation}$ corresponds to the apparent reaction rate for lipase catalyzed *O*-acylation. From Equation 1:

$[\text{Intermediate}] = V_{O\text{-}acylation}/k_{acyl\ migration}$

By using the nomenclature in Table 1, $V_{O\text{-}acylation}$ is given by:

$V_{O\text{-}acylation} = k_{cat,app} * E_0$ **(2)**

where E_0 is the amount of enzyme. The rate constant for *O*- to *N*-acyl migration is much less than 1 min^{-1}. By using this value (i.e. setting $k_{acyl\ migration} = 1\ min^{-1}$) acyl migration is assumed to be much more important than what has been found experimentally. In Table 1 it is shown that $k_{cat,app}$ is at least 54 min^{-1} for the *O*-acylation of a secondary hydroxyl. By using 10 mg beads with immobilized enzyme in a 2 mL reaction volume (corresponding to an enzyme concentration of 7.1 μM as determined by active site titration) the following steady state concentration is obtained:

$[\text{Intermediate}] = 54\ min^{-1} * 7.1 * 10^{-6}\ M/(1\ min^{-1}) = 0.4\ mM.$

A concentration of 0.4 mM of the *O*-acylated intermediate corresponds to a "minimal" concentration since acyl migration proceeds much more slowly than 60 h^{-1} as discussed in the paper. The detection limit of the *O*-acylated intermediate in our experimental setup is 2 μM. The minimal concentration of the presumed *O*-acylated intermediate is thus at least 200 times higher than the detection limit.

For comparison by using $k_{acyl\ migration}$= 1 h^{-1} and $k_{cat,app}$ = 260 min^{-1} (the value for the lipase catalyzed acylation of a primary hydroxyl group, Table 1) a steady-state concentration of 100 mM is obtained!

As no *O*-acylated intermediate was observed in any experiment it can be concluded that acyl migration is of minor importance in lipase catalyzed *N*-acylation of amino alcohols.

Table S3: Gradient elution for HPLC analysis of products resulting from acylation of 1,2-propanediol

Time [min]	Flow rate [ml/min]	% A	% B
0	0,75	100	0
30	0,75	100	0
32	0,75	0	100
57	0,75	0	100
59	0,75	100	0
82	0,75	100	0

Table S4: Gradient elution for HPLC analysis of products resulting from acylation of amino-alcohols

Time [min]	Flow rate [ml/min]	% A	% B
0	1	100	0
20	1	100	0
23	1	0	100
80	1	0	100
82	1	100	0
90	1	100	0

Cartesian coordinates of calculated structures

Conformations of amino alcohols, geometry optimization by employing B3LYP/6-31G(d,p)

(*R*)-alaninol, conformations in the same order as in Table 2

```
E = -249.5586 hartrees

14
Frame 1
C -5.6458 3.7655 -0.0065
C -4.1147 3.6880 -0.0476
H -5.9035 4.8120 0.2092
N -6.2417 2.9590 1.0644
C -6.2553 3.3770 -1.3535
H -3.7235 4.3463 -0.8407
H -3.8085 2.6549 -0.2884
O -3.6308 4.0839 1.2338
H -2.6701 3.9913 1.2374
H -5.7436 3.1667 1.9287
H -6.0643 1.9718 0.8747
H -5.8943 4.0251 -2.1590
H -7.3448 3.4510 -1.3072
H -5.9985 2.3424 -1.6160


E = -249.5623 hartrees

14
Frame 1
C -5.6777 3.8828 -0.0473
C -4.1410 3.8108 -0.0980
H -5.9687 4.9350 0.1157
N -6.0929 3.0000 1.0620
C -6.3120 3.3909 -1.3491
H -3.7320 4.2849 0.8134
H -3.7578 4.3724 -0.9576
O -3.7008 2.4728 -0.2195
H -4.2938 1.9802 0.3757
H -7.0910 2.8121 1.0171
H -5.9218 3.4536 1.9572
H -6.0300 4.0405 -2.1834
H -7.4061 3.3898 -1.2821
H -5.9728 2.3766 -1.5751
```

(*R*)-4-amino-1-pentanol,

conformations in the same order as in Table 2

```
E = -328.1300 hartrees

20
Frame 1
C -5.7544 4.0260 -0.1711
C -4.2115 3.9995 -0.2024
H -6.0258 5.0918 -0.1702
N -6.2530 3.4810 1.1025
C -6.3891 3.3854 -1.4189
H -3.8596 4.4487 0.7350
H -3.8875 4.6686 -1.0107
C -3.4817 2.6580 -0.4176
H -6.0907 2.4732 1.0962
H -7.2631 3.6086 1.1412
H -3.7892 2.1843 -1.3583
C -3.5797 1.6096 0.6888
H -2.4146 2.8900 -0.5341
O -4.8327 0.9173 0.5891
H -3.4771 2.0892 1.6740
H -2.7549 0.8901 0.5755
H -4.8730 0.2739 1.3088
H -5.9897 3.8133 -2.3472
H -7.4737 3.5457 -1.4211
H -6.2126 2.3050 -1.4362


E = -328.1400 hartrees

20
Frame 1
C -5.7378 4.0409 -0.1810
C -4.1937 4.0288 -0.1866
H -6.0374 5.1018 -0.2360
N -6.2493 3.4264 1.0667
C -6.3614 3.3135 -1.3749
H -3.8464 4.4638 0.7634
H -3.8743 4.7336 -0.9654
C -3.4613 2.6934 -0.4251
H -7.2673 3.4523 1.0765
H -5.9380 3.9636 1.8740
H -3.7527 2.2685 -1.3937
C -3.6258 1.6038 0.6450
H -2.3895 2.9250 -0.5041
O -4.9074 1.0098 0.6775
H -3.3456 2.0199 1.6309
H -2.9134 0.7979 0.4308
H -5.5242 1.7235 0.9593
H -5.9554 3.6930 -2.3180
H -7.4473 3.4644 -1.3973
H -6.1642 2.2403 -1.3104
```

Cartesian coordinates of calculated structures using the small active site model of a serine hydrolase consisting of 47 atoms

Geometries optimized at the B3LYP/6-31G(d,p) level

Proton shuttle mechanism for *N*-acylation of ethanol amine:

Starting complex ("ES-complex") for the proton shuttle mechanism of *N*-acylation

```
E = -1125.1373 hartrees

47
Frame 1
C -5.5163 27.4631 20.1411
O -5.5393 27.7376 21.5327
H -5.4262 26.8866 21.9968
C -3.6296 23.5254 20.2375
C -3.1954 23.7394 24.2481
O -3.8845 24.8528 24.8737
O -3.2862 24.8081 20.7182
H -3.7987 24.9670 21.5319
C -0.3737 21.9992 26.9740
O 0.8305 22.1714 27.2147
O -1.2560 22.8713 26.6615
H 1.9629 24.5576 26.7553
C 1.3449 25.3483 26.3575
N -0.0113 25.1716 26.2641
H -0.5287 24.2576 26.4929
C 1.6019 26.6032 25.8523
H 2.5525 27.1108 25.7539
C -0.5181 26.2954 25.7139
H -1.5723 26.4207 25.5061
N 0.4251 27.1969 25.4444
H -0.0547 28.5782 24.3355
C -1.6659 27.4478 22.5843
H -1.9288 27.0607 21.5930
H -1.1551 26.6354 23.1136
N -2.8960 27.7878 23.3200
H -3.5703 28.2164 22.6868
C -4.7145 25.5695 24.1314
O -4.9652 25.3252 22.9497
C -5.4165 26.6359 24.9310
H -0.7759 20.9505 27.0364
C -0.6900 28.6302 22.4731
H -5.3876 28.4146 19.6135
H -6.4595 27.0112 19.7884
H -4.6916 26.7928 19.8653
H -3.0471 23.3448 19.3277
H -4.6970 23.4354 19.9777
H -3.3886 22.7233 20.9528
H -2.5995 24.1003 23.4063
H -3.9327 23.0153 23.8885
H -2.5640 23.3100 25.0308
H 0.2490 28.2842 22.0038
O -0.4640 29.2480 23.7252
H -1.1156 29.4028 21.8154
H -2.6285 28.4986 24.0020
H -6.2436 26.1744 25.4840
H -5.8144 27.3973 24.2608
H -4.7283 27.0838 25.6475
```

TS for the proton shuttle mechanism of *N*-acylation

```
E = -1125.1104 hartrees

47
Frame 1
C -5.8146 28.2932 20.1613
O -5.7443 28.2974 21.5736
H -5.6471 27.3466 21.8681
C -5.0842 24.3147 19.4788
C -3.4977 23.8981 23.2245
O -3.2470 25.1813 23.7813
O -4.1183 25.2011 19.9861
H -4.4091 25.4653 20.9079
C 1.0781 22.1267 28.6511
O 2.0448 22.8492 28.8350
O 0.0347 22.3515 27.8901
H 2.0822 25.1312 27.5785
C 1.2924 25.4507 26.9140
N 0.1960 24.6434 26.7022
H 0.0952 23.2951 27.3984
C 1.1509 26.5988 26.1737
H 1.7847 27.4666 26.0695
C -0.5835 25.3039 25.8471
H -1.5358 24.9697 25.4570
N -0.0446 26.4912 25.5011
H -0.4963 27.2134 24.8201
C -2.1014 27.0483 21.9762
H -2.3546 27.2858 20.9415
H -1.9151 25.9776 22.0547
N -3.2000 27.3834 22.9099
H -3.8239 28.0845 22.4971
C -4.1578 26.2334 23.3565
O -4.9874 25.8951 22.3896
C -4.8562 26.7514 24.6267
H 0.9907 21.1396 29.1508
C -0.8788 27.8699 22.5398
H -5.5326 29.2872 19.7893
H -6.8367 28.0866 19.7959
H -5.1424 27.5474 19.7143
H -4.7771 24.0030 18.4708
H -6.0873 24.7689 19.3931
H -5.1930 23.3998 20.0881
H -3.3954 23.8899 22.1339
H -4.4998 23.5290 23.4773
H -2.7483 23.2336 23.6665
H 0.0389 27.2683 22.4231
O -1.1579 28.1745 23.8717
H -0.7382 28.7858 21.9340
H -2.4362 27.8502 23.7206
H -5.5552 25.9811 24.9644
H -5.4259 27.6589 24.4006
H -4.1411 26.9609 25.4279
```

Proton shuttle mechanism for *O*-acylation of ethanol amine:

Starting complex ("ES-complex") for the proton shuttle mechanism of *O*-acylation

This structure had one very small imaginary frequency (-9.6) that we neglected since it will have a minimal impact on the energy.

```
E = -1125.1273 hartrees

47
Frame 1
C -5.5372 27.7611 20.3391
O -6.5733 27.1207 21.0808
H -6.1521 26.3768 21.5465
C -6.0002 24.1034 19.3736
C -2.9445 23.8982 23.6033
O -3.6272 25.0017 24.2341
O -4.6399 24.3145 19.7093
H -4.6084 24.5052 20.6605
C 0.7839 22.0007 28.4994
O 1.9387 22.4501 28.3985
O -0.3123 22.4840 28.0610
H 2.3206 24.5826 27.1946
C 1.5297 25.1698 26.7515
N 0.2359 24.7288 26.8456
H -0.0392 23.7959 27.3462
C 1.4797 26.3632 26.0660
H 2.2975 27.0157 25.7872
C -0.5359 25.6522 26.2297
H -1.6120 25.5632 26.1571
N 0.1743 26.6671 25.7372
H -0.5770 28.2206 24.7608
C -1.6268 27.4092 22.3531
H -1.5929 27.1856 21.2803
H -1.3788 26.4892 22.9052
O -2.9360 27.8582 22.6830
C -4.6405 25.5495 23.5632
O -5.0218 25.1365 22.4726
C -5.3102 26.6581 24.3276
H 0.6553 21.0284 29.0527
C -0.6110 28.4950 22.7302
H -4.7496 28.1639 20.9890
H -5.9963 28.5864 19.7836
H -5.0685 27.0761 19.6185
H -6.0537 23.9738 18.2871
H -6.6371 24.9542 19.6519
H -6.4173 23.1935 19.8376
H -2.5458 24.2055 22.6345
H -3.6312 23.0593 23.4646
H -2.1374 23.6321 24.2839
H 0.4120 28.1045 22.6044
N -0.9352 28.9275 24.0947
H -0.4823 29.8117 24.3064
H -0.7299 29.3496 22.0511
H -2.7548 28.4314 23.4607
H -6.0123 26.2204 25.0466
H -5.8595 27.2886 23.6276
H -4.5699 27.2395 24.8768
```

TS for the proton shuttle mechanim of *O*-acylation

The TS-structure could not be fully relaxed at the B3LYP/6-31G(d,p) level. Therefore an optimization with constraints were performed to obtain a TS-model. The His $N_{\varepsilon 2}$-H bond length was kept fixed at 1.08 Å and the distance between the hydroxyl proton and oxygen of the amino alcohol was set to 1.18 Å. These were the distances found in TS at the HF/6-31G(d,p) level (the TS-structure could be fully relaxed at the HF/6-31G(d,p) level). Our TS-model at the B3LYP/6-31G(d,p) level had one imaginary frequency of 946.3i cm^{-1} corresponding to nucleophilic attack by the oxygen atom of ethanol amine and the transfer of two protons.

```
E = -1125.0805 hartrees

47
Frame 1
C -5.3418 27.9087 20.1135
O -6.4962 27.3448 20.7331
H -6.1623 26.6671 21.3478
C -5.8698 24.1809 19.3366
C -3.3310 23.9185 23.5024
O -3.8681 25.0723 24.1718
O -4.5428 24.3312 19.8072
H -4.6073 24.6895 20.7086
C 1.2013 22.0434 28.7014
O 2.3036 22.5561 28.5946
O 0.0653 22.4597 28.1942
H 2.4849 24.7434 27.1852
C 1.6229 25.2273 26.7495
N 0.3751 24.6538 26.8592
H 0.1885 23.3576 27.6394
C 1.5155 26.4029 26.0462
H 2.2543 27.1327 25.7508
C -0.4580 25.4796 26.2289
H -1.5242 25.3405 26.1139
N 0.1877 26.5467 25.7228
H -0.3214 27.3363 25.1821
C -1.8849 27.2565 22.2488
H -1.8255 27.2969 21.1489
H -1.6754 26.2103 22.5485
O -3.1335 27.6835 22.7141
C -4.7861 25.7744 23.4926
O -5.2177 25.4071 22.4031
C -5.3508 26.9163 24.2882
H 1.0499 21.1094 29.2802
C -0.8146 28.1757 22.9065
H -4.5941 28.2263 20.8517
H -5.6736 28.7787 19.5337
H -4.8605 27.2001 19.4219
H -5.8171 23.9418 18.2678
H -6.4620 25.0986 19.4585
H -6.4087 23.3551 19.8346
H -2.8037 24.2154 22.5937
H -4.1288 23.2168 23.2429
H -2.6355 23.4688 24.2111
H 0.1747 27.6791 22.8518
N -1.3162 28.4099 24.2596
H -1.0761 29.3673 24.5237
H -0.7300 29.1010 22.3054
```

```
H -2.7138 28.2980 23.6299
H -6.1766 26.5407 24.9064
H -5.7307 27.6667 23.5960
H -4.5819 27.3448 24.9291
```

Cartesian coordinates of calculated structures using the small active site model of a serine hydrolase consisting of 48 atoms

Geometries optimized at the B3LYP/6-31G(d,p) level

<u>Proton shuttle mechanism for *N*-acylation of 1,2-diaminoethane</u>

This computed transition state structure shows that the proton shuttle mechanism is possible for other substrate assisting groups than a hydroxyl.

```
E = -1105.2313 hartrees

48
Frame 1
C -5.7893 28.2462 20.0685
O -5.7562 28.2845 21.4814
H -5.6693 27.3400 21.8027
C -4.7842 24.2805 19.4794
C -3.6172 23.9486 23.4521
O -3.3621 25.2694 23.9088
O -3.9540 25.2458 20.0751
H -4.3447 25.4754 20.9707
C 1.0050 22.0482 28.5553
O 2.0699 22.6832 28.6377
O -0.0557 22.3345 27.9046
H 2.2852 24.7887 27.4112
C 1.5069 25.2283 26.8036
N 0.3068 24.5763 26.6826
H 0.1036 23.6082 27.1892
C 1.4047 26.3762 26.0536
H 2.1409 27.1536 25.8934
C -0.4730 25.3273 25.8824
H -1.4850 25.0677 25.6011
N 0.1529 26.4352 25.4732
H -0.6284 27.5389 24.5639
C -2.1763 27.0463 22.0902
H -2.4176 27.1230 21.0287
H -1.9240 26.0096 22.3144
N -3.2895 27.4304 22.9769
H -3.8984 28.1069 22.5043
C -4.2614 26.2898 23.3972
O -5.0315 25.9079 22.3932
C -5.0511 26.8370 24.6003
H 0.9321 21.0801 29.1217
C -0.9846 27.9700 22.4908
H -5.5119 29.2355 19.6806
H -6.7974 28.0160 19.6820
H -5.0941 27.5005 19.6586
H -4.3645 24.0147 18.5001
H -5.8142 24.6396 19.3097
H -4.8561 23.3516 20.0705
H -3.4530 23.8449 22.3735
H -4.6419 23.6254 23.6736
H -2.9127 23.3080 23.9907
H -0.0215 27.4888 22.3011
N -1.1818 28.2365 23.9348
H -0.9582 29.1908 24.2014
H -1.0203 28.9150 21.9380
H -2.3873 27.9772 23.8804
```

H -5.7562 26.0650 24.9207
H -5.6236 27.7227 24.3042
H -4.3958 27.0888 25.4400

Cartesian coordinates of calculated structures for the different mechanisms using the large active site model of *Candida antarctica* lipase B consisting of 205 atoms

Geometries calculated by employing B3LYP/6-31G(d,p)

The following atoms were kept fixed for the production of the final B3LYP/6-31G(d,p) geometries and hessian calculations (corresponding to backbone atoms in the enzyme):

Atom 23 (G41), Atom 67 (D187), Atom 103 (V190), Atom 135 (H224), Atom 140 (L278), Atom 157 (A281), Atom 165 (I285)

Proton shuttle mechanism of *N-acylation:*

ES-complex for the proton shuttle mechanism of *N*-acylation

```
E = -4049.9792 hartrees

205
Frame 1
C -12.1536 20.8916 5.1907
H -11.8649 21.8048 5.7173
H -12.1119 20.0388 5.8724
H -13.1846 21.0209 4.8456
C -11.2405 20.7251 3.9868
O -10.9599 21.6822 3.2528
N -10.7788 19.4698 3.7732
H -11.0418 18.7410 4.4257
C -9.7790 19.1595 2.7468
H -9.1125 20.0280 2.6861
C -10.4697 18.9714 1.3729
O -10.6155 17.8705 0.8439
C -8.9577 17.9086 3.1334
H -9.6113 17.0338 3.0194
O -8.4645 18.0011 4.4664
H -9.2003 17.8129 5.0707
C -7.7484 17.7422 2.2190
H -8.0606 17.6264 1.1793
H -7.1870 16.8542 2.5216
H -7.0849 18.6099 2.3079
N -10.8915 20.1341 0.8133
H -10.8842 20.9591 1.4124
C -11.6534 20.1296 -0.4193
H -12.7209 19.9262 -0.2535
H -11.5551 21.1007 -0.9122
H -11.2639 19.3487 -1.0745
C -16.2054 18.2172 10.3070
H -15.9303 19.0244 10.9983
H -17.0929 17.7238 10.7104
C -15.0898 17.1756 10.3216
O -15.2831 15.9910 10.5787
C -16.5186 18.8310 8.9275
H -17.1968 19.6802 9.0931
H -15.6024 19.2762 8.5085
C -17.1379 17.8957 7.9267
C -17.2948 16.5287 8.0022
H -17.0063 15.8487 8.7917
C -17.6980 18.2959 6.6606
N -17.9075 16.0540 6.8611
```

H -18.1781 15.0864 6.6957
C -18.1705 17.1126 6.0224
C -17.8507 19.5304 6.0041
H -17.4917 20.4486 6.4632
C -18.7758 17.1429 4.7600
H -19.1254 16.2297 4.2872
C -18.4580 19.5628 4.7542
H -18.5782 20.5118 4.2382
C -18.9138 18.3791 4.1372
H -19.3820 18.4344 3.1580
N -13.8353 17.6541 10.0458
H -13.6963 18.6389 9.8760
C -12.6618 16.7959 10.1594
H -12.8930 16.0313 10.9052
C -11.4743 17.6045 10.7268
O -10.9684 17.3314 11.8069
C -12.3404 16.0350 8.8659
H -13.2381 15.5321 8.4976
H -11.5605 15.2967 9.0732
O -11.8936 16.9741 7.8650
N -11.0896 18.6778 9.9679
H -11.3243 18.6412 8.9826
C -9.9493 19.4897 10.3681
H -9.9732 20.4351 9.8205
H -10.0126 19.6879 11.4394
H -8.9923 18.9894 10.1720
C -17.0980 7.2870 8.7218
C -17.6769 5.9805 8.1718
H -18.2164 5.4214 8.9444
H -16.8703 5.3517 7.7838
H -18.3748 6.1698 7.3480
H -17.8855 7.9637 9.0684
H -16.4693 7.0653 9.5964
C -16.2035 8.0502 7.7244
O -15.4534 7.3667 6.9714
O -16.2651 9.3141 7.7721
N -14.1490 6.0300 4.7932
C -14.3737 4.7846 4.2959
O -13.6841 4.2472 3.4282
C -15.5591 4.0581 4.9236
H -16.0436 3.4502 4.1561
H -16.2851 4.7376 5.3782
H -15.1890 3.3814 5.7025
H -14.7804 6.4066 5.4999
C -12.9974 6.8358 4.3994
H -12.4521 6.2502 3.6575
C -12.0003 7.0233 5.5650
O -10.7898 6.8873 5.3821
C -13.4289 8.2017 3.7925
H -13.9598 8.7455 4.5855
C -14.4358 8.0329 2.6311
H -15.3313 7.5316 3.0166
H -14.7553 9.0383 2.3255
C -12.2140 9.0464 3.3759
H -11.6190 8.5460 2.6044
H -11.5422 9.2355 4.2172
H -12.5452 10.0126 2.9802
C -13.9252 7.2622 1.4050
H -13.0449 7.7404 0.9621
H -14.6994 7.2249 0.6293
H -13.6631 6.2303 1.6588

N -12.5422 7.3627 6.7685
H -13.5572 7.4379 6.8673
C -11.7265 7.4295 7.9713
H -12.2203 6.8445 8.7600
H -10.7766 6.9453 7.7311
C -11.4539 8.8551 8.5030
H -10.7591 8.7227 9.3479
C -10.7546 9.7287 7.4530
H -11.4263 9.9331 6.6118
H -9.8673 9.2335 7.0467
H -10.4502 10.6905 7.8832
C -12.7254 9.5248 9.0428
H -13.4995 9.6107 8.2729
H -12.5119 10.5332 9.4170
H -13.1584 8.9508 9.8707
C -18.8269 10.9094 6.1751
H -19.6699 10.2215 6.3224
H -18.2262 10.8965 7.0869
C -19.3565 12.3161 5.9454
O -18.8173 13.3246 6.3994
C -17.9640 10.3970 4.9880
H -17.7890 9.3276 5.1500
H -18.5244 10.4877 4.0495
C -16.6491 11.0951 4.8379
N -15.6222 10.8924 5.7330
H -15.6957 10.2343 6.5606
C -16.1630 11.9926 3.9136
H -16.6654 12.4002 3.0467
C -14.5821 11.6530 5.3259
H -13.6355 11.6753 5.8476
N -14.8656 12.3393 4.2245
H -14.7717 15.6505 5.6666
N -20.4856 12.3825 5.1775
H -20.8429 11.5242 4.7861
C -21.0980 13.6360 4.7740
H -20.6868 14.0167 3.8286
H -22.1759 13.4992 4.6571
H -20.9129 14.3780 5.5518
C -20.0788 12.8176 -0.9771
C -19.5972 14.2326 -0.6389
H -20.4443 14.9122 -0.4916
H -18.9793 14.6444 -1.4454
H -18.9979 14.2557 0.2766
H -20.6855 12.4273 -0.1463
H -20.7531 12.8715 -1.8434
C -18.9593 11.8042 -1.2885
H -18.3512 12.2225 -2.1057
C -18.0317 11.5663 -0.0871
H -18.5967 11.1752 0.7691
H -17.5289 12.4836 0.2340
H -17.2530 10.8350 -0.3276
C -19.5562 10.4768 -1.7803
H -18.7705 9.7598 -2.0411
H -20.1866 10.6238 -2.6650
H -20.1781 10.0162 -1.0020
C -16.3855 17.3141 -0.2890
C -15.2107 17.5496 -1.2397
H -15.2270 18.5650 -1.6530
H -15.2310 16.8513 -2.0842
H -14.2505 17.4163 -0.7283
H -16.3649 16.3001 0.1238

```
H -17.3469 17.4450 -0.7994
H -16.3628 18.0107 0.5560
C -9.7886 14.6773 -2.5699
C -9.8394 15.8793 -3.5235
H -10.3052 15.6158 -4.4800
H -8.8284 16.2507 -3.7375
H -10.4090 16.7079 -3.0867
H -10.8236 14.3494 -2.3872
C -9.1851 15.0890 -1.2121
H -8.1434 15.4067 -1.3755
H -9.7194 15.9712 -0.8379
C -9.0338 13.5097 -3.2235
H -7.9836 13.7775 -3.4002
H -9.4746 13.2465 -4.1926
H -9.0476 12.6101 -2.6008
C -9.2247 14.0015 -0.1325
H -8.6287 13.1236 -0.4057
H -10.2513 13.6663 0.0537
H -8.8324 14.3837 0.8155
C -11.2039 16.5929 6.7684
N -13.7820 15.6309 5.4170
H -13.5708 14.6458 5.2538
C -13.6044 16.3151 4.1181
H -12.5368 16.5577 4.0278
C -13.9350 15.3937 2.9299
H -15.0178 15.1822 2.9263
H -13.6966 15.9179 1.9920
O -13.1757 14.2024 2.9904
H -13.7534 13.4880 3.3568
C -14.4003 17.6174 4.0856
H -14.1827 18.1829 3.1730
H -14.1488 18.2439 4.9474
H -15.4803 17.4277 4.1173
O -10.8852 17.4822 5.9932
C -10.7710 15.1492 6.6415
H -10.0720 14.9505 7.4694
H -11.6428 14.5115 6.8157
C -10.1077 14.8004 5.3043
H -10.8437 14.9032 4.4999
H -9.2999 15.5119 5.1008
C -9.5563 13.3712 5.3048
H -9.0943 13.1351 4.3418
H -8.7971 13.2311 6.0841
H -10.3493 12.6346 5.4758
```

TS for the proton shuttle mechanism of *N*-acylation

One imaginary frequency (1028.1i cm^{-1}) corresponded to nucleophilic attack and the transfer of two protons.

```
E = -4049.9472 hartrees

205
Frame 1
C -12.1806 21.0232 5.1359
H -11.7800 21.9084 5.6384
H -12.2333 20.1931 5.8452
```

H -13.1892 21.2737 4.7914
C -11.3020 20.7133 3.9340
O -11.0242 21.5929 3.1017
N -10.8678 19.4389 3.8454
H -11.1142 18.7625 4.5794
C -9.8680 19.0365 2.8552
H -9.1958 19.8922 2.7160
C -10.5541 18.7362 1.5004
O -10.7805 17.5936 1.0962
C -9.0528 17.8126 3.3432
H -9.6866 16.9279 3.2054
O -8.6586 17.9440 4.6960
H -9.4446 17.7138 5.2448
C -7.7902 17.6423 2.5021
H -8.0307 17.5314 1.4410
H -7.2484 16.7515 2.8324
H -7.1295 18.5073 2.6322
N -10.8755 19.8513 0.7950
H -10.8608 20.7276 1.3186
C -11.6121 19.7519 -0.4490
H -12.6853 19.5739 -0.2931
H -11.4917 20.6790 -1.0159
H -11.2190 18.9176 -1.0339
C -16.2605 18.1657 10.3457
H -15.9759 18.9625 11.0449
H -17.1440 17.6695 10.7549
C -15.1452 17.1179 10.3564
O -15.3304 15.9785 10.7798
C -16.5926 18.7999 8.9831
H -17.2924 19.6279 9.1654
H -15.6943 19.2811 8.5653
C -17.1908 17.8710 7.9634
C -17.3026 16.4990 8.0048
H -16.9885 15.8091 8.7761
C -17.7736 18.2846 6.7123
N -17.9109 16.0332 6.8550
H -18.1192 15.0568 6.6573
C -18.2111 17.1046 6.0435
C -17.9767 19.5329 6.0972
H -17.6518 20.4479 6.5865
C -18.8254 17.1556 4.7857
H -19.1371 16.2485 4.2773
C -18.5976 19.5842 4.8549
H -18.7597 20.5446 4.3726
C -19.0150 18.4051 4.2043
H -19.4898 18.4730 3.2291
N -13.9279 17.5466 9.9135
H -13.8380 18.4568 9.4875
C -12.7372 16.7029 9.9760
H -12.9197 15.9767 10.7710
C -11.5400 17.5600 10.4524
O -11.2134 17.5891 11.6364
C -12.4922 15.9173 8.6788
H -13.3694 15.2766 8.4984
H -11.6268 15.2636 8.8424
O -12.2783 16.8316 7.6121
N -10.9384 18.3072 9.4886
H -11.1667 18.0885 8.5187
C -9.7846 19.1303 9.8030
H -9.6186 19.8391 8.9886
H -9.9666 19.6739 10.7332

H -8.8743 18.5318 9.9386
C -16.7937 7.2324 8.5672
C -17.6512 6.2055 7.8208
H -18.0744 5.4656 8.5090
H -17.0524 5.6788 7.0747
H -18.4854 6.6908 7.3007
H -17.3805 7.7759 9.3128
H -15.9853 6.7127 9.0987
C -16.1439 8.2415 7.6152
O -15.5074 7.8033 6.6189
O -16.2970 9.4748 7.8965
N -14.1441 6.0235 4.7906
C -14.3816 4.7860 4.2750
O -13.6804 4.2461 3.4204
C -15.6055 4.0839 4.8580
H -15.8063 3.1888 4.2683
H -16.4859 4.7349 4.8511
H -15.4165 3.7906 5.8968
H -14.7989 6.4291 5.4583
C -12.9918 6.8287 4.3940
H -12.4415 6.2342 3.6633
C -12.0010 7.0257 5.5650
O -10.7977 6.8226 5.4109
C -13.4182 8.1874 3.7667
H -13.9436 8.7464 4.5526
C -14.4304 8.0074 2.6114
H -15.3281 7.5186 3.0078
H -14.7455 9.0107 2.2922
C -12.1925 9.0072 3.3320
H -11.5978 8.4754 2.5819
H -11.5258 9.2187 4.1718
H -12.5072 9.9637 2.9003
C -13.9317 7.2186 1.3919
H -13.0547 7.6890 0.9348
H -14.7126 7.1715 0.6236
H -13.6690 6.1902 1.6581
N -12.5444 7.4500 6.7431
H -13.5507 7.5986 6.7977
C -11.7469 7.5624 7.9574
H -12.2507 7.0095 8.7629
H -10.7978 7.0627 7.7470
C -11.4744 9.0063 8.4330
H -10.7889 8.9065 9.2890
C -10.7658 9.8364 7.3549
H -11.4336 10.0185 6.5054
H -9.8818 9.3203 6.9675
H -10.4522 10.8089 7.7509
C -12.7493 9.6980 8.9340
H -13.5061 9.7670 8.1450
H -12.5365 10.7145 9.2846
H -13.2035 9.1502 9.7680
C -18.8361 10.8130 6.0346
H -19.7224 10.1674 6.0057
H -18.3466 10.6693 7.0012
C -19.2336 12.2755 5.9075
O -18.5542 13.1856 6.3828
C -17.8628 10.3795 4.9037
H -17.6570 9.3099 5.0244
H -18.3400 10.5089 3.9258
C -16.5703 11.1318 4.9108
N -15.6761 11.0177 5.9533

H -15.8398 10.3464 6.8220
C -16.0260 12.0267 4.0234
H -16.4073 12.3915 3.0821
C -14.6387 11.8163 5.6958
H -13.7777 11.9324 6.3361
N -14.8154 12.4436 4.5304
H -13.7602 16.0387 6.1658
N -20.3720 12.5101 5.1940
H -20.8598 11.7221 4.7966
C -20.8406 13.8482 4.8831
H -20.4242 14.2243 3.9400
H -21.9313 13.8503 4.8077
H -20.5400 14.5223 5.6861
C -20.0491 12.8504 -0.9507
C -19.5359 14.2562 -0.6199
H -20.3685 14.9534 -0.4737
H -18.9125 14.6518 -1.4300
H -18.9353 14.2716 0.2951
H -20.6658 12.4768 -0.1195
H -20.7208 12.9144 -1.8180
C -18.9509 11.8120 -1.2555
H -18.3271 12.2184 -2.0663
C -18.0389 11.5535 -0.0460
H -18.6207 11.1690 0.8023
H -17.5256 12.4628 0.2822
H -17.2702 10.8102 -0.2823
C -19.5724 10.4985 -1.7533
H -18.8006 9.7660 -2.0133
H -20.1946 10.6619 -2.6406
H -20.2082 10.0488 -0.9800
C -16.3572 17.3260 -0.2581
C -15.1765 17.5905 -1.1957
H -15.1162 18.6501 -1.4687
H -15.2670 17.0164 -2.1246
H -14.2256 17.3155 -0.7275
H -16.4229 16.2660 0.0107
H -17.3097 17.6080 -0.7214
H -16.2639 17.8942 0.6736
C -9.7614 14.6815 -2.6096
C -9.7624 15.8626 -3.5917
H -10.2097 15.5859 -4.5534
H -8.7393 16.2071 -3.7884
H -10.3251 16.7127 -3.1905
H -10.8070 14.3739 -2.4522
C -9.1951 15.1148 -1.2427
H -8.1554 15.4481 -1.3838
H -9.7524 15.9906 -0.8868
C -9.0080 13.4875 -3.2149
H -7.9490 13.7334 -3.3689
H -9.4269 13.2089 -4.1894
H -9.0538 12.6033 -2.5720
C -9.2422 14.0390 -0.1520
H -8.5949 13.1855 -0.3813
H -10.2615 13.6591 -0.0157
H -8.9203 14.4522 0.8087
C -11.6867 16.4059 6.2940
N -12.9813 15.9452 5.5155
H -12.9667 14.8002 4.9216
C -13.3103 16.6070 4.2306
H -12.3656 16.9797 3.8320
C -13.8066 15.4244 3.3279

H -14.9099 15.3700 3.3557
H -13.4970 15.5896 2.2893
O -13.2209 14.2498 3.8588
H -14.0967 13.2500 4.1312
C -14.3175 17.7427 4.3431
H -14.5634 18.1306 3.3476
H -13.9166 18.5667 4.9377
H -15.2528 17.4062 4.8065
O -11.1082 17.4305 5.7583
C -10.7984 15.1537 6.4902
H -10.0682 15.3911 7.2750
H -11.4006 14.3119 6.8581
C -10.0423 14.7203 5.2275
H -10.7437 14.5918 4.3953
H -9.3475 15.5169 4.9489
C -9.2657 13.4154 5.4371
H -8.7039 13.1421 4.5376
H -8.5493 13.5056 6.2626
H -9.9367 12.5802 5.6719

Traditional mechanism:

Note that this would the pathway for a (monosubstituted) amine whereas short amino alcohols have been shown to exist exclusively as ring structures with an intramolecular hydrogen bond. We modeled a hydrogen bond to the backbone of T40 donated by the open chain amino alcohol hydroxyl. This hydrogen bond lowers the energy for all structures of the hypothetical traditional reaction mechanism and since it is fully developed in the ES-complex, it does not contribute to catalysis ($k_{cat,app}$).

ES-complex for the traditional mechanism of *N*-acylation

```
E = -4049.9870 hartrees

205
Frame 1
C -12.5850 20.4309 5.2354
H -12.4058 21.3606 5.7812
H -12.4594 19.5752 5.9035
H -13.6197 20.4514 4.8777
C -11.6483 20.3860 4.0399
O -11.4943 21.3696 3.3020
N -11.0234 19.2027 3.8336
H -11.1525 18.4534 4.5090
C -10.0110 19.0335 2.7904
H -9.4443 19.9708 2.7401
C -10.7134 18.8081 1.4328
O -10.8848 17.6847 0.9437
C -9.0367 17.8805 3.1283
H -9.5924 16.9377 3.0406
O -8.5084 18.0358 4.4373
H -9.1600 17.6642 5.0561
C -7.8622 17.8586 2.1552
H -8.2013 17.7042 1.1283
H -7.1832 17.0458 2.4261
H -7.3021 18.7991 2.2135
N -11.1180 19.9499 0.8331
H -11.1544 20.7713 1.4383
C -11.8717 19.9268 -0.4056
H -12.9354 19.7073 -0.2449
H -11.7847 20.8988 -0.8975
H -11.4643 19.1511 -1.0577
C -16.1022 18.3897 10.0363
H -15.7312 19.2189 10.6538
H -17.0174 18.0405 10.5232
C -15.0870 17.2597 10.2105
O -15.0820 16.5727 11.2247
C -16.4080 18.9120 8.6263
H -17.0394 19.8052 8.7396
H -15.4847 19.2948 8.1619
C -17.0977 17.9412 7.7065
C -17.4133 16.6174 7.9267
H -17.2203 15.9937 8.7889
C -17.5922 18.2548 6.3898
N -18.0701 16.0910 6.8367
H -18.3861 15.1262 6.7476
C -18.1928 17.0691 5.8773
```

C -17.5964 19.4186 5.5999
H -17.1495 20.3389 5.9689
C -18.7817 17.0278 4.6078
H -19.2318 16.1144 4.2312
C -18.1847 19.3795 4.3414
H -18.2004 20.2752 3.7260
C -18.7705 18.1936 3.8503
H -19.2233 18.1928 2.8625
N -14.1311 17.1133 9.2279
H -14.2966 17.5330 8.3226
C -13.1898 15.9996 9.2771
H -13.5868 15.2713 9.9926
C -11.7781 16.3805 9.7783
O -10.8929 15.5277 9.8280
C -13.0342 15.3263 7.9140
H -13.9927 15.0247 7.4857
H -12.3948 14.4548 8.0291
O -12.4487 16.3031 7.0215
N -11.5854 17.6776 10.1056
H -12.3746 18.3007 10.0233
C -10.2875 18.1764 10.5232
H -10.2343 19.2510 10.3324
H -10.1020 17.9946 11.5888
H -9.5071 17.6684 9.9514
C -16.8089 6.8310 8.7367
C -17.9330 6.1258 7.9616
H -18.3308 5.2699 8.5208
H -17.5631 5.7628 6.9981
H -18.7659 6.8111 7.7659
H -17.1900 7.2345 9.6797
H -16.0243 6.0999 8.9708
C -16.1484 7.9751 7.9380
O -15.4708 7.6518 6.9162
O -16.3263 9.1523 8.3613
N -14.1388 6.4971 4.6904
C -14.3653 5.3382 4.0181
O -13.6945 4.9437 3.0632
C -15.5711 4.5477 4.5199
H -15.3823 3.4845 4.3559
H -16.4596 4.8259 3.9409
H -15.7797 4.7317 5.5778
H -14.7603 6.7610 5.4567
C -13.0109 7.3753 4.3937
H -12.4843 6.9312 3.5476
C -11.9785 7.3829 5.5420
O -10.7754 7.2729 5.3037
C -13.4770 8.8169 4.0404
H -13.9980 9.2060 4.9255
C -14.5085 8.8261 2.8886
H -15.4001 8.2801 3.2185
H -14.8235 9.8682 2.7420
C -12.2844 9.7403 3.7426
H -11.7043 9.3860 2.8838
H -11.5930 9.8007 4.5874
H -12.6392 10.7532 3.5242
C -14.0327 8.2372 1.5530
H -13.1493 8.7581 1.1673
H -14.8189 8.3288 0.7939
H -13.7867 7.1750 1.6478
N -12.4825 7.5395 6.7998
H -13.4927 7.6121 6.9290

C -11.6264 7.4348 7.9707
H -12.0511 6.6849 8.6547
H -10.6645 7.0596 7.6136
C -11.4132 8.7520 8.7496
H -10.6841 8.5088 9.5388
C -10.8047 9.8474 7.8639
H -11.5069 10.1392 7.0756
H -9.8867 9.5046 7.3755
H -10.5688 10.7409 8.4538
C -12.6999 9.2321 9.4376
H -13.4997 9.4279 8.7157
H -12.5226 10.1561 10.0004
H -13.0794 8.4830 10.1427
C -18.8005 10.9655 6.3638
H -19.5669 10.1831 6.2929
H -18.4348 10.9801 7.3925
C -19.4245 12.3158 6.0474
O -19.0901 13.3647 6.6001
C -17.6266 10.6102 5.4054
H -17.3912 9.5498 5.5478
H -17.9502 10.7298 4.3647
C -16.3849 11.4127 5.6307
N -15.5487 11.1474 6.6917
H -15.7136 10.3627 7.3790
C -15.8035 12.4664 4.9587
H -16.1594 12.9636 4.0657
C -14.5203 12.0262 6.6139
H -13.7044 12.0213 7.3240
N -14.6328 12.8493 5.5779
H -13.3525 14.2942 4.3510
N -20.3904 12.2859 5.0805
H -20.5777 11.4055 4.6253
C -21.0556 13.4770 4.5839
H -20.5413 13.9121 3.7170
H -22.0837 13.2362 4.2976
H -21.0717 14.2206 5.3830
C -19.8343 12.7156 -0.7505
C -19.6143 14.2326 -0.7225
H -20.5198 14.7663 -1.0313
H -18.8061 14.5278 -1.4026
H -19.3499 14.5898 0.2777
H -20.6460 12.4490 -0.0565
H -20.1883 12.4279 -1.7503
C -18.5933 11.8658 -0.4104
H -17.7907 12.1588 -1.1048
C -18.0854 12.1092 1.0192
H -18.8662 11.8722 1.7547
H -17.7821 13.1485 1.1782
H -17.2184 11.4782 1.2415
C -18.8834 10.3739 -0.6339
H -17.9935 9.7633 -0.4485
H -19.2176 10.1800 -1.6597
H -19.6723 10.0228 0.0439
C -16.5835 17.7317 -0.7463
C -15.3616 17.4309 -1.6192
H -14.9069 18.3526 -1.9976
H -15.6336 16.8189 -2.4867
H -14.5943 16.8861 -1.0588
H -17.0382 16.8103 -0.3670
H -17.3538 18.2750 -1.3061
H -16.3151 18.3430 0.1223

```
C -9.9680 14.6921 -2.5577
C -9.8122 15.8497 -3.5547
H -10.3234 15.6364 -4.5013
H -8.7538 16.0300 -3.7837
H -10.2281 16.7811 -3.1526
H -11.0421 14.5599 -2.3586
C -9.2904 15.0385 -1.2162
H -8.2056 15.1264 -1.3841
H -9.6364 16.0301 -0.8986
C -9.4360 13.3875 -3.1716
H -8.3605 13.4664 -3.3783
H -9.9392 13.1661 -4.1202
H -9.5860 12.5283 -2.5110
C -9.5632 14.0484 -0.0782
H -9.2206 13.0356 -0.3175
H -10.6329 14.0043 0.1540
H -9.0449 14.3598 0.8351
C -11.2814 16.1121 6.3729
N -12.7104 15.0011 3.9798
H -12.1542 14.5528 3.2524
C -13.4545 16.1033 3.3545
H -12.7731 16.9672 3.2921
C -13.8849 15.7971 1.9100
H -14.5641 14.9344 1.9022
H -14.4403 16.6593 1.5018
O -12.7903 15.4500 1.0710
H -12.1843 16.2121 1.0297
C -14.6494 16.5036 4.2197
H -15.1946 17.3496 3.7877
H -14.3145 16.7870 5.2208
H -15.3534 15.6710 4.3315
O -10.8146 17.0898 5.8032
C -10.5897 14.7720 6.4498
H -10.2636 14.6300 7.4900
H -11.3296 13.9962 6.2299
C -9.4078 14.6463 5.4850
H -9.7798 14.8021 4.4669
H -8.6804 15.4429 5.6759
C -8.7278 13.2777 5.5907
H -7.8910 13.2034 4.8889
H -8.3354 13.1010 6.5990
H -9.4260 12.4650 5.3613
```

TS for nitrogen inversion (the rate limiting TS)

The TS for nitrogen inversion has a "flat" sp^2 like nitrogen and is concerted with amide bond synthesis at the B3LYP/6-31G(d,p) level. One imaginary frequency of 441.6i cm^{-1} corresponded to nitrogen inversion and amide bond synthesis.

```
E = -4049.9546 hartrees

205
Frame 1
C -13.0173 20.3758 5.2851
H -12.7768 21.3030 5.8114
H -12.9841 19.5337 5.9806
H -14.0349 20.4696 4.8920
C -12.0446 20.2106 4.1294
```

O -11.7759 21.1493 3.3648
N -11.5151 18.9727 3.9926
H -11.6873 18.2690 4.7187
C -10.4316 18.7168 3.0453
H -9.7799 19.5990 3.0563
C -10.9787 18.5471 1.6036
O -11.2357 17.4447 1.0996
C -9.6080 17.4824 3.5000
H -10.2024 16.5845 3.2867
O -9.3134 17.5693 4.8820
H -10.0956 17.2125 5.3799
C -8.2883 17.3980 2.7371
H -8.4506 17.3511 1.6562
H -7.7442 16.5012 3.0457
H -7.6635 18.2682 2.9682
N -11.1071 19.7093 0.9177
H -11.1510 20.5448 1.5013
C -11.6121 19.7519 -0.4490
H -12.7056 19.6742 -0.4952
H -11.3013 20.6907 -0.9142
H -11.1906 18.9136 -1.0077
C -16.0917 18.2533 10.0824
H -15.6859 19.0356 10.7377
H -17.0028 17.8763 10.5537
C -15.0965 17.0904 10.1036
O -15.3420 16.0530 10.7213
C -16.4214 18.8729 8.7155
H -17.0259 19.7735 8.8959
H -15.5028 19.2484 8.2379
C -17.1557 17.9716 7.7644
C -17.4449 16.6332 7.8955
H -17.1951 15.9507 8.6960
C -17.7124 18.3809 6.5012
N -18.1493 16.1841 6.7956
H -18.4405 15.2182 6.6652
C -18.3256 17.2330 5.9196
C -17.7535 19.6046 5.8107
H -17.2926 20.4923 6.2374
C -18.9635 17.2970 4.6746
H -19.4165 16.4173 4.2281
C -18.3886 19.6666 4.5760
H -18.4216 20.6068 4.0318
C -18.9870 18.5210 4.0136
H -19.4694 18.5936 3.0423
N -13.9097 17.2998 9.4729
H -13.7653 18.1265 8.9134
C -12.7967 16.3603 9.6004
H -12.8931 15.9107 10.5927
C -11.4728 17.1506 9.6808
O -10.8989 17.2751 10.7653
C -12.9036 15.1633 8.6232
H -13.7770 14.6092 8.9912
H -12.0261 14.5223 8.7799
O -13.1578 15.4086 7.2475
N -11.0431 17.7245 8.5352
H -11.3891 17.3892 7.6073
C -9.7820 18.4492 8.5283
H -9.5183 18.6755 7.4925
H -9.8585 19.3842 9.0962
H -8.9789 17.8579 8.9840
C -16.5277 6.8991 8.6004

C -17.6512 6.2055 7.8208
H -17.9428 5.2668 8.3024
H -17.3316 5.9807 6.7997
H -18.5415 6.8426 7.7658
H -16.8461 7.1362 9.6185
H -15.6554 6.2376 8.6543
C -16.0995 8.1762 7.8946
O -15.5343 8.1340 6.7890
O -16.4082 9.2718 8.5251
N -14.1680 6.5820 4.5867
C -14.4448 5.4136 3.9383
O -13.7454 4.9415 3.0455
C -15.7095 4.7072 4.4191
H -15.9362 3.8920 3.7312
H -16.5617 5.3939 4.4664
H -15.5567 4.2933 5.4225
H -14.8068 6.9178 5.3029
C -12.9631 7.3643 4.3141
H -12.4371 6.8370 3.5174
C -11.9855 7.3361 5.5109
O -10.8060 7.0323 5.3531
C -13.2951 8.8149 3.8650
H -13.8232 9.2990 4.6994
C -14.2607 8.8487 2.6577
H -15.2099 8.3870 2.9559
H -14.4858 9.9040 2.4509
C -12.0099 9.6148 3.5962
H -11.4038 9.1548 2.8090
H -11.3805 9.6806 4.4876
H -12.2534 10.6351 3.2805
C -13.7612 8.1756 1.3716
H -12.8258 8.6204 1.0162
H -14.5005 8.2933 0.5708
H -13.5965 7.1030 1.5138
N -12.5126 7.6842 6.7234
H -13.5038 7.8914 6.7885
C -11.7469 7.5624 7.9574
H -12.2605 6.8575 8.6285
H -10.7915 7.1154 7.6725
C -11.5050 8.8836 8.7136
H -10.8908 8.6092 9.5847
C -10.7110 9.8897 7.8704
H -11.2919 10.2086 6.9984
H -9.7764 9.4525 7.5040
H -10.4660 10.7834 8.4543
C -12.8134 9.4943 9.2346
H -13.4707 9.7797 8.4070
H -12.6167 10.3936 9.8288
H -13.3630 8.7906 9.8717
C -18.6462 10.9760 6.0886
H -19.3233 10.2436 5.6315
H -18.5174 10.7021 7.1392
C -19.2473 12.3706 6.0377
O -18.8488 13.2888 6.7552
C -17.2646 10.9135 5.3774
H -16.9444 9.8658 5.3595
H -17.3702 11.2396 4.3364
C -16.2188 11.7375 6.0601
N -15.7482 11.3938 7.3124
H -16.0910 10.1835 7.9894
C -15.6181 12.9114 5.6787

H -15.7197 13.5037 4.7844
C -14.8948 12.3465 7.6683
H -14.3464 12.3758 8.5969
N -14.7836 13.2834 6.7074
H -14.1807 14.1443 6.7668
N -20.2406 12.5488 5.1205
H -20.4746 11.7851 4.5050
C -20.8406 13.8482 4.8831
H -20.3114 14.4099 4.1040
H -21.8827 13.7245 4.5753
H -20.8079 14.4243 5.8093
C -19.7655 12.7442 -0.7275
C -19.5359 14.2562 -0.6199
H -20.4499 14.8098 -0.8636
H -18.7542 14.5877 -1.3131
H -19.2325 14.5567 0.3873
H -20.5408 12.4382 -0.0086
H -20.1734 12.5167 -1.7221
C -18.5108 11.8766 -0.5032
H -17.7491 12.2020 -1.2283
C -17.9209 12.0543 0.9041
H -18.6617 11.7911 1.6715
H -17.6008 13.0841 1.0888
H -17.0475 11.4093 1.0504
C -18.8208 10.3982 -0.7802
H -17.9249 9.7764 -0.6771
H -19.2141 10.2555 -1.7932
H -19.5720 10.0171 -0.0763
C -16.3705 17.6265 -0.2381
C -15.1765 17.5905 -1.1957
H -15.0099 18.5690 -1.6602
H -15.3353 16.8676 -2.0046
H -14.2550 17.3091 -0.6759
H -16.5457 16.6450 0.2152
H -17.2912 17.9223 -0.7541
H -16.2057 18.3376 0.5781
C -9.8390 14.6792 -2.6138
C -9.7624 15.8626 -3.5917
H -10.1677 15.5963 -4.5752
H -8.7226 16.1834 -3.7378
H -10.3275 16.7235 -3.2182
H -10.8982 14.3999 -2.5044
C -9.3209 15.0855 -1.2187
H -8.2473 15.3161 -1.2997
H -9.8144 16.0174 -0.9137
C -9.0887 13.4669 -3.1875
H -8.0203 13.6921 -3.3040
H -9.4774 13.1909 -4.1751
H -9.1734 12.5870 -2.5427
C -9.5450 14.0451 -0.1147
H -9.0604 13.0887 -0.3424
H -10.6122 13.8590 0.0471
H -9.1377 14.3991 0.8376
C -12.0033 15.5377 6.1374
N -12.6287 15.0642 4.9179
H -12.5263 14.0987 4.6479
C -13.3603 15.9797 4.0523
H -12.7339 16.8541 3.8610
C -13.5790 15.3123 2.6849
H -14.1566 14.3841 2.8157
H -14.1949 15.9855 2.0660

O -12.3804 14.9444 2.0262
H -11.9281 15.7646 1.7529
C -14.6843 16.4901 4.6418
H -15.1030 17.2952 4.0257
H -14.5222 16.8703 5.6519
H -15.4400 15.6986 4.7093
O -11.6290 16.8125 6.0745
C -10.9053 14.5214 6.5528
H -10.4314 14.8786 7.4732
H -11.3806 13.5575 6.7881
C -9.8114 14.2923 5.4973
H -10.2737 14.0401 4.5360
H -9.2613 15.2247 5.3384
C -8.8306 13.1842 5.8989
H -8.0597 13.0457 5.1326
H -8.3224 13.4195 6.8420
H -9.3411 12.2223 6.0310

Proton shuttle mechanism of *O-acylation:*

ES-complex for the proton shuttle mechanism of *O*-acylation

```
E = -4049.9759 hartrees

205
Frame 1
C -12.0078 20.9580 5.1906
H -11.7230 21.8860 5.6926
H -11.9291 20.1181 5.8848
H -13.0507 21.0621 4.8734
C -11.1297 20.7872 3.9624
O -10.9043 21.7287 3.1908
N -10.6379 19.5392 3.7677
H -10.8395 18.8274 4.4606
C -9.6809 19.2302 2.7027
H -9.0383 20.1112 2.5888
C -10.4433 18.9972 1.3763
O -10.6679 17.8745 0.9210
C -8.8071 18.0119 3.0728
H -9.4452 17.1190 3.0253
O -8.2337 18.1588 4.3665
H -8.9297 18.0089 5.0276
C -7.6523 17.8442 2.0900
H -8.0207 17.6911 1.0735
H -7.0526 16.9781 2.3823
H -7.0049 18.7279 2.1148
N -10.8318 20.1488 0.7739
H -10.7901 20.9901 1.3490
C -11.6534 20.1296 -0.4193
H -12.7212 20.0020 -0.1933
H -11.5215 21.0672 -0.9658
H -11.3419 19.2959 -1.0508
C -16.1775 18.3542 10.2744
H -15.8517 19.1891 10.9092
H -17.0542 17.9038 10.7454
C -15.0850 17.2880 10.2997
O -15.2909 16.1355 10.6645
C -16.5449 18.9047 8.8825
H -17.2055 19.7700 9.0391
H -15.6446 19.3191 8.4023
C -17.2213 17.9338 7.9556
C -17.3976 16.5745 8.1008
H -17.0823 15.9249 8.9055
C -17.8287 18.2857 6.6974
N -18.0719 16.0614 7.0138
H -18.3332 15.0857 6.8867
C -18.3482 17.0832 6.1360
C -17.9931 19.4920 5.9937
H -17.6084 20.4248 6.3995
C -19.0041 17.0680 4.8995
H -19.3761 16.1395 4.4777
C -18.6525 19.4791 4.7697
H -18.7825 20.4067 4.2183
C -19.1507 18.2766 4.2269
H -19.6546 18.2931 3.2642
N -13.8376 17.7113 9.9085
H -13.6939 18.6806 9.6673
C -12.6696 16.8528 10.0607
H -12.9654 16.0555 10.7468
```

C -11.5327 17.6222 10.7720
O -11.1620 17.3162 11.8977
C -12.2434 16.1531 8.7637
H -13.1038 15.6719 8.2915
H -11.4821 15.4050 9.0025
O -11.7099 17.1328 7.8426
N -11.0386 18.6976 10.0830
H -11.1857 18.7028 9.0808
C -9.9391 19.4830 10.6220
H -9.9707 20.4923 10.2033
H -10.0479 19.5327 11.7061
H -8.9606 19.0387 10.3977
C -17.2491 7.3892 8.5823
C -17.6769 5.9805 8.1718
H -18.3583 5.5360 8.9077
H -16.7993 5.3377 8.0727
H -18.1909 5.9881 7.2041
H -18.1045 8.0687 8.6577
H -16.7943 7.3620 9.5829
C -16.2061 8.0248 7.6430
O -15.4168 7.2405 7.0428
O -16.2053 9.2882 7.5883
N -14.1370 6.0361 4.7834
C -14.3832 4.7983 4.2787
O -13.7075 4.2580 3.4010
C -15.5794 4.0857 4.9006
H -16.2007 3.6728 4.1010
H -16.1799 4.7318 5.5456
H -15.2103 3.2427 5.4952
H -14.7593 6.4163 5.4973
C -12.9776 6.8284 4.3888
H -12.4284 6.2283 3.6614
C -11.9885 7.0346 5.5600
O -10.7737 6.9475 5.3694
C -13.3968 8.1852 3.7511
H -13.9274 8.7489 4.5301
C -14.4008 8.0042 2.5891
H -15.2972 7.5072 2.9775
H -14.7201 9.0066 2.2740
C -12.1750 9.0146 3.3235
H -11.5679 8.4845 2.5821
H -11.5177 9.2360 4.1681
H -12.5029 9.9631 2.8834
C -13.8880 7.2206 1.3721
H -13.0075 7.6946 0.9243
H -14.6617 7.1749 0.5962
H -13.6265 6.1918 1.6383
N -12.5394 7.3347 6.7682
H -13.5570 7.3818 6.8722
C -11.7265 7.4295 7.9713
H -12.1906 6.8151 8.7546
H -10.7534 6.9931 7.7254
C -11.5231 8.8629 8.5123
H -10.8151 8.7610 9.3505
C -10.8778 9.7793 7.4633
H -11.5672 9.9566 6.6304
H -9.9702 9.3319 7.0465
H -10.6206 10.7522 7.8992
C -12.8224 9.4634 9.0671
H -13.6029 9.5348 8.3021
H -12.6525 10.4714 9.4640

H -13.2247 8.8517 9.8837
C -18.9139 10.9034 6.2987
H -19.7528 10.2630 6.6023
H -18.2025 10.9334 7.1257
C -19.4405 12.3119 6.0582
O -18.9948 13.3069 6.6285
C -18.2275 10.2730 5.0574
H -18.0403 9.2191 5.2897
H -18.9041 10.2866 4.1939
C -16.9420 10.9355 4.6710
N -15.7998 10.7867 5.4263
H -15.7486 10.1810 6.2850
C -16.5887 11.7703 3.6329
H -17.2117 12.1271 2.8234
C -14.8306 11.5188 4.8305
H -13.8244 11.5823 5.2208
N -15.2622 12.1302 3.7356
H -12.9094 14.9418 5.1072
N -20.4781 12.3870 5.1712
H -20.7561 11.5417 4.6965
C -21.0980 13.6360 4.7740
H -20.6949 14.0189 3.8265
H -22.1786 13.5022 4.6633
H -20.9093 14.3727 5.5551
C -20.1233 12.8301 -0.9675
C -19.5972 14.2326 -0.6389
H -20.4236 14.9287 -0.4572
H -19.0012 14.6360 -1.4656
H -18.9657 14.2358 0.2556
H -20.7094 12.4494 -0.1177
H -20.8269 12.9039 -1.8087
C -19.0392 11.7923 -1.3226
H -18.4541 12.1991 -2.1622
C -18.0738 11.5338 -0.1566
H -18.6136 11.1484 0.7178
H -17.5448 12.4410 0.1503
H -17.3153 10.7908 -0.4248
C -19.6836 10.4791 -1.7913
H -18.9249 9.7440 -2.0811
H -20.3441 10.6396 -2.6513
H -20.2857 10.0323 -0.9897
C -16.6021 17.5050 -0.6049
C -15.2107 17.5496 -1.2397
H -15.0072 18.5328 -1.6814
H -15.1166 16.8088 -2.0419
H -14.4240 17.3452 -0.5087
H -16.8134 16.5197 -0.1768
H -17.3858 17.7199 -1.3399
H -16.6965 18.2385 0.2028
C -9.8189 14.7027 -2.5376
C -9.8394 15.8793 -3.5235
H -10.2827 15.5908 -4.4837
H -8.8219 16.2398 -3.7223
H -10.4167 16.7215 -3.1257
H -10.8594 14.3803 -2.3764
C -9.2556 15.1524 -1.1750
H -8.2136 15.4782 -1.3168
H -9.8087 16.0371 -0.8354
C -9.0483 13.5167 -3.1375
H -7.9944 13.7795 -3.2978
H -9.4668 13.2247 -4.1080

H -9.0769 12.6357 -2.4892
C -9.3112 14.0905 -0.0710
H -8.6719 13.2288 -0.2893
H -10.3336 13.7185 0.0674
H -8.9832 14.5115 0.8851
C -10.9049 16.7994 6.8140
O -13.0857 15.8246 5.5167
H -12.6253 14.4121 2.6115
C -13.5488 16.5445 4.3826
H -12.7174 17.0833 3.8934
C -14.1728 15.5470 3.3819
H -15.1312 15.2171 3.8004
C -14.3985 16.1795 2.0105
N -13.3112 14.3528 3.3610
H -13.8891 13.5136 3.2337
H -14.2871 17.2882 4.7051
H -15.0453 17.0625 2.0776
H -13.4441 16.4949 1.5693
H -14.8737 15.4661 1.3292
O -10.5334 17.7194 6.0977
C -10.4072 15.3763 6.6872
H -9.6760 15.2155 7.4952
H -11.2332 14.6869 6.8786
C -9.7675 15.0743 5.3283
H -10.5032 15.2967 4.5486
H -8.9159 15.7425 5.1636
C -9.3242 13.6133 5.2135
H -8.8653 13.4231 4.2383
H -8.5896 13.3509 5.9837
H -10.1739 12.9291 5.3155

TS model for the proton shuttle mechanism of *O*-acylation

Using constrained distances, see Figure S12.

```
E = -4049.9139 hartrees

205
Frame 1
C -11.9948 20.9602 5.1750
H -11.7045 21.8791 5.6912
H -11.9198 20.1092 5.8556
H -13.0366 21.0748 4.8582
C -11.1127 20.8058 3.9473
O -10.8750 21.7620 3.1955
N -10.6253 19.5611 3.7326
H -10.8607 18.8291 4.3942
C -9.6380 19.2682 2.6905
H -9.0066 20.1599 2.5970
C -10.3566 19.0286 1.3400
O -10.4697 17.9133 0.8315
C -8.7594 18.0630 3.0933
H -9.3875 17.1632 3.0420
O -8.2213 18.2301 4.4001
H -8.9365 18.0870 5.0428
C -7.5771 17.8935 2.1446
H -7.9197 17.7261 1.1218
H -6.9794 17.0355 2.4643
H -6.9368 18.7824 2.1774
N -10.8395 20.1677 0.7796
H -10.8386 20.9986 1.3718
C -11.6534 20.1296 -0.4193
H -12.7213 19.9936 -0.1967
H -11.5286 21.0612 -0.9786
H -11.3283 19.2899 -1.0346
C -16.1418 18.4268 10.3362
H -15.8022 19.2673 10.9564
H -17.0179 17.9908 10.8219
C -15.0582 17.3515 10.3644
O -15.2690 16.2121 10.7687
C -16.5176 18.9622 8.9415
H -17.1752 19.8306 9.0902
H -15.6193 19.3694 8.4508
C -17.1969 17.9839 8.0241
C -17.3583 16.6233 8.1656
H -17.0265 15.9742 8.9640
C -17.8134 18.3345 6.7701
N -18.0387 16.1082 7.0803
H -18.2583 15.1280 6.9296
C -18.3251 17.1313 6.2055
C -17.9857 19.5427 6.0724
H -17.6050 20.4756 6.4817
C -18.9855 17.1175 4.9717
H -19.3485 16.1878 4.5442
C -18.6482 19.5314 4.8505
H -18.7848 20.4605 4.3034
C -19.1411 18.3283 4.3048
H -19.6471 18.3462 3.3432
N -13.8197 17.7549 9.9346
H -13.6829 18.7056 9.6247
C -12.6573 16.8827 10.0396
```

H -12.9490 16.0767 10.7165
C -11.5067 17.6308 10.7552
O -11.1596 17.3276 11.8900
C -12.2683 16.2086 8.7177
H -13.1416 15.7455 8.2505
H -11.5127 15.4465 8.9286
O -11.7413 17.1972 7.8071
N -10.9796 18.6883 10.0653
H -11.1231 18.6981 9.0623
C -9.8849 19.4689 10.6195
H -9.9097 20.4808 10.2062
H -10.0054 19.5128 11.7027
H -8.9042 19.0251 10.4033
C -17.2707 7.4133 8.5283
C -17.6769 5.9805 8.1718
H -18.3219 5.5464 8.9448
H -16.7874 5.3556 8.0657
H -18.2228 5.9473 7.2229
H -18.1406 8.0719 8.6173
H -16.7780 7.4247 9.5110
C -16.2801 8.0423 7.5339
O -15.4575 7.2784 6.9653
O -16.3543 9.3044 7.3957
N -14.1174 6.0474 4.7637
C -14.3609 4.8061 4.2639
O -13.6793 4.2624 3.3944
C -15.5620 4.0997 4.8835
H -16.1917 3.7007 4.0835
H -16.1532 4.7458 5.5372
H -15.1991 3.2476 5.4685
H -14.7491 6.4325 5.4649
C -12.9524 6.8365 4.3817
H -12.4030 6.2429 3.6493
C -11.9700 7.0277 5.5595
O -10.7556 6.9283 5.3823
C -13.3617 8.2046 3.7637
H -13.8837 8.7582 4.5564
C -14.3737 8.0455 2.6059
H -15.2758 7.5595 2.9954
H -14.6787 9.0537 2.2931
C -12.1340 9.0294 3.3441
H -11.5309 8.5011 2.5987
H -11.4755 9.2396 4.1904
H -12.4496 9.9850 2.9101
C -13.8761 7.2611 1.3837
H -12.9908 7.7256 0.9366
H -14.6527 7.2294 0.6105
H -13.6276 6.2278 1.6446
N -12.5295 7.3391 6.7621
H -13.5447 7.3851 6.8555
C -11.7265 7.4295 7.9713
H -12.1969 6.8126 8.7498
H -10.7530 6.9929 7.7323
C -11.5254 8.8606 8.5204
H -10.8345 8.7508 9.3715
C -10.8557 9.7783 7.4885
H -11.5285 9.9685 6.6450
H -9.9445 9.3269 7.0842
H -10.5978 10.7459 7.9343
C -12.8301 9.4682 9.0549
H -13.5919 9.5517 8.2718

H -12.6602 10.4730 9.4592
H -13.2546 8.8562 9.8599
C -18.9342 10.8357 6.1509
H -19.7789 10.1935 6.4310
H -18.2066 10.7993 6.9631
C -19.4258 12.2649 5.9749
O -18.8795 13.2426 6.4811
C -18.2924 10.2742 4.8524
H -18.1223 9.2023 4.9986
H -18.9797 10.3749 4.0054
C -16.9929 10.9334 4.5091
N -15.8798 10.7209 5.2996
H -15.8921 10.0842 6.1803
C -16.6151 11.8184 3.5260
H -17.1862 12.2400 2.7147
C -14.8833 11.4584 4.8117
H -13.8959 11.5579 5.2338
N -15.2858 12.1247 3.7261
H -12.8699 14.7995 4.9321
N -20.5332 12.3693 5.1808
H -20.8973 11.5266 4.7631
C -21.0980 13.6360 4.7740
H -20.7008 13.9834 3.8104
H -22.1857 13.5558 4.6941
H -20.8545 14.3816 5.5332
C -20.1258 12.8245 -0.9309
C -19.5972 14.2326 -0.6389
H -20.4216 14.9335 -0.4640
H -19.0078 14.6184 -1.4780
H -18.9586 14.2580 0.2501
H -20.7043 12.4613 -0.0680
H -20.8360 12.8800 -1.7675
C -19.0427 11.7821 -1.2731
H -18.4625 12.1742 -2.1224
C -18.0697 11.5495 -0.1079
H -18.6069 11.1831 0.7769
H -17.5405 12.4657 0.1723
H -17.3123 10.8010 -0.3638
C -19.6872 10.4591 -1.7118
H -18.9296 9.7198 -1.9933
H -20.3532 10.6036 -2.5702
H -20.2842 10.0272 -0.8983
C -16.5873 17.5509 -0.5707
C -15.2107 17.5496 -1.2397
H -14.9790 18.5305 -1.6722
H -15.1600 16.8143 -2.0500
H -14.4204 17.3084 -0.5230
H -16.8183 16.5717 -0.1387
H -17.3825 17.7966 -1.2843
H -16.6352 18.2830 0.2427
C -9.8168 14.7226 -2.5139
C -9.8394 15.8793 -3.5235
H -10.2866 15.5728 -4.4772
H -8.8207 16.2331 -3.7341
H -10.4108 16.7309 -3.1399
H -10.8580 14.4087 -2.3407
C -9.2436 15.1938 -1.1627
H -8.1978 15.5033 -1.3143
H -9.7829 16.0915 -0.8376
C -9.0552 13.5203 -3.0930
H -7.9999 13.7735 -3.2604

H -9.4778 13.2104 -4.0563
H -9.0868 12.6534 -2.4259
C -9.3085 14.1567 -0.0355
H -8.6795 13.2822 -0.2343
H -10.3349 13.8019 0.1162
H -8.9744 14.5967 0.9097
C -10.9512 16.8616 6.7610
O -13.0651 15.8640 5.4023
H -12.7187 14.0233 2.9809
C -13.6649 16.4141 4.2637
H -12.9296 16.9574 3.6318
C -14.2737 15.2312 3.4390
H -15.2743 15.0410 3.8653
C -14.4437 15.6218 1.9707
N -13.4709 14.0261 3.6783
H -14.5535 12.8642 3.4376
H -14.4483 17.1356 4.5430
H -15.0405 16.5382 1.8693
H -13.4647 15.8112 1.5104
H -14.9384 14.8314 1.3926
O -10.5536 17.7904 6.0714
C -10.4690 15.4348 6.6337
H -9.7674 15.2573 7.4653
H -11.3157 14.7612 6.7817
C -9.7876 15.1352 5.2973
H -10.5093 15.3466 4.5024
H -8.9362 15.8089 5.1537
C -9.3285 13.6773 5.2065
H -8.8422 13.4807 4.2459
H -8.6117 13.4286 5.9988
H -10.1768 12.9892 5.2937

Shockwave Flash movies

Reaction path for the proton shuttle of *N*-acylation

alaninol_protonshuttle_large_B3LYP_631Gdp.swf

This movie shows the reaction path for the proton shuttle mechanism of *N*-acylation of (*R*)-alaninol in the large active site model of *Candida antarctica* lipase B consisting of 205 atoms.

Nitrogen inversion

Small active site model

NMe_inversion_small_MP2_631Gdp.swf

This movie shows the reaction path for nitrogen inversion for methyl amine in the small serine hydrolase active site model using MP2/6-31G(d,p) level of theory. The reaction path goes through the sp^2 like transition state for nitrogen inversion, which is a separate TS from amide bond synthesis at this level of theory.

NMe_inversion_small_B3LYP_631Gdp.swf

This movie shows the computed IRC for methyl amine in the small active site model using B3LYP/6-31G(d,p) level of theory. Amide bond synthesis is concerted with nitrogen inversion at this level of theory.

Large active site model

The reaction paths were calculated in the large active site model consisting of 205 atoms.

alaninol_inversion_large_HF_631Gdp.swf

This movie shows the reaction path for nitrogen inversion for (*R*)-alaninol in the large active site model using HF/6-31G(d,p) level of theory. The reaction path goes through the sp^2 like transition state for nitrogen inversion, which is a separate TS from amide bond synthesis at this level of theory. The transition state for nitrogen inversion breaks the hydrogen bond between the catalytic His $N_{\varepsilon 2}$ and the scissile nitrogen atom which causes the catalytic base to move towards S105.

alaninol_inversion_large_B3LYP_631Gdp.swf

This movie shows the reaction path for nitrogen inversion for (*R*)-alaninol in the large active site model using B3LYP/6-31G(d,p) level of theory. Only the first 18 points of the reaction path are shown for each direction. The movie shows how nitrogen inversion is concerted with amide bond synthesis at this level of theory and how the catalytic base (H224) moves towards S105.

Supplementary references

[1] a) T. D. Smith, J. B. Gerken, P. V. Jog, J. D. Roberts, *Org. Lett.* **2007**, *9*, 4555-4557; b) P. Butz, R. T. Kroemer, N. A. Macleod, E. G. Robertson, J. P. Simons, *J. Phys. Chem. A* **2001**, *105*, 1050-1056.

[2] P. Deslongchamps, *Tetrahedron* **1975**, *31*, 2463-2490.

[3] P.-O. Syren, K. Hult, *ChemCatChem* **2011**, *3*, 853-860.

[4] a) H. K. Hall, Jr., *J. Am. Chem. Soc.* **1957**, *79*, 5441-5444; b) V. S. Bryantsev, M. S. Diallo, W. A. Goddard, III, *J. Phys. Chem. A* **2007**, *111*, 4422-4430; c) F. Khalili, A. Henni, A. L. L. East, *J. Mol. Struct.: THEOCHEM* **2009**, *916*, 1-9.